Università degli Studi di Ferrara

Doctoral Course in Mathematics

XXIX cycle

Coordinator: Prof. Massimiliano Mella

Optimal control and stability in complex systems: epidemiological and landscape models

Scientific Disciplinary Sector: MAT/07

Elena Bonacini

Advisor: Prof.ssa Maria Groppi

Co-advisor: Luca Bolzoni, PhD

Years 2014/2016

Ph.D. Thesis

Advisors:

Prof.ssa Maria Groppi

Department of Mathematical, Physical and Computer Sciences
Università degli Studi di Parma

Luca Bolzoni, PhD

Risk Analysis Unit, Istituto Zooprofilattico Sperimentale della Lombardia e dell'Emilia Romagna

Department of Mathematical, Physical and Computer Sciences
Università degli Studi di Parma
Parco Area delle Scienze 53/A,
43124 Parma, Italy

Acknowledgments

I wish to thank Maria Groppi for introducing me to the beauty of applied mathematics, for her precious support and empathy during all these years and for her endless patience. I thank Luca Bolzoni for his enthusiastic collaboration: he gave me hints and interesting ideas and, with his practical expertise, really improved this work. I am grateful to Cinzia Soresina for her deep friendship: our office felt like home and I have been so lucky in sharing this journey with her. I thank all my family and my very-patient quasi-husband: they are my roots and my lifeblood. A special mention goes to my daughter Milla, who actively contributed to the writing of this thesis with sleepless nights and unconditioned love.

Summary

This thesis deals with epidemiological and environmental complex systems; their evolution and potentialities are analysed by means of qualitative analysis and optimal control techniques.

In the first part of the thesis we analyse a controlled SIR epidemiological model, focusing on four different control policies: prophylactic vaccination, isolation, non-selective culling and reduction of transmission controls. We thoroughly investigate the problem of minimizing the epidemic duration both with theoretical and numerical tools. In particular, for each policy, we prove the existence of an optimal control and we prove that the optimal strategy is to apply the control at the maximum rate until the eradication of the disease, possibly delaying the control action some amount of time. To complete the analytical study, we perform an extensive numerical study, exploring the solution of the time-optimal control problem on a wide range of parameter settings describing different epidemiological conditions, different possible control efforts and different numbers of initially introduced infected individuals in the population. The numerical simulations show that using the maximum control for the entire epidemic duration may not be the optimal strategy (even in unconstrained conditions) and that minimizing the epidemic duration does not always imply minimizing the total infectious burden, and vice versa.

The subsequent parts of the thesis focus on network models.

The second part deals with a network of dynamical systems devised to simulate the spread of an epidemic in highly populated cities. We model the city structure by identifying the nodes of the graph with the neighbourhoods of the city, and using directed weighted edges to represent the fraction of people moving from one neighbourhood to another due to their daily routine activities. The evolution of the disease inside each neighbourhood is described by the generalized model by Capasso and Serio in order to take into account psychological effects that can arise if a significant part of the neighbourhood is infected. The non-linear incidence term of this model is a generic unspecified function characterized by some meaningful properties. The equations of the model are obtained starting from the Capasso-Serio model and taking into account the influence of the infected individuals that come from other districts. We define the basic reproduction number for our epidemiological network and perform an analytical study for two particular network and parameters configurations, in order to analyse the stability of the disease free equilibrium. We prove that in an homogeneous (with respect to the epidemiological parameters) network

the mobility of people is irrelevant, while in a slightly heterogeneous network it could be an essential ingredient in avoiding an epidemic.

In the third part of the thesis we study an environmental network devised to simulate an heterogeneous territory distributed in several landscape units, that are regions whose borders are identified by natural or anthropic barriers. The state of each landscape unit is described by the percentage of high quality green areas and by the bio-energy; they depend on several environmental parameters. Each landscape unit is represented by a node of the graph, while the interaction between them is simulated using weighted directed arcs, that mimic the capability of transmission of bio-energy. The interaction between landscape units has the same mathematical structure as the electrical coupling in neural networks. The equilibria of the isolated landscape unit and their stability properties are analysed in terms of two bifurcation parameters. In order to study the equilibria of the environmental network a proper reduced model is considered. Its equilibria and their stability properties are analysed by means of four bifurcation parameters, with the aim of obtaining information about the robustness of the environmental system under strong perturbations due to human land uses impact or to natural events.

Riassunto

Questa tesi tratta sistemi complessi in ambito epidemiologico ed ambientale, utilizzando tecniche di controllo ottimo e analisi qualitativa dei sistemi dinamici per fornire indicazioni sull'evoluzione dei sistemi.

Nella prima parte della tesi viene studiato un problema di controllo ottimo di tipo *time-optimal* applicato a modelli epidemiologici di tipo SIR, considerando quattro possibili politiche di controllo dell'epidemia: vaccinazione, isolamento, abbattimento non selettivo e interventi per la riduzione della trasmissione dell'infezione. L'obiettivo dello studio è determinare per ogni politica la strategia (cioè la funzione) di controllo che minimizza il tempo di eradicazione della malattia. Sfruttando la teoria di Pontryagin, viene dimostrata l'esistenza di una soluzione del problema di controllo a tempo ottimo per le quattro politiche di controllo dell'epidemia. Inoltre, si dimostra che il controllo ottimo è di tipo bang-bang, ossia la strategia ottimale che minimizza la durata dell'epidemia può essere l'applicazione della politica di controllo all'insorgere dell'infezione, oppure l'intervento ritardato di una certa quantità di tempo, che può essere anche consistente. Dai risultati ottenuti, si può osservare che, in varie configurazioni dei parametri, applicare il controllo al massimo delle sue potenzialità per l'intera durata dell'epidemia può allungarne il decorso e che in alcuni casi la strategia che minimizza la durata di un'infezione non corrisponde a quella che minimizza il numero di individui che vengono infettati, e viceversa.

Il resto della tesi riguarda lo studio di modelli su network.

Nella seconda parte della tesi viene considerato un modello epidemiologico definito su grafo, costruito per simulare la diffusione di un'epidemia all'interno di una città densamente popolata. I nodi del grafo rappresentano i quartieri della città, mentre gli archi diretti e pesati descrivono la frazione di popolazione di un dato quartiere che giornalmente si sposta verso un altro quartiere per motivi di studio o di lavoro. La dinamica di infezione all'interno di ciascun quartiere è descritta da un modello epidemiologico di tipo SIR generalizzato proposto da Capasso e Serio nel 1973, in modo da poter includere nel modello la risposta psicologica della popolazione ad un forte aumento del numero degli infetti. Per analizzare la diffusione dell'epidemia viene definito il numero riproduttivo di base specifico di questo modello epidemiologico su grafo: se il suo valore supera la soglia critica 1 allora si avrà diffusione dell'epidemia, in caso contrario si estinguerà monotonicamente. In questa tesi sono stati considerati due particolari tipi di modelli epidemiologici definiti su grafo: il caso di network omogeneo (in cui ogni nodo presenta gli stessi parametri epidemiologici)

e un particolare caso di network eterogeneo. Nel primo caso si osserva che, indipendentemente dalla geometria del grafo, esiste una soglia critica al di sopra della quale si ha diffusione della malattia, mentre al di sotto si ha estinzione monotona. Nel secondo caso invece la diffusione dell'epidemia è fortemente influenzata dai flussi di persone tra i quartieri.

Nella terza parte della tesi è stato analizzato un sistema complesso definito su un grafo, messo a punto per descrivere l'evoluzione di un sistema ambientale. Il sistema ambientale viene suddiviso in unità territoriali, che sono porzioni di territorio i cui confini sono delimitati da barriere naturali o antropiche. Ogni nodo del grafo rappresenta un'unità territoriale, il cui stato è descritto dalla percentuale di aree verdi di buona qualità e dal valore di bio-energia, mentre la loro dinamica dipende da alcuni parametri territoriali. L'interazione tra le unità territoriali è modellizzata tramite un arco diretto e pesato in cui il peso descrive la facilità di scambio di bio-energia tra le diverse unità, e viene descritto analiticamente mediante un termine di accoppiamento di tipo "elettrico", analogo a quello usato nel campo delle reti neurali. L'obiettivo dello studio è determinare gli equilibri del sistema complesso e la loro stabilità, per valutare la "resistenza" di un equilibrio del sistema a forti perturbazioni dovute a eventi naturali o all'intervento umano. Inizialmente sono stati individuati e studiati gli equilibri della singola unità territoriale al variare di due parametri. Per lo studio del sistema complesso si è dimostrato che non sono presenti attrattori periodici o caotici, ma il sistema tende sempre ad un equilibrio. Successivamente, per lo studio degli equilibri, è stato costruito un opportuno modello ridotto. Su questo modello ridotto è stata condotta un'analisi teorica degli equilibri e della loro stabilità al variare di quattro parametri del sistema. Successivamente i risultati dell'analisi qualitativa effettuata sono stati testati su un esempio reale, relativo ad un sistema ambientale nella provincia nord di Torino.

Contents

Introduction 1

1 Preliminaries 5
1.1 Pontryagin's theory 5
1.2 Networks of dynamical systems and graph theory 8
Directed graphs 8
Weighted graphs 9

Part I Time-optimal control problem applied to SIR model

2 Introduction 13

3 Theoretical and numerical study 17
3.1 Optimal control problem: general setting 17
3.1.1 Eradication time 19
3.2 Admissible control strategies 21
3.3 Existence of an optimal control 23
3.4 Numerical method 26
3.5 Linear term policies 27
3.5.1 Vaccination 29
3.5.2 Isolation 33
3.5.3 Culling 35
3.6 Reduction of transmission policy 35

4 Discussion and conclusions 41
4.1 Perspectives 44

Part II Capasso-Serio epidemic model applied to a network

5 Introduction 49

6 The Capasso-Serio epidemic model on a network 55
6.1 The model 55
6.2 The basic reproduction number 58

7 The analytical study 63
7.1 Homogeneous epidemic network models 64
7.2 Heterogeneous fully connected epidemic network models with constant fluxes 66
7.2.1 Conditions for stability 67
7.2.2 The case $\zeta < 1/\mathcal{R}_0^{hom}$ 70
7.2.3 The case $\zeta > 1/\mathcal{R}_0^{hom}$ 71

8 Discussion and conclusions 75

Part III A network landscape model: stability analysis and numerical tests

9 Introduction 81

10 The network landscape model 85

11 Theoretical and numerical study 89
11.1 Equilibria and stability properties: the case of a single LU 89
11.2 A preliminary analysis of network dynamics 94
11.2.1 The simplified system 95
11.2.2 Equilibria and their asymptotic stability 96
11.2.3 Stability regions 99
11.3 Application to a case study in Northern Italy 101

12 Discussion and Conclusions 109

References

List of Figures

3.1 Schematization of the four types of admissible optimal control 23
3.2 Switching function and adjoint variables for an optimal vaccination problem with delayed control 31
3.3 Optimal vaccination problem 32
3.4 Optimal isolation problem 34
3.5 Optimal culling problem 36
3.6 Optimal reduction of transmission problem 38

11.1 Existence and stability regions of the equilibria of the single landscape model (SLM) 92
11.2 Bifurcation diagrams for the single lanscape model (SLM) 93
11.3 Existence and stability regions of the equilibria of the simplified model 102
11.4 Time evolution of the solutions of SLM and NLM relevant to Turin Province 106
11.5 Trajectories relevant to Turin Province for the SLM, NLM and simplified model 107
11.6 Position in the parameters planes of Turin Province LUs 108

List of Tables

11.1 Data of the landscapes in the considered environmental system. 103
11.2 Geometric parameters and connectivity indices that describe the interaction between the LUs. 103

Introduction

Mathematical modelling has become an important tool for predicting the evolution of real systems in different fields: biological and chemical systems, disease transmission [71], landscape ecology [73], neural networks, social phenomena, Internet, technological and transportation infrastructures [12]. These models are created with the aim of both understanding the essential underlying mechanisms and calibrating the response to these dynamics in order to control or improve them.

There is an astonishing number and variety of models and explanations for the spread and cause of epidemic outbreaks [3, 4, 8, 26, 30, 45, 47, 71]. The reason is that epidemiological models are useful experimental tools for building and testing theories, assessing quantitative conjectures, answering specific questions, determining sensitivities to changes in parameter values, and estimating key parameters in a field where data on human-to-human contacts are rare, often incomplete and complicated by many factors not of direct interest. Moreover, they allow to do "experiments" in a field where real experiments are impossible or unethical. Understanding the transmission characteristics of infectious diseases in communities, regions, and countries can lead to better approaches to decrease their spreading. Mathematical models are used in comparing, planning, evaluating, and optimizing various detection, prevention, therapy, and control programs [46].

In the first part of the thesis we model outbreaks of infectious diseases in domestic animals considering a controlled SIR epidemiological model. The emergence and re-emergence of infectious diseases represent a major threat to public health and may cause heavy economic and social losses. Recent epidemics of Ebola in West Africa and MERS-CoV in South Korea highlighted once again the requirement for strong public health interventions for fast disease eradication [32, 61]. Also outbreaks of infectious diseases in domestic animals may cause significant consequences for both the sustainability of the livestock industry and the costs associated to disease surveil-

lance, control, and eradication. Moreover, the economic burdens imposed by livestock diseases exceed the agricultural compartment, by affecting also commerce, tourism, and even human health in the infected areas. Consequently, minimizing the time period needed for outbreaks eradication in the affected areas represents a public health priority. In our study, in order to minimize outbreaks eradication, we focus on four different control policies: prophylactic vaccination, isolation, non-selective culling and reduction of transmission controls. The evolution of the epidemic described by a SIR model, even if uncontrolled, is well known: in some amount of time the disease will disappear. Obviously, we are not interested in modifying the evolution of the dynamical system. Instead, we are interested in minimizing the eradication time. In this thesis, we prove that for each policy the optimal strategy that minimizes the epidemic duration is to apply the control at the maximum rate until the eradication of the disease, possibly delaying the control action some amount of time. This type of control is called bang-bang control with at most one switch from no control to maximum rate control. This result is obtained by applying the Pontryagin's Maximum Principle (PMP), which is a classical result from optimal control theory that provides a necessary condition that must be satisfied by an optimal solution. We observe that this result is in contrast with previous findings on the unconstrained problems of minimizing the total infectious burden over an outbreak, where the optimal strategy is to use the maximal control for the entire epidemic. Then, the critical consequence of our results is that, in a wide range of epidemiological circumstances, it may be impossible to minimize the total infectious burden while minimizing the epidemic duration, and vice versa.
To complete the analytical study, we perform an extensive numerical study with a simple ad-hoc numerical method, exploring the solution of the optimal control problem on a wide range of parameter settings describing different epidemiological conditions, different possible control efforts and different number of initially introduced infected individuals in the population. The numerical simulations show that in some cases the optimal control can be delayed also when the control reproduction number is lower than one and that the optimal implementation of the control can even occur after the peak of infection has been reached. Our results are especially important for livestock diseases where the minimization of outbreaks duration is a priority due to sanitary restrictions imposed to farms during ongoing epidemics, such as animal movements and export bans, that cause a huge economic impact.

In the second part of the thesis we consider a human-to-human disease which is supposed to spread in a highly populated city and which is modelled by means of an epidemic network model. As said before, there is a huge amount of epidemic models. In this part of the thesis, we choose the generalized model by Capasso and Serio,

which combines simplicity to flexibility – since the incidence function must satisfy some constraints, but is not specified – and also a smidgen of realism, taking into account psychological effects that can arise if a significant part of the city is infected. We want to introduce and quantify spatial effet, focusing on the impact of daily-routine human mobility and heterogeneity of epidemiological parameters on the occurrence of an epidemic outbreak. Metapopulation models are commonly used to describe the dynamics of an epidemic in heterogeneous environment [5, 57]. We choose to partition the city into neighbourhoods, containing many hundreds or thousands of people. This seems reasonable, if we want to focus on daily-routine human mobility. Moreover, this scale allows tu collect enough data both for the neighbourhoods parameters and for the mobility data, which can be obtained from road traffic studies and public transportation companies. Mathematically, we model the city structure by identifying the nodes of a graph with the neighbourhoods of the city, and using directed weighted edges to represent the fraction of people moving from one neighbourhood to another due to their daily routine activities. Then, the equations of the model are obtained starting from the Capasso-Serio model and taking into account the influence of the infected individuals that come from other districts.
We define the basic reproduction number for our epidemiological network and perform an analytical study for two particular network and parameters configurations, in order to analyse the stability of the disease free equilibrium, and hence the potential outbreak of the disease. First we consider an homogeneous (with respect to the epidemiological parameters) network and prove that, in this framework, mobility of people between neighbourhoods is irrelevant. Then we consider a slightly heterogeneous network, where a node of the network has different epidemiological parameters from other nodes. This latter case might represent different behaviours of the population in different neighbourhoods, due to different social status or wealth; it could also model a vector-diffusion disease, such as dengue fever, where mosquitoes are considered as a background and humans act like vectors between localized mosquitoes populations [85]. In case of slightly heterogeneous network, we prove that human mobility might be an essential ingredient in avoiding, or facilitating, the epidemic outbreak.

Another recent field of application of mathematical modelling is the Landscape Ecology, which focuses on the problem of a quantitative evaluation of an environment, aiming at managing and planning the territory through government, conservation and protection of landscapes. In this context, in the third part of the thesis we investigate an environmental network devised to simulate an heterogeneous territory distributed in several landscape units, that are regions whose borders are identified by natural or anthropic barriers. Our purpose is to study the long term evolution of

the system in order to achieve informations about the robustness of the environment under strong perturbations due to human land uses impact and to natural events. To do this, we construct a network of dynamical systems that describes the evolution in time and in space of an environmental system and we determine the equilibria and their stability properties. We describe the state of each landscape unit by the percentage of high quality green areas and by the bio-energy value; they depend on several environmental parameters, such as solar exposure, relative humidity or presence of built-up areas. The territory is partitioned in several landscape units, which are considered as nodes of the graph underlying the environmental network. Then, the interaction between landscape units is described by a coupling linear term that has the same mathematical structure as the electrical coupling in neural networks. Moreover, all the coupling information are contained in the weight matrix relevant to the graph underlying the environmental network.
First, we perform a stability analysis of the isolated landscape unit by means of two bifurcation parameters, detecting general conditions for the number of equilibria, for their existence and stability. Then, in order to study the equilibria of the complex network, a proper reduced model is considered. Its equilibria and their stability properties are analysed; their dynamics are completely determined in terms of four bifurcation parameters. We also show some numerical tests relevant to an environmental system of the northern side of the Turin Province (Italy). The obtained results are compared with those of the simplified system and of the isolated landscape unit, in order to underline how the coupling between the ecological sectors may modify the scenarios, thanks to the exchange of bio-energy, and also underlying how the simplified system is able to give information about the asymptotic behaviour of the network model, in accordance with the stability analysis performed.

The final pages of this thesis present the publications coauthored by the candidate and the list of presented talks and posters.

1

Preliminaries

This Chapter introduces some basic concepts on Pontryagin's theory and network of dynamical systems that are used in this thesis.

First we present the theory of the Pontryagin's Maximum Principle (PMP), which is a classical result in Optimal Control theory. For this argument, we follow the notation of the notes [22]. Then, we introduce the general concept of graph and the definition of network of dynamical systems (or complex system), following the notation used in the review article by Boccaletti et al.[12].

1.1 Pontryagin's theory

After more than three hundred years of evolution, optimal control theory has been formulated as an extension of the calculus of variations. The Pontryagin's Maximum Principle (PMP) [78] is a classical result in Optimal Control theory which provides a necessary condition that must be satisfied by a solution to be optimal. There are various versions of PMP for problem statements of varying generality, depending con the considered constraints such as conditions at the boundary or path constraints. We present a version that is suitable for the types of problems discussed in this thesis; for more general versions see [11, 22, 36]. We want to remark that however, despite the PMP being a fundamental tool, optimal control theory is by no means complete, especially when it comes to the question whether an optimal control exists for a given problem.

Let $[t_0, t_f] \subset \mathbb{R}$ and $\boldsymbol{u} : [t_0, t_f] \to U$ be a piecewise continuous function, where U is a bounded subset of $\mathbb{R}^m$. Suppose that $\boldsymbol{x} : [t_0, t_f] \to \mathbb{R}^n$ is the solution of the autonomous system of ordinary differential equations

$$\dot{\boldsymbol{x}}(t) = F(\boldsymbol{x}(t), \boldsymbol{u}(t)); \quad \boldsymbol{x}(t_0) = \boldsymbol{x}_0,$$

where $F : \mathbb{R}^n \times U \to \mathbb{R}^n$ is continuous in the variable $\boldsymbol{u}$ and continuously differentiable on $\mathbb{R}^n$.

We will denote $\boldsymbol{u}(t)$ the *control* applied at time t and $\boldsymbol{x}(t)$ the *system trajectory* (or state, or response) corresponding to control $\boldsymbol{u}$ and initial condition $\boldsymbol{x}_0$. Notice that in order to define a system trajectory a corresponding control and initial condition must be specified.

Given function $\ell : \mathbb{R}^n \times U \to \mathbb{R}$ that is continuous on U and continuously differentiable on $\mathbb{R}^n$ we define the *cost functional*

$$J(\boldsymbol{x}, \boldsymbol{u}, t_0, t_f) = \int_{t_0}^{t_f} \ell(\boldsymbol{x}(t), \boldsymbol{u}(t))dt.$$

Roughly speaking, the goal is then to find a control $\boldsymbol{u}$ that minimizes J, along with the corresponding $\boldsymbol{x}$, t_0 and t_f. There are different variations of this problem depending on the specific constraints placed on t_0, t_f, $\boldsymbol{x}(t_0)$ and $\boldsymbol{x}(t_f)$.

In our specific framework, the initial time t_0 and the initial condition $\boldsymbol{x}(t_0)$ are given, while the terminal time t_f is free. We require also that the final condition $\boldsymbol{x}(t_f)$ belongs to a certain smooth manifold X_f (target set) of dimension $n_f \leq n$.

Before stating the Pontryagin's Maximum Principle, some notation is needed.

Definition 1.1 (The extended problem). *For a given control $\boldsymbol{u}$ and the corresponding trajectory $\boldsymbol{x}$ we define the* dynamic cost variable

$$c(t) = \int_{t_0}^{t} \ell(\boldsymbol{x}(\tau), \boldsymbol{u}(\tau))d\tau.$$

Then we can consider the extended trajectory $\tilde{\boldsymbol{x}}(t)^\mathsf{T} = (c(t), \boldsymbol{x}(t)^\mathsf{T})^\mathsf{T}$ *and the* extended system $\tilde{F}(\boldsymbol{x}, \boldsymbol{u})^\mathsf{T} = (\ell(\boldsymbol{x}, \boldsymbol{u}), F(\boldsymbol{x}, \boldsymbol{u})^\mathsf{T})^\mathsf{T}$. *Then we have to find a control $\boldsymbol{u}$ and a final time t_f such that the $(n+1)$-dimensional solution of*

$$\dot{\tilde{\boldsymbol{x}}}(t) = \tilde{F}(\boldsymbol{x}(t), \boldsymbol{u}(t)), \qquad \tilde{\boldsymbol{x}}(t_0) = \begin{pmatrix} 0 \\ \boldsymbol{x}_0 \end{pmatrix},$$

terminates at

$$\begin{pmatrix} c(t_f) \\ \boldsymbol{x}_f \end{pmatrix},$$

where $\boldsymbol{x}_f \in X_f$ and $c(t_f)$ taking the least possible value.

The following result gives a necessary condition for a control to be optimal. This of course does not guarantee the existence of the optimal control, but if it exists then it belongs to the class of functions that satisfies the Pontryagin's Maximum Principle. Sufficient conditions and existence results are more difficult to obtain and are typically more case-specific [22].

Theorem 1.2 (Pontryagin's Maximum Principle for autonomous problems with free terminal time and terminal target set).
Consider the optimal control problem

$$\begin{aligned} \textit{minimize:} \quad & J(\boldsymbol{u}, t_f) = \int_{t_0}^{t_f} \ell(\boldsymbol{x}(t), \boldsymbol{u}(t)) dt \\ \textit{subject to:} \quad & \dot{\boldsymbol{x}}(t) = F(\boldsymbol{x}(t), \boldsymbol{u}(t)), \quad t \geq 0; \\ & \boldsymbol{x}(t_0) = \boldsymbol{x}_0, \quad \boldsymbol{x}(t_f) \in X_f \\ & \boldsymbol{u} : [t_0, t_f] \to U \textit{ piecewise continuous}, \end{aligned}$$

with fixed initial time t_0 and free terminal time t_f and where the target set X_f is a smooth manifold of dimension $n_f \leq n$. Let ℓ and F be continuous in $(\boldsymbol{x}, \boldsymbol{u})$ and have continuous first partial derivatives with respect to $\boldsymbol{x}$, for all $(\boldsymbol{x}, \boldsymbol{u}) \in \mathbb{R}^n \times \mathbb{R}^m$. Suppose that $\boldsymbol{u}^*$ and t_f^* are minimizer for the problem and let $\tilde{\boldsymbol{x}}^*$ denote the optimal extended trajectory. Then, there exists a piecewise continuously differentiable vector function (called adjoint variable) $\tilde{\boldsymbol{\lambda}}^* = (\lambda_0, \lambda_1, \ldots, \lambda_n)^\mathsf{T} \neq (0, 0, \ldots, 0)^\mathsf{T}$ such that

$$\dot{\tilde{\boldsymbol{\lambda}}}^*(t) = -\nabla_{\tilde{\boldsymbol{x}}} \mathcal{H}(\boldsymbol{x}^*(t), \boldsymbol{u}^*(t), \tilde{\boldsymbol{\lambda}}^*(t)),$$

where

$$\mathcal{H}(\boldsymbol{x}, \boldsymbol{u}, \tilde{\boldsymbol{\lambda}}) = \tilde{\boldsymbol{\lambda}}^\mathsf{T} \tilde{F}(\boldsymbol{x}, \boldsymbol{u}).$$

Moreover:

i) for each $t_0 \leq t \leq t_f^*$, the function $\mathcal{H}(\boldsymbol{x}^*(t), \boldsymbol{w}, \tilde{\boldsymbol{\lambda}}^*(t))$ attains a minimum on U at $\boldsymbol{w} = \boldsymbol{u}^*(t)$:

$$\mathcal{H}(\boldsymbol{x}^*(t), \boldsymbol{u}^*(t), \tilde{\boldsymbol{\lambda}}^*(t)) \leq \mathcal{H}(\boldsymbol{x}^*(t), \boldsymbol{w}, \tilde{\boldsymbol{\lambda}}^*(t)), \ \forall \boldsymbol{w} \in U$$

ii) for each $t_0 \leq t \leq t_f$:

$$\begin{aligned} \lambda_0^*(t) &= \textit{const.} \geq 0 \\ \mathcal{H}(\boldsymbol{x}^*(t), \boldsymbol{u}^*(t), \tilde{\boldsymbol{\lambda}}^*(t)) &= 0 \end{aligned}$$

iii) at the optimal final time $\boldsymbol{\lambda}^*(t_f^*)$ *is orthogonal to the tangent plane of* X_f *at* $\boldsymbol{x}^*(t_f^*)$, $\mathcal{T}(\boldsymbol{x}^*(t_f^*))$*:*

$$\boldsymbol{\lambda}^*(t_f^*)^\mathsf{T}\boldsymbol{d} = 0, \quad \forall \boldsymbol{d} \in \mathcal{T}(\boldsymbol{x}^*(t_f^*)).$$

Note that if $\lambda_0(t_f) = 0$, then the necessary conditions of optimality become independent on the cost functional. This is called the *abnormal case*. On the contrary, if $\lambda_0(t_f) > 0$, then this is known as the *normal case* and it is common practice to normalize the adjoint vector $\tilde{\boldsymbol{\lambda}}$ by taking $\lambda_0(t) = 1$, $t_0 \leq t \leq t_f$.

1.2 Networks of dynamical systems and graph theory

Many systems in nature and in technology can be seen as a large number of highly interconnected dynamical units. Typical examples include large communication systems (the Internet, the telephone network, the World Wide Web), transportation infrastructures (rail-road and airline routes), biological systems (gene and protein interaction networks, neural networks), and a variety of social interaction structures. A possible approach to capture the global properties of such systems is to model them as graphs whose nodes represent the dynamical units (for instance the neurons in the brain or the individuals in a social system) and the links stand for the interactions between the units. Of course, this is a very strong approximation, since it means translating the interaction between two dynamical units, which is usually depending on time, space and many more other details, into simple numbers: the existence or not and the magnitude of a link between the two corresponding nodes. Nevertheless, in many cases of practical interest, such an approximation provides a simple but still very informative representation of the entire system.

Then, to define a network of dynamical system we need some rigorous definitions of graph theory.

Directed and undirected graphs

A *directed graph* $G = (\mathcal{V}, \mathcal{L})$ consists of two sets: a nonempty set $\mathcal{V} = \{1, 2, \ldots, M\}$ and $\mathcal{L}$, that is a set of ordered pairs of elements of $\mathcal{V}$. The elements of the first set are the *nodes* of the graph, while the elements of $\mathcal{L}$ are its *links*. The couple (i, j), that represents a link from node i to node j, is denoted by $i \to j$. In our definition we do not allow multiple edges (couples of nodes connected by more than one link). Two nodes are *adjacent* if there exist a link between them.

It is often useful to consider a matricial representation of a graph. A graph G can be completely described by giving the *adjacency* (or connectivity) matrix A, a

$M \times M$ square matrix whose entry a_{ij} $(i, j = 1, \ldots, M)$ is equal to 1 when the link $i \to j$ exists, and zero otherwise.

Two important quantities in directed graphs are the out-degree of the node i

$$k_i^{out} = \sum_{j=1}^{M} a_{ij},$$

that represents the number of out-going links from node i, and the in-degree

$$k_i^{in} = \sum_{j=1}^{M} a_{ji},$$

which analogously represents the number of in-going links to node i.

We further note that an *undirected graph* can be seen as a directed graph where the adjacency matrix is symmetric.

Weighted graphs

Typically, pair of nodes of a real network are connected with different intensity. Then it is convenient to describe them using a *directed weighted graph* $G = (\mathcal{V}, \mathcal{L}, \mathcal{W})$ consisting of three sets: the sets of nodes $\mathcal{V}$ and and links $\mathcal{L}$, as in the simple directed graph, and the set of weights $\mathcal{W}$ that are real numbers, one for each link. In this context, instead of being described by the adjacency matrix, G is completely determined by the *weights matrix* W whose entry w_{ij} is the weight related to the link $i \to j$ and, of course, $w_{ij} = 0$ if there is no link between the two nodes. For weighted graphs we allow w_{ii} to be different from zero.

The corresponding quantities of in and out-degrees are the out-strength of node i

$$s_i^{out} = \sum_{j=1}^{M} w_{ij},$$

and the in-strength of node i

$$s_i^{in} = \sum_{j=1}^{M} w_{ji}.$$

Networks of dynamical systems

A network of dynamical systems is a system of ordinary differential equations that describes the evolution in time of M units (individuals, cities, neurons, ...) that

interact and influence each other. Each unit is represented by a node of the graph, whose state at time t is represented by a vector $\boldsymbol{x}(t) \in \mathbb{R}^d$, while the links (that we suppose without loss of generality directed and weighted) mimic the interaction between different parts. The network of dynamical systems will then be represented by a system of dM ordinary differential equations:

$$\begin{cases} \dot{\boldsymbol{x}}_i = \boldsymbol{F}_i(\boldsymbol{x}_i) + \boldsymbol{H}_i(\boldsymbol{x}_1, \ldots, \boldsymbol{x}_M; W) \\ i = 1, \ldots, M, \end{cases}$$

where $\dot{\boldsymbol{x}}_i = \boldsymbol{F}_i(\boldsymbol{x}_i)$ are the vector dynamics of the node i when isolated from the others, whereas the term $\boldsymbol{H}_i$ describes the interaction of the i-th unit with the others and, thus, $\boldsymbol{H}_i$ depends on all the state variables of the system and on the magnitude of the pairwise interactions, that are described by the elements of the weights matrix W.

Part I

Time-optimal control problem applied to SIR model

2

Introduction

The emergence and re-emergence of infectious diseases represent a major threat to public health and may cause heavy economic and social losses. Recent epidemics of Ebola in West Africa and MERS-CoV in South Korea highlighted once again the requirement for strong public health interventions for fast disease eradication [32, 61].

In a similar way, outbreaks of infectious diseases in domestic animals may cause significant consequences for both the sustainability of the livestock industry and the costs associated to disease surveillance, control, and eradication. Moreover, the economic burdens imposed by livestock diseases exceed the agricultural compartment, by affecting also commerce, tourism, and even human health in the infected areas. Consequently, minimizing the time period needed for outbreaks eradication in the affected areas represents a public health priority.

There exist several examples of livestock epidemics causing huge sanitary and economic impacts, such as the 1996 epidemic of classical swine fever in The Netherlands [68], the 2001 epidemic of foot-and-mouth in the UK [28], and the 2015 epidemic of high pathogenic avian influenza in Midwestern USA [52]. From the epidemiological point of view, the main indicators generally used to describe the severity of these infection events in livestock are: (*i*) the total number of infected animals and farms during an epidemic, and (*ii*) the duration of the epidemic. The rationale behind these indicators is based on the evidence that epidemic surveillance and control costs are directly related to spatial and temporal extension of the epidemic events [50]. Furthermore, the effect of the epidemic duration on the socio-economic burdens associated to livestock diseases is larger than in human diseases. This is due to the sanitary restrictions imposed to farms in infected areas during ongoing outbreaks, such as animal movement and export bans. Moreover, the block or the restriction of farm activities can go over the time of infection, carrying on until the disease-free status is formally regained [51]. Examples of costly restrictions for the livestock in-

dustry include: the export ban of UK cattle because of the 1996 bovine spongiform encephalopathy epidemic [40] and the export ban of poultry and poultry related products in Hong Kong, Laos, Thailand, and The Netherlands due to outbreaks of highly pathogenic avian influenza [60, 74, 75].

By using a stochastic modelling framework for classical swine fever in The Netherlands pig farms, Mangen et al. [66] showed that the increase of the epidemic duration affects the sanitary costs associated to disease outbreaks more than a proportional growth in the number of infected farms. This prediction followed from the observation that longer epidemics are more widespread, involving a larger number of animals slaughtered. The estimate of the epidemic duration appears almost invariably in the simulation outputs of data-driven mathematical models developed to evaluate the effectiveness and the efficiency of surveillance and control policies for several infections in livestock, such as foot-and-mouth disease [80], classical swine fever [33], bovine tuberculosis [81], and avian influenza [64]. However, few attempts have been made to address the problem of minimizing the epidemic duration from a theoretical point of view by using optimal control theory. To our knowledge, the only example of analytic characterization of the control function in a time-optimal framework is due to Jiang [55], who focused on the analysis of isolation strategies in a subsystem of the model proposed in Zhang et al. [90] to describe SARS spread. On the other hand, the optimal control theory has been widely applied to solve the problem of minimizing the total number of infected individuals (or the total infectious burden) in basic SIR (Susceptible-Infected-Recovered) epidemic models by means of different control policies, such as: the implementation of emergency prophylactic vaccination plans, the isolation of infected individuals, the reduction of disease transmission through the limitation of contacts between individuals, and non-selective culling [1, 2, 9, 17, 44, 69, 88].

Prophylactic vaccination consists in the vaccination of susceptible individuals; its goal is to prevent the development of diseases. Isolation consists in the quarantine of infected individuals. As regards livestock diseases, in SIR models isolation is mathematically equivalent to removal of infected individuals through test-and-cull procedures. Non-selective culling consists in the slaughtering of both infected and healthy individuals and it is usually implemented in wildlife and livestock when no other options are available (e.g. no diagnostic tests available, lack of time or resources). The rationale for culling healthy individuals resides in the positive relationship between the rate at which individuals become infected and the abundance of susceptible individuals. Among humans, the reduction of transmission can be obtained through information campaigns or emergency movement bans (e.g. school closures, flight lim-

itations), while in livestock it can be obtained by imposing limitations on animal, vehicle, and personnel movements among farms.

Those cited studies solved the optimal control problem for the minimization of the infectious burden in unconstrained conditions (i.e. without costs of control or resource limitations). They showed that the optimal strategy always relies in the adoption of the maximum control for the entire epidemic. In this context, maximum control is intended as the implementation of the control policy at its maximum available rate.

In this Part[1] of the thesis we consider a controlled SIR epidemiological model, focusing on four different control policies: prophylactic vaccination, isolation, non-selective culling or reduction of transmission controls. We thoroughly investigate the problem of minimizing the epidemic duration both with theoretical and numerical tools. In particular, for each policy, we investigate the optimal control strategy that minimizes the epidemic duration, proving that the optimal strategy is to apply the control at the maximum rate until the eradication of the disease, possibly delaying the control action some amount of time. To complete the analytical study, we perform an extensive numerical study, exploring the solution of the optimal control problem on a wide range of parameter settings describing different epidemiological conditions, different possible control efforts and different number of initially introduced infected individuals in the population. The numerical simulations show that the optimal control can be delayed also when the control reproduction number is lower than one and that the optimal implementation of the control can even occur after the peak of infection has been reached. Consequently, our results lead to the conclusion that: (*i*) using the maximum control for the entire epidemic duration may not be the optimal strategy (even in unconstrained conditions); and (*ii*) minimizing the epidemic duration does not always imply minimizing the total infectious burden, and vice versa.

This Part is organized as follows. In Section 3.1 the basic assumptions and the equations of the time-optimal epidemiological control model are presented. In Sections 3.2 and 3.3 we present theoretical results regarding the particular type of admissible controls and the proof of the existence of a solution for the optimal control problem, respectively. In Section 3.4 we describe the numerical method; results of the simulations and proofs of the optimal control strategy for the choosen policies are included in Sections 3.5 and 3.6. Finally, in Chapter 4 we include some concluding remarks and work perspectives.

[1] Most of the contents of this Part appears on arXiv:1706.04447 [math.OC], revised version submitted to *Mathematical Biosciences* in April 2017 [13]

3

Theoretical and numerical study

3.1 Optimal control problem: general setting

We describe the evolution of the infection in a host population with a standard deterministic SIR model. The classical theoretical papers on epidemic models by Kermack and McKendrick [58, 59] have had a major influence in the development of mathematical models and they are still relevant in many situations. In particular, the authors introduced a simple deterministic model, the SIR model, where the population is divided into three compartments:

- the susceptibles (S), i.e. the class of individuals who can catch the disease and become infective,
- the infectives (I) who have the disease and can transmit it to other susceptible individuals,
- the removed class (R) which includes the individuals who do not catch or transmit the disease any more, such as dead or recovered (thus immunized) individuals.

Their evolution in time is described by the differential system of equations:

$$\begin{cases} \dot{S} = -\beta SI \\ \dot{I} = \beta SI - \mu I \\ \dot{R} = \mu I, \end{cases} \tag{3.1}$$

where β is the transmission rate of the infection and μ represents the loss rate of infected individuals through both mortality and recovery. The SIR model ignores almost every detail of a real epidemic, such as incubation, demographic and social structure of the population and spatial distribution of the individuals. Conversely, it assumes that the population is uniformly mixed, namely that each individual has the

same probability to get in contact with another one. The interaction term between susceptible and infected individuals is therefore a mass action term proportional to a constant parameter, β. The model neglects also birth and natural death phenomena, since the time scale progress of the epidemic is considered much more shorter than lifetime, leading to a constant population in time. If we supplement the model with a set of initial conditions

$$S(0) = S_0 \geq 0 \quad I(0) = I_0 \geq 0 \quad R(0) = 0, \tag{3.2}$$

one can prove that the Cauchy problem (3.1)-(3.2) has a unique solution, which is a global solution on $\mathbb{R}_+$ and always positive. The dynamical system admits an infinite number of equilibrium points [71], which are characterized by the I component equal to zero; their stability depends on the value of the S component: the equilibrium is stable if $S < \mu/\beta$, unstable otherwise.

It is easy to prove that the total population $N(t) = S(t) + I(t) + R(t)$ is constant in time, since from (3.1) $\dot{N} = 0$. Therefore, we can focus on the dynamics of susceptibles and infected individuals only, and then obtain the removed ones from $R(t) = N - S(t) - I(t)$.

We will then consider the following system of two ordinary differential equations (ODEs):

$$\begin{cases} \dot{S} = f_1(S, I) = -\beta SI \\ \dot{I} = f_2(S, I) = \beta SI - \mu I \end{cases}. \tag{3.3}$$

If we denote by $\boldsymbol{x}(t) = (S(t), I(t))^\mathsf{T}$ the column vector that describes the state of the system at time t, we can rewrite system (3.3) in the more compact form $\dot{\boldsymbol{x}} = f(\boldsymbol{x})$.

In our analysis, we consider four different control policies, namely: vaccination, isolation, culling, and reduction of transmission. We denote the generic control policy rate applied at time t by $u(t)$, which is assumed to be a piecewise continuous function that takes values in a positive bounded set $U = [0, u^{max}]$. We apply the different policies separately by adding a linear term in the control variable $u(t)$ to model (3.3), namely considering the general system

$$\dot{\boldsymbol{x}}(t) = f(\boldsymbol{x}(t)) + u(t)g(\boldsymbol{x}(t)), \tag{3.4}$$

where the function g depends on the chosen control policy. Specifically, we define a general linear term policy

$$g_l(\boldsymbol{x}) = \begin{pmatrix} -\alpha_1 S \\ -\alpha_2 I \end{pmatrix} \tag{3.5}$$

which is a linear function of S and I that allows to model

$$\text{Vaccination} \qquad \alpha_1 = 1, \alpha_2 = 0 : \qquad g_v(\boldsymbol{x}) = \begin{pmatrix} -S \\ 0 \end{pmatrix} \tag{3.6}$$

$$\text{Isolation} \qquad \alpha_1 = 0, \alpha_2 = 1 : \qquad g_i(\boldsymbol{x}) = \begin{pmatrix} 0 \\ -I \end{pmatrix} \tag{3.7}$$

$$\text{Culling} \qquad \alpha_1 = 1, \alpha_2 = 1 : \qquad g_c(\boldsymbol{x}) = \begin{pmatrix} -S \\ -I \end{pmatrix} \tag{3.8}$$

and, in addition, we consider the nonlinear term policy

$$\text{Reduction of transmission} \qquad g_r(\boldsymbol{x}) = \begin{pmatrix} \beta SI \\ -\beta SI \end{pmatrix}. \tag{3.9}$$

We define the *basic reproduction number* for model (3.3) as $\mathcal{R}_0 = \beta S(0)/\mu$, which represents the average number of secondary infections produced by a single infected individual in a completely susceptible population in the absence of control [3]. In addition, for each policy we will define the *control reproduction number* $\mathcal{R}_C$ that represents the average number of secondary infections produced by a single infected individual in a completely susceptible population with control measures in place [19]. From this definition, it follows that, when $\mathcal{R}_C < 1$, control measures applied at the beginning of the epidemic are able to immediately reduce the number of the infected individuals (i.e. $\dot{I}(0) < 0$).

3.1.1 Eradication time

The target will be the minimization of the eradication time of the infection.

Definition 3.1 (Eradication Time)**.** *The eradication time T of the controlled SIR problem (3.4) is the first time at which the number of infected individuals reaches the threshold ε from above, where $\varepsilon < 1$ is a fixed positive constant.*

Existence of the eradication time in problem (3.4) is guaranteed by the following results.

Remark 1. If we consider non-negative initial data $S(0)$ and $I(0)$, then the solution of the differential system (3.4) is non-negative at each time $t > 0$.

Proof. Indeed, for all the chosen policies, the I axis is a trajectory for the system; the S axis is also a trajectory (for vaccination and culling policies) or is a set of stationary points (for isolation and reduction of transmission policies).

□

Remark 2. For each $k > 0$ the set $\mathcal{Q}_k = \{S \geq 0,\, I \geq 0,\, S + I \leq k\}$ is a positively invariant trapping region.

Proof. Using results of Remark 1 it is sufficient to prove that for $S, I > 0$ the vector field evaluated on the boundary line $S+I = k$ points towards the internal part of the region $\mathcal{Q}_k$ [41]; it is straightforward for each policy since the scalar product of the vector field $f(\boldsymbol{x})$ and the outward pointing normal vector of the boundary $\hat{n} = (1,1)^\mathsf{T}$ is negative in all cases.

□

Corollary 3.2. *Given an initial condition $\boldsymbol{x}_0 = (S(0), I(0)) \in \mathbb{R}^2_+$, let $\boldsymbol{x}(t) = (S(t), I(t))$ be the solution of (3.4). Then $I(t) \to 0$ as $t \to +\infty$ for all control policies.*

Proof. By Remark 2 we know that the set $\mathcal{Q}_{N_0}$, where $N_0 = S(0)+I(0)$, is a trapping region. Moreover, in this region the function $\dot{S}(t)$ has a constant negative sign, so there cannot be periodic trajectories and all orbits must converge to a stationary point $\bar{\boldsymbol{x}} \in \mathcal{Q}_{N_0}$. It is easy to prove that the number of infected individuals of a stationary point is always zero. In fact, for the vaccination and culling policies, the only stationary point is $\bar{\boldsymbol{x}} = (0, 0)$, while for isolation and reduction of transmission policies the stationary points are all those of the S axis.

□

We will chose initial conditions of infected individuals $I(0)$ strictly greater than ε. As a consequence, T being the first time at which the variable I reaches ε, it holds that $\dot{I}(T) < 0$.

We can then write the optimal control problem [78] where the goal is:

$$\begin{aligned} \text{minimize:} \quad & J(u) = \int_0^T 1dt \quad \text{(Eradication time)} \\ \text{subject to:} \quad & \dot{\boldsymbol{x}}(t) = f(\boldsymbol{x}(t)) + u(t)g(\boldsymbol{x}(t)), \quad t \geq 0; \\ & \boldsymbol{x}(0) = \boldsymbol{x}_0, \quad \boldsymbol{x}(T) \in \mathcal{C} = \{(S, I) \,:\, I = \varepsilon\} \\ & u : [0, +\infty) \to U = [0, u^{max}] \text{ piecewise continuous,} \end{aligned} \tag{3.10}$$

where g is defined by the chosen control policy.

3.2 Admissible control strategies

Given the optimal control problem (3.10) with $f, g \in \mathcal{C}^\infty(\mathbb{R}^2)$, we apply the Pontryagin's Maximum Principle (see Section 1.1) in order to find a characterization of the optimal control strategy.

Theorem 3.3 (Pontryagin's Maximum Principle for linear time-optimal control problem). *Suppose that $u^*(t)$ is a minimizer for the optimal control problem (3.10) and let $\boldsymbol{x}^*(t) = (S^*(t), I^*(t))^\mathsf{T}$ and T^* denote the optimal solution of problem (3.4) and the optimal eradication time, respectively. Then, there exists a piecewise $\mathcal{C}^1$ vector function $\boldsymbol{\lambda}^*(t) = (\lambda_S^*(t), \lambda_I^*(t))^\mathsf{T} \neq 0$ such that*

$$\dot{\boldsymbol{\lambda}}^*(t) = -\nabla_x \mathcal{H}(\boldsymbol{x}^*(t), u^*(t), \boldsymbol{\lambda}^*(t))^\mathsf{T},$$

where the Hamiltonian is defined as $\mathcal{H}(\boldsymbol{x}, u, \boldsymbol{\lambda}) = 1 + \boldsymbol{\lambda}^\mathsf{T}(f(\boldsymbol{x}) + ug(\boldsymbol{x}))$, and:

i) the function $h(w) = \mathcal{H}(\boldsymbol{x}^*(t), w, \boldsymbol{\lambda}^*(t))$ attains its minimum on U at $w = u^*(t)$:

$$\mathcal{H}(\boldsymbol{x}^*(t), u^*(t), \boldsymbol{\lambda}^*(t)) \leq \mathcal{H}(\boldsymbol{x}^*(t), w, \boldsymbol{\lambda}^*(t)), \quad \forall w \in U$$

for every $t \in [0, T^*]$;

ii) the Hamiltonian is constant equal to zero along the optimal solution:

$$\mathcal{H}(\boldsymbol{x}^*(t), u^*(t), \boldsymbol{\lambda}^*(t)) = 0;$$

iii) the following transversality condition holds: $\lambda_S^*(T^*) = 0$.

Moreover, because the Hamiltonian is linear in the control variable, the value of $u^*(t)$ is determined by the sign of the switching function $\psi(\boldsymbol{x}, \boldsymbol{\lambda}) = \boldsymbol{\lambda}^T g(\boldsymbol{x})$ for all the time instants t at which $\psi(\boldsymbol{x}^*(t), \boldsymbol{\lambda}^*(t))$ does not vanish:

$$u^*(t) = \begin{cases} 0 & \text{if } \psi(\boldsymbol{x}^*(t), \boldsymbol{\lambda}^*(t)) > 0 \\ u^{max} & \text{if } \psi(\boldsymbol{x}^*(t), \boldsymbol{\lambda}^*(t)) < 0. \end{cases}$$

Proof. This formulation of the Theorem derives from the more general PMP given in Theorem 1.2. We omit the superscript $*$ for the optimal quantities, in order to simplify the notation.

We only take into account normal case, therefore $\lambda_0(t) = 1$ for each $t \geq 0$ and $\mathcal{H}(\boldsymbol{x}, u, \boldsymbol{\lambda}) = \lambda_0 \ell + \boldsymbol{\lambda}^\mathsf{T} F(\boldsymbol{x}, \boldsymbol{u}) = 1 + \boldsymbol{\lambda}^\mathsf{T}(f(\boldsymbol{x}) + ug(\boldsymbol{x}))$.

We prove that condition iii) of Theorem 1.2 results in a simple condition over $\lambda_S(T)$. As stated at the end of Chapter 3, the target set for our problem is defined

as $X_f = \mathcal{C} = \{(S, I) \ : \ I = \varepsilon\}$, which can be equivalently seen as the hypersurface $\chi(S, I) = 0$, with $\chi(S, I) = I - \varepsilon$. Then the tangent set is

$$\mathcal{T}(\boldsymbol{x}(T)) = \{d \in \mathbb{R}^2 \ : \ \nabla_{\boldsymbol{x}} \chi(\boldsymbol{x}(T)) d = 0\},$$

namely $\mathcal{T}(\boldsymbol{x}(T)) = \{(d_1, d_2) \in \mathbb{R}^2 \ : \ d_2 = 0\}$.

Then the transversal condition of Theorem 1.2 $\boldsymbol{\lambda}(T)^\mathsf{T} \boldsymbol{d} = 0$ simply results in $\lambda_S(T) = 0$.

Finally, we prove the last observation. Suppose that condition i) of the Theorem holds, then

$$\begin{aligned} h(u(t)) &\leq h(w) \\ \boldsymbol{\lambda}^\mathsf{T}(f(\boldsymbol{x}) + u(t) g(\boldsymbol{x})) &\leq \boldsymbol{\lambda}^\mathsf{T}(f(\boldsymbol{x}) + w g(\boldsymbol{x})) \\ u(t) \boldsymbol{\lambda}^\mathsf{T} g(\boldsymbol{x}) &\leq w \boldsymbol{\lambda}^\mathsf{T} g(\boldsymbol{x}). \end{aligned}$$

If $\boldsymbol{\lambda}^\mathsf{T} g(\boldsymbol{x})$ is positive, then condition i) reduces to $u(t) \leq w$, $\forall w \in U$ and therefore $u(t) = 0$. On the contrary, if $\boldsymbol{\lambda}^\mathsf{T} g(\boldsymbol{x})$ is negative, condition i) implies that the control assumes the maximum possible value, that is $u(t) = u^{max}$.

□

Using this result, what we will prove in Sections 3.5-3.6 can be summarized in the following Theorem.

Theorem 3.2.1. *For each considered control policy the optimal control for problem (3.10) is bang-bang. The optimal strategy consists either in a constant control $u^*(t) \equiv u^{max}$ or in a delayed control $0 \to u^{max}$ with a single switching time τ_s^*, namely $u^*(t) = 0$ for $t \in [0, \tau_s^*)$ and $u^*(t) = u^{max}$ for $t \in (\tau_s^*, T^*]$. In addition, if the optimal control is delayed, three different behaviors are allowed, depending on the position of the switching time τ_s^* compared to the peak of infection, leading to the four different types of admissible optimal control sketched in Fig. 3.1.*

We will denote the set of such admissible optimal controls by

$$\begin{aligned} \mathcal{A} = \Big\{ & u : [0, +\infty) \to \{0, u^{max}\} \text{ piecewise constant with at most} \\ & \text{one jump from 0 to } u^{max} \ , \lim_{t \to +\infty} u(t) = u^{max} \Big\}. \end{aligned} \tag{3.11}$$

We point out that, although mathematically accurate, in practical application a constant control $u(t) = u^{max}$ for $t \to +\infty$ is unrealistic. On the contrary, we

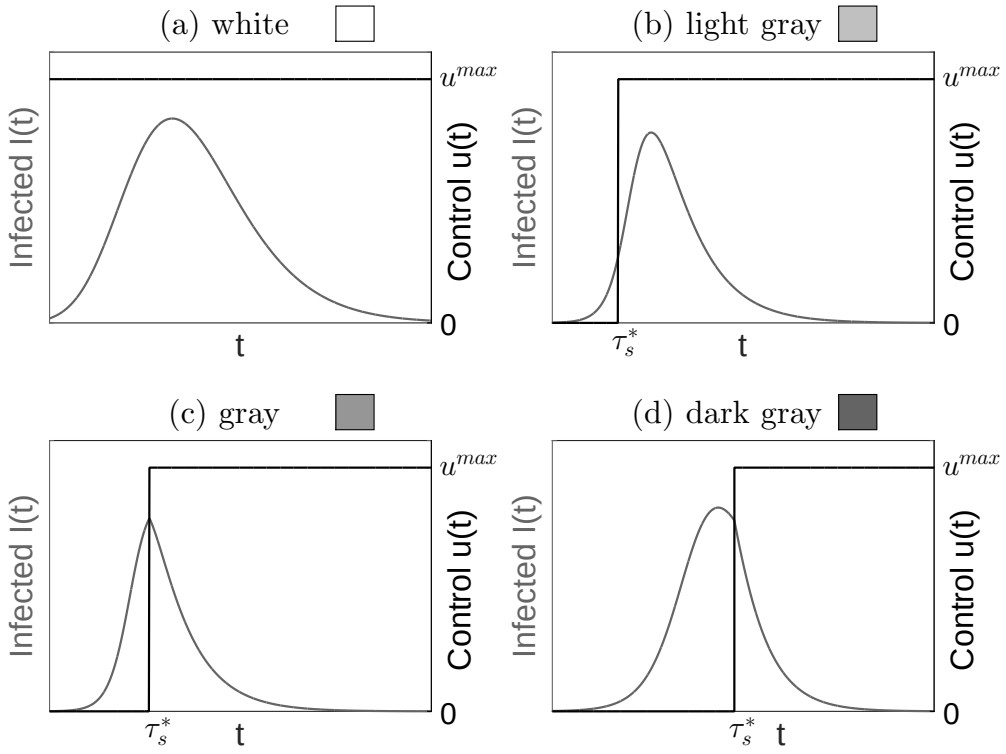

Fig. 3.1. Schematization of the four types of admissible optimal control and legend of the plot colors that will be used throughout the thesis. White (panel a) denotes a constant control at its maximum value. Different shades of gray denote delayed controls applied at the switching time τ_s^*. We distinguish three different behaviors, depending on the position of τ_s^* with respect to the infectious dynamics: the switch occurs before the peak of the infection (panel b, light gray), in correspondence of the peak (panel c, gray) or after the peak of infection (panel d, dark gray).

reasonably expect that the considered control policies will be suspended after the complete eradication of the disease. However, this fact does not affect the efficiency of our study, since we will focus on the actual epidemic evolution only, from its onset to the eradication.

3.3 Existence of an optimal control

To prove the existence of an optimal control we strongly rely on the particular form of the admissible controls proved in Theorem 3.2.1. Our idea is to identify each bang-bang function $u(t) \in \mathcal{A}$ with a real parameter. Since the delayed optimal control

function is not defined at the switching time instant, for our purpose and especially for numerical simulations we fix by convention $u^*(\tau_s^*) = u^{max}$. Then, we can generalize the idea of switching time, defined as the zero of the switching function ψ, introducing the *starting intervention time*

$$\tau = \begin{cases} 0 & \text{in case of constant maximum control} \\ \tau_s & \text{in case of delayed control} \end{cases} \tag{3.12}$$

which represents the first time instant at which the control $u(t) \in \mathcal{A}$ assumes the value u^{max}. Since a delayed control can be characterized by its switching time τ_s, we can then identify each admissible optimal control in $\mathcal{A}$, constant or delayed, by the value of τ and write it in the more general form:

$$u(t;\tau) = \begin{cases} 0 & 0 < t < \tau \\ u^{max} & \tau \leq t < +\infty. \end{cases} \tag{3.13}$$

Therefore, the functional to be minimized $J(u)$ can be seen as the function

$$\begin{array}{ccc} J : [0, +\infty) & \to & [0, +\infty) \\ \tau & \to & T \end{array} \tag{3.14}$$

that links the starting intervention time $\tau \geq 0$ to the eradication time T of the problem

$$\begin{array}{c} \dot{\boldsymbol{x}}(t) = f(\boldsymbol{x}(t)) + u(t;\tau)g(\boldsymbol{x}(t)), \quad t \geq 0; \\ \boldsymbol{x}(0) = \boldsymbol{x}_0, \quad \boldsymbol{x}(T) \in \mathcal{C} = \{(S, I) \ : \ I = \varepsilon\}. \end{array} \tag{3.15}$$

In the next Theorem we prove that J always admits at least a minimum value, therefore an optimal control u^* is identified by a starting intervention time such that $\tau^* = \operatorname{argmin} J$.

Theorem 3.3.1. *There exists an optimal solution of the optimal control problem* (3.10).

Proof. By definition, there exists an optimal solution of (3.10) if the functional $J(u)$, which gives the eradication time of the controlled SIR problem (3.4) as a function of the control, has (at least) a minimum point u^* on the set of admissible controls. For each policy Theorem 3.2.1 holds, namely the set of admissible controls is $\mathcal{A}$ given in (3.11). As stated before, we can see J as a function that links the starting intervention time τ (3.12) to the eradication time T (see (3.14)). Since the starting intervention time cannot be larger than the eradication time of the uncontrolled

epidemic T_{unc}, then the domain of the function J is restricted to the interval $[0, \tau^{max}]$, where $\tau^{max} = T_{unc}$. We prove that J admits at least a minimum point τ^* by proving that it is a continuous function on the compact interval $[0, \tau^{max}]$.

First we prove that J is a continuous function in 0, namely that

$$\lim_{h \to 0^+} J(h) = J(0).$$

We observe that by definition $J(0)$ is the eradication time $T_0 (= T_{\tau=0})$ of the solution $\boldsymbol{x}(t)$ of the controlled problem

$$\begin{cases} \dot{\boldsymbol{x}}(t) = f(\boldsymbol{x}(t)) + u^{max} g(\boldsymbol{x}(t)), \quad t \geq 0 \\ \boldsymbol{x}(0) = \boldsymbol{x}_0, \quad \boldsymbol{x}(T_0) \in \mathcal{C} = \{(S, I) \, : \, I = \varepsilon\} \end{cases},$$

while $J(h)$ is the eradication time T_h of the solution

$$\boldsymbol{y}(t) = \begin{cases} \boldsymbol{y}_1(t) & 0 \leq t < h \\ \boldsymbol{y}_2(t) & t \geq h \end{cases},$$

where $\boldsymbol{y}_1$ is the solution of the uncontrolled problem

$$\begin{cases} \dot{\boldsymbol{y}}_1(t) = f(\boldsymbol{y}_1(t)), \quad 0 \leq t \leq h \\ \boldsymbol{y}_1(0) = \boldsymbol{x}_0 \end{cases},$$

and $\boldsymbol{y}_2$ is the solution of

$$\begin{cases} \dot{\boldsymbol{y}}_2(t) = f(\boldsymbol{y}_2(t)) + u^{max} g(\boldsymbol{y}_2(t)), \quad t \geq h \\ \boldsymbol{y}_2(h) = \boldsymbol{y}_1(h), \quad \boldsymbol{y}_2(T_h) \in \mathcal{C} \end{cases}.$$

By the Continuous Dependence on Initial Conditions Theorem, for a generic $t \geq h$ it holds:

$$\begin{aligned} ||\boldsymbol{y}(t) - \boldsymbol{x}(t)||_\infty &\leq e^{L(t-h)} ||\boldsymbol{y}(h) - \boldsymbol{x}(h)||_\infty \\ &\leq e^{L(t-h)} ||\boldsymbol{y}(h) - \boldsymbol{x}_0|| + ||\boldsymbol{x}_0 - \boldsymbol{x}(h)||_\infty \\ &\leq e^{L(t-h)} (c_{\boldsymbol{y}} + c_{\boldsymbol{x}}) h, \end{aligned}$$

where the last inequality follows from the Mean Value Theorem. This is true in particular for $t = T_h$: $||\boldsymbol{y}(T_h) - \boldsymbol{x}(T_h)||_\infty \leq \tilde{c}\, h$. Let us consider only the infected component of the two solutions: $I_{\boldsymbol{x}}(t)$ and $I_{\boldsymbol{y}}(t)$. Then $|I_{\boldsymbol{y}}(T_h) - I_{\boldsymbol{x}}(T_h)| \leq \tilde{c}\, h$, which leads to $|I_{\boldsymbol{x}}(T_0) - I_{\boldsymbol{x}}(T_h)| \leq \tilde{c} h$, since $I_{\boldsymbol{y}}(T_h) = \varepsilon = I_{\boldsymbol{x}}(T_0)$. This is equivalent to

$$\lim_{h\to 0^+} I_{\boldsymbol{x}}(T_h) = I_{\boldsymbol{x}}(T_0).$$

$I_{\boldsymbol{x}}(t)$ being a continuous positive function that is strictly monotone in a neighborhood of T_0, it is invertible and therefore we can state that $\lim_{h\to 0^+} T_h = T_0$, namely $\lim_{h\to 0^+} J(h) = J(0)$. The proof of the continuity of J in a generic starting intervention time τ follows from the continuity in 0, using translation arguments. □

3.4 Numerical method

In optimal control, many methods have been proposed in recent years. Several powerful, yet time-expensive, direct methods based on nonlinear programming can be found, such as NUDOCCCS [20] or MUSCOD [29]. On the other hand, the indirect methods based on PMP, such as shooting methods [56], are both fast and accurate, but tend to suffer from great sensitivity to the initialization.

More specifically, several numerical methods for the optimal solution of both minimum time and bang-bang control problems can be found in literature. Such techniques are mainly based on shooting methods [56, 62, 67], smooth regularizations of the control function [83], or pseudospectral methods [82]. However, since our problem is characterized by the particular class of optimal controls $\mathcal{A}$ in (3.11), for our numerical simulations we will use a simpler ad hoc numerical scheme that turns out to be much faster and accurate. The method strongly relies on the idea of identifying each bang-bang function $u(t) \in \mathcal{A}$ with a real parameter that has been formulated in Section 3.3.

Indeed, the numerical solution is computed by evaluating the function $J(\tau)$ over a suitable interval and looking for its minimum values. More specifically, we fix a uniform mesh $\{\tau_i,\, i = 1,\dots,M\}$ over the interval $[0, \tau^{max}]$, where as stated before $\tau^{max} = T_{unc}$ is the eradication time of the uncontrolled epidemic. Then for each mesh point we consider the related control function $u(t;\tau_i)$ defined in (3.13) and numerically integrate the Cauchy problem (3.15) using the Crank-Nicholson method with uniform time steps $\{t_k,\, k = 1,\dots,N\}$, obtaining the numerical solution $\boldsymbol{x}_k^{(i)} = (S_k^{(i)}, I_k^{(i)})^\intercal,\ k = 1,\dots,N$. Then, we set the eradication time T_i relevant to the mesh point τ_i as the first time step $t_{\bar{k}}$ at which the computed solution $I_{\bar{k}}^{(i)} \le \varepsilon$. Finally, we take the minimum over the set of computed eradication times $T_j = \min\{T_i,\, i = 1,\dots,M\}$ as the optimal eradication time, and set the corresponding τ_j as the optimal starting intervention time. Since the minimum is not necessarily unique, if there are more switching times $\tau_{i_1},\dots,\tau_{i_r}$ for which the eradication time is the same minimum value T_{min}, we choose by convention the smallest starting in-

tervention time as the optimal one.

In the following sections we investigate the four different control policies considered. For each policy we will present theoretical and numerical results. In our numerical simulations, we set $\varepsilon = 0.5$, as in [44]. Then, through a sensitivity analysis, we explore the solutions of optimal control problems (3.6)–(3.9) on a wide range of parameter settings describing different epidemiological conditions (represented by $\mathcal{R}_0 = \beta S(0)/\mu$), different possible control efforts (represented by u^{max}), and a different number of initially introduced infected individuals in the population (represented by $I(0)$).

3.5 Linear term policies

We consider SIR model (3.3) with the general linear term control, denoted by $u_l(t)$, obtaining an optimal control problem as the one defined in (3.10), with $g_l(\boldsymbol{x})$ as in (3.5).

Theorem 3.5.1. *If u_l^* is the optimal control strategy for the linear term control problem, then u_l^* is a bang-bang control with at most one switching time τ_s^* from no control to maximum control.*

Proof. Throughout all the proofs we omit the superscript $*$ for the optimal quantities, in order to simplify the notation.

Let $\boldsymbol{x}(t) = (S(t), I(t))^\mathsf{T}$ denote the optimal solution for the control problem with linear term policy, suitable to model vaccination, isolation or culling for proper values of parameters α_1 and α_2; $u_l(t)$ be the control term, $\boldsymbol{\lambda}(t) = (\lambda_S(t), \lambda_I(t))^\mathsf{T}$ the corresponding adjoint variables and T the optimal eradication time. By the Pontryagin's Minimum Principle, the Hamiltonian function, the switching function and its derivative are respectively:

$$\mathcal{H}(\boldsymbol{x}, \boldsymbol{\lambda}, u_l) = 1 - (\beta SI + \alpha_1 u_l S)\lambda_S + (\beta SI - \mu I - \alpha_2 u_l I)\lambda_I \tag{3.16}$$

$$\psi(\boldsymbol{x}, \boldsymbol{\lambda}) = -\alpha_1 S\lambda_S - \alpha_2 I\lambda_I, \qquad \dot{\psi}(\boldsymbol{x}, \boldsymbol{\lambda}) = \beta SI(\alpha_1\lambda_I - \alpha_2\lambda_S), \tag{3.17}$$

and the adjoint variables satisfy the following system of ODEs:

$$\begin{cases} \dot{\lambda_S} &= (\lambda_S - \lambda_I)\beta I + \alpha_1 u_l \lambda_S \\ \dot{\lambda_I} &= (\lambda_S - \lambda_I)\beta S + \mu\lambda_I + \alpha_2 u_l \lambda_I. \end{cases} \tag{3.18}$$

The sketch of the proof is as follows.

(i) First we prove that the control is non-singular, namely that the function ψ vanishes only in isolated points. Suppose in fact that ψ vanishes in an open interval B. Then also all the derivatives vanish there and in particular $\psi = \dot{\psi} = 0$ in B, which yields by some algebra $\lambda_S = \lambda_I = 0$ by (3.17), since $S, I > 0$ when $S(0), I(0) > 0$ (see Remark 1). This is in contradiction with Theorem 3.3, as the adjoint variables λ_S and λ_I cannot vanish simultaneously by construction, therefore ψ vanishes only in isolated points. As a consequence, the control is a piecewise constant function $u_l(t)$ that can assume only two values: 0 and u^{max}. The switching times are defined as the time instants at which the function $\psi(t)$ changes its sign and, consequently, the function $u_l(t)$ changes its value. Therefore two types of switch can occur: either the value of $u_l(t)$ is 0 in a left-neighbourhood of the switching time and is u^{max} in a right-neighbourhood, and we denote it by $0 \to u^{max}$, or the converse, which is denoted by $u^{max} \to 0$.

(ii) Next we show that the optimal control in a left-neighbourhood of the eradication time T must be equal to u^{max}. By condition 3 of Theorem 3.3 $\psi(T) = -\alpha_2 I(T)\lambda_I(T)$ and $\dot{\psi}(T) = \alpha_1 \beta S(T) I(T) \lambda_I(T)$. The sign of the function ψ in the left-neighbourhood of T will then be determined by the sign of $\lambda_I(T)$. Substituting $\lambda_S(T) = 0$ in (3.16) and by condition 2 of Theorem 3.3 we get $\lambda_I(T) = -\dot{I}(T)^{-1}$, which is positive, since $\dot{I}(T) < 0$. As a consequence, $\psi(T) \leq 0$ and $\dot{\psi}(T) \geq 0$. Since they cannot vanish simultaneously, as α_1 and α_2 are not simultaneously zero, ψ is negative in a left-neighbourhood of T.

(iii) Now we prove that there can be at most one switching time, relevant to the switch $0 \to u^{max}$. Let τ_s be a generic switching time, namely $\psi(\tau_s) = 0$. Then $-\alpha_1 S(\tau_s)\lambda_S(\tau_s) = \alpha_2 I(\tau_s)\lambda_I(\tau_s)$ by (3.17). Suppose $\alpha_2 \neq 0$, then at the switching time $\lambda_I = -\frac{\alpha_1 S \lambda_S}{\alpha_2 I}$. Substituting this relation in (3.16) and by condition 2 of Theorem 3.3, we can write λ_S, and therefore λ_I and $\dot{\psi}$, as functions of $Q(t) = \beta I(t) + \frac{\alpha_1}{\alpha_2}(\beta S(t) - \mu)$, which is a decreasing function since $\dot{Q}(t) < 0$:

$$\lambda_S(\tau_s) = (Q(\tau_s)S(\tau_s))^{-1}, \qquad \lambda_I(\tau_s) = -\frac{\alpha_1}{\alpha_2}(Q(\tau_s)I(\tau_s))^{-1}, \qquad \dot{\psi} = -\frac{\beta}{Q}\left(\frac{\alpha_1^2}{\alpha_2}S + \alpha_2 I\right).$$

In particular, we can see that the sign of $\dot{\psi}$ is opposite to the sign of Q. Suppose that there are multiple switching times $\tau_s^{(j)}$, $j = 1, \ldots, n$. We have already proved that $u_l(T) = u^{max}$, so at the last switching time $\dot{\psi}(\tau_s^{(n)}) < 0$ must hold, thus $Q(\tau_s^{(n)}) > 0$. Since Q is a decreasing function, this means that Q is positive in the interval $[0, \tau_s^{(n)}]$, and it implies that all the switching times $\tau_s^{(j)}$ are from no control (positive values of ψ) to maximum control (negative values of ψ). This is not possible, therefore there can be at most a unique switch from no control to the maximum control rate u^{max}, namely $\dot{\psi}(\tau_s) < 0$.

Now suppose $\alpha_2 = 0$. We still prove that there can be at most one switching time, relevant to the switch $0 \to u^{max}$ and that, in addition, the switch can only occur before the peak time. Let τ_s be a generic switching time, namely $\psi(\tau_s) = 0$. Then $\lambda_S(\tau_s) = 0$ by (3.17) and, analogously to what happens at the eradication time T, $\lambda_I(\tau_s) = -\dot{I}(\tau_s)^{-1}$. Thus, the sign of $\dot{\psi}(\tau_s)$ is opposite to the sign of $\dot{I}(\tau_s)$, which is positive (respectively, negative) before (resp. after) the peak time of the infection t_p. The only possible change in sign of the function ψ after the peak is then from negative to positive, which is not admissible, since we proved that ψ is negative in a left-neighbourhood of T. Thus the switch can only occur before the peak and, being $\dot{\psi}(\tau_s)$ always negative, it must be unique. Moreover, since ψ changes its sign from positive to negative values, the control switches from 0 to the maximum rate u^{max}. □

We proceed now to analyse the peculiarities of each policy involved in the general formulation.

3.5.1 Vaccination

We consider the vaccination control, denoted by $u_v(t)$ in the optimal control problem (3.10), with $g_v(\boldsymbol{x})$ as in (3.6). The control reproduction number for vaccination is defined as $\mathcal{R}_C^v = \mathcal{R}_0 = \beta S(0)/\mu$.

For this policy, it is easy to prove that there exists a unique time instant t_p (possibly 0) at which the function $\dot{I}$ changes sign. In particular, $\dot{I}(t) > 0$ for $t < t_p$ and $\dot{I}(t) < 0$ for $t > t_p$. We call t_p the peak time, because it represents the time at which the number of infected individuals reaches its maximum. Therefore, in addition to the general results of Theorem 3.5.1, it is possible to prove the following.

Theorem 3.5.2. *The switch of the optimal control u_v^* can occur only before the peak of the infection. Moreover, if $\mathcal{R}_0 < 1$ or $u_v^{max} > \mu$, the optimal control is the constant control $u_v^*(t) \equiv u_v^{max}$.*

Proof. The sketch of the proof is as follows.

(i) The position of the switch with respect to the peak of infection follows from the proof of Theorem 3.5.1, point (iii) (case $\alpha_2 = 0$).

(ii) By definition of the basic reproduction number, we know that if $\mathbb{R}_0 < 1$ then the number of infected individual is monotonically decreasing in time, namely the peak of the infection is $t_p = 0$. As we already proved that there cannot be a switch for $t > t_p$, in this case the optimal control must be $u_v(t) \equiv u_v^{max}$.

Suppose that $\mathbb{R}_0 > 1$ and that the optimal control is delayed with switch $0 \to u_v^{max}$ at time $\tau_s > 0$. Then we prove that the relation $\mu > u_v^{max}$ must hold.

First we prove that, under those hypotheses, the function ψ has a minimum point m_ψ in (τ_s, T) at which $\lambda_I(m_\psi) < \lambda_S(m_\psi)$, as sketched in Fig. 3.2. The function ψ vanishes at τ_s (by definition) and at T (by the transversality condition), while it is strictly negative between the two points, therefore it must have at least a minimum point. Since ψ is a $\mathcal{C}^1$ function, in such points $\dot{\psi} = 0$ and thus also $\lambda_I = 0$, by (3.17). Substituting this latter value in the second derivative of the switching function and recalling the definition of ψ in (3.17) we obtain

$$\ddot{\psi} = \beta SI(\beta S\lambda_S - \beta I\lambda_I - u^{max}\lambda_I) = \beta^2 S^2 I\lambda_S = -\beta^2 SI\psi.$$

Then $\ddot{\psi}$ is positive and we can state that ψ has only an extremal point in that interval, and more specifically that it is a minimum point, which we denote by m_ψ. Moreover, since $\lambda_I(m_\psi) = 0$ and $\lambda_S(m_\psi) > 0$, it is straightforward that $\lambda_I(m_\psi) < \lambda_S(m_\psi)$.

Similarly, we prove that the function λ_S has a unique maximum M_{λ_S} in the interval $[\tau_s, T]$ at which $\lambda_I(M_{\lambda_S}) > \lambda_S(M_{\lambda_S})$, as sketched in Fig. 3.2. In fact, it vanishes at τ_s (since $\psi(\tau_s) = 0$) and at T (for the transversality condition) and it is strictly positive between the two points, since $\psi < 0$. On the interval $[\tau_s, T]$, being $u(t) = u_v^{max}$, λ_S is a $\mathcal{C}^1$ function, therefore its maximum and minimum points are characterized by $\dot{\lambda}_S = 0$, namely $\lambda_S = \beta I\lambda_I/(\beta I + u_v^{max})$ from (3.18). Substituting this value in (3.16) and recalling that $\mathcal{H} = 0$ we obtain that in the extremal points $\lambda_I = 1/(\mu I)$. Substituting those values in the second derivative of λ_S we obtain:

$$\ddot{\lambda}_S = \lambda_S[(\beta I + u_v^{max})^2 - \mu\beta I] - \lambda_I \beta I(\beta I + u_v^{max}) = -\beta^2 I/(\beta I + u_v^{max}),$$

which is negative and therefore in the interval (τ_s, T) the function λ_S has a unique maximum point, which we denote by M_{λ_S}. Moreover

$$\lambda_S(M_{\lambda_S}) = \beta I(M_{\lambda_S})\lambda_I(M_{\lambda_S})/(\beta I(M_{\lambda_S}) + u_v^{max}) < \lambda_I(M_{\lambda_S}).$$

Evaluating $\dot{\lambda}_S$ at the point m_ψ, by (3.18) we obtain

$$\dot{\lambda}_S(m_\psi) = (\beta I(m_\psi) + u_v^{max})\lambda_S(m_\psi) > 0,$$

therefore $m_\psi < M_{\lambda_S}$. Being $\lambda_I(m_\psi) < \lambda_S(m_\psi)$ and $\lambda_I(M_{\lambda_S}) > \lambda_S(M_{\lambda_S})$, there must exist a point $\sigma \in (m_\psi, M_{\lambda_S})$ such that $\lambda_S(\sigma) = \lambda_I(\sigma)$ and $\dot{\lambda}_I(\sigma) > \dot{\lambda}_S(\sigma)$, as sketched in Fig. 3.2. This last inequality reduces to $\mu\lambda_I(\sigma) > u_v^{max}\lambda_S(\sigma)$, therefore $\mu > u_v^{max}$ is a necessary condition for having a positive switching time. In conclusion, if $u_v^{max} > \mu$ the optimal control is the constant control $u_v(t) \equiv u_v^{max}$.

□

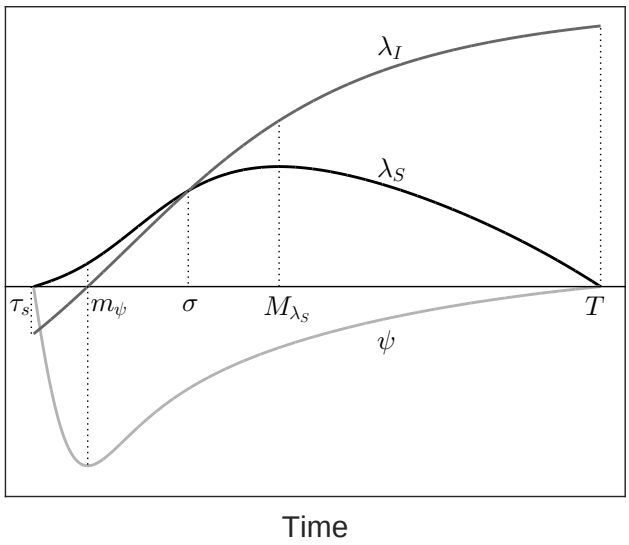

Fig. 3.2. Optimal vaccination problem with delayed control. Schematization of the switching function $\psi(t)$ and of the adjoint variables $\lambda_S(t)$, $\lambda_I(t)$ on the interval $[\tau_s, T]$.

The numerical analyses on the time-optimal vaccination problem are illustrated in Fig. 3.3. In Fig. 3.3(a), we show the results of the simulations performed in the parameter space $[u_v^{max}, \mathcal{R}_0(\beta)]$. As explained in the color codes in Fig. 3.1, the light gray and white regions in Fig. 3.3(a) represent the combinations of parameters $[u_v^{max}, \mathcal{R}_0(\beta)]$ for which the time-optimal vaccination problem selects for delayed and constant control, respectively. As highlighted by the analytic results, Fig. 3.3(a) displays that the switching time always occurs before the peak of infection and that higher vaccination efforts always select for a constant control. Fig. 3.3(b) shows the optimal starting intervention time (τ^*), the eradication time for the optimal vaccination strategy (T^*, solid curve), and the eradication time for the constant vaccination ($T_{\tau=0}$, dashed curve) as functions of the maximum effort, u_v^{max}. In Fig. 3.3(b), we notice that the optimal starting intervention time undergoes a discontinuous transition from delayed to constant control for increasing values of u_v^{max}. Then, small changes in u_v^{max} can cause an abrupt change in the starting point of the optimal vaccination campaign. On the other hand, Fig. 3.3(b) shows that, when delaying the onset of vaccination is optimal, the differences in the final time of the epidemic between optimal control and constant control (i.e. variation in the objective function) is marginal.

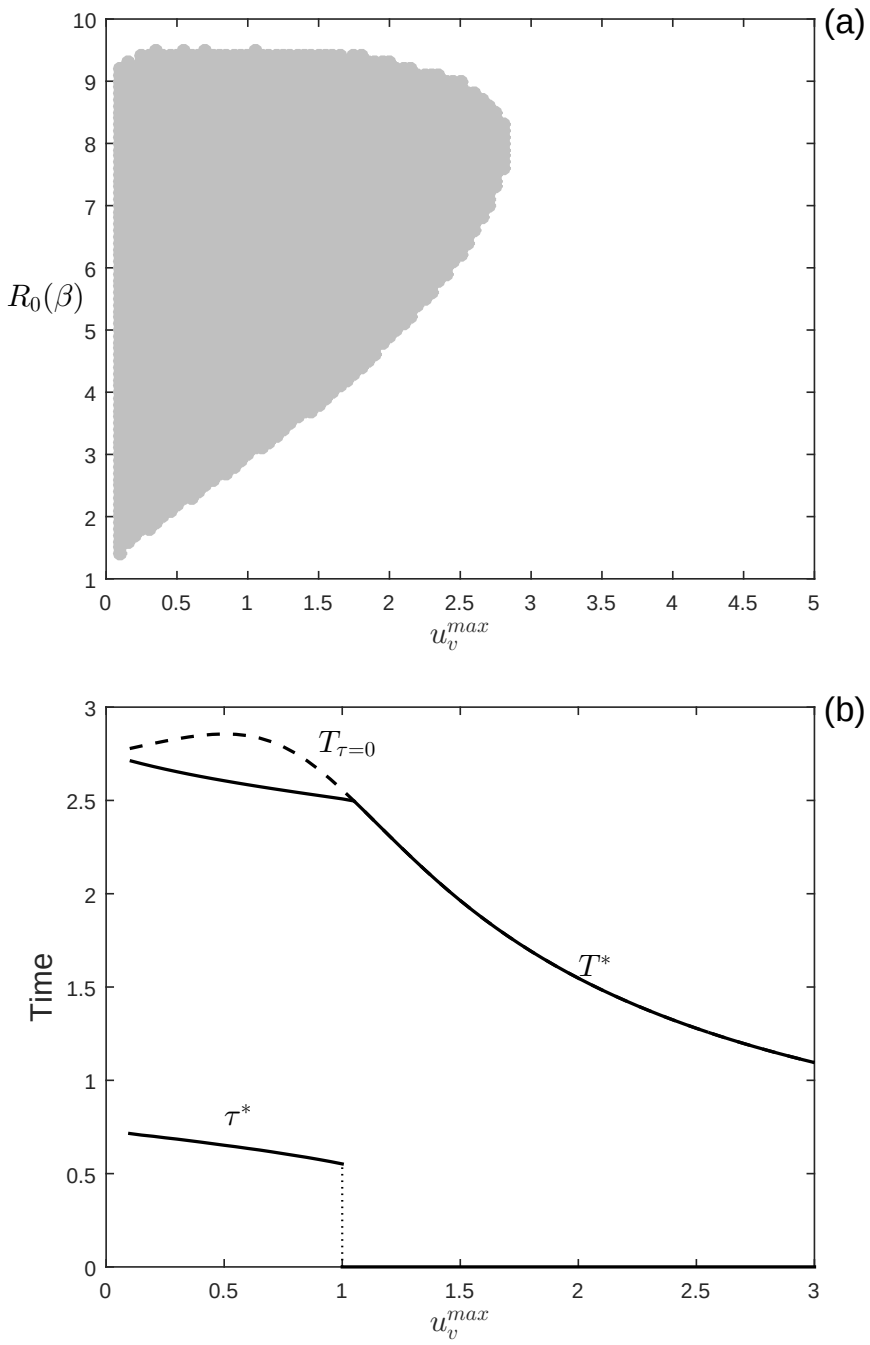

Fig. 3.3. Numerical analysis of the optimal vaccination problem. (a) Different colors represent different optimal control types obtained by varying u_v^{max} (that ranges from 0 to μ) and $\mathcal{R}_0(\beta)$. Color meanings are specified in Fig. 3.1. (b) Plot of the optimal starting intervention time τ^*, the optimal eradication time T^*, and the eradication time $T_{\tau=0}$ as functions of u_v^{max}, with $\mathcal{R}_0(\beta) = 3$. Other parameters: $S(0) = 2000$, $\mu = 5$, $I(0) = 1$, $\varepsilon = 0.5$.

3.5.2 Isolation

We consider SIR model (3.3) with isolation control, denoted by $u_i(t)$, obtaining an optimal control problem as the one defined in (3.10), with $g_i(\boldsymbol{x})$ as in (3.7). The control reproduction number for isolation is defined as $\mathcal{R}_C^i = \beta S(0)/(\mu + u_i^{max})$.

The numerical analyses on the time-optimal isolation problem are illustrated in Fig. 3.4. In Fig. 3.4(a), we show the results of the simulations performed in the parameter space $[u_i^{max}, \mathcal{R}_0(\beta)]$. Conversely to vaccination, our results show that the time-optimal isolation problem can select for delayed strategies also for high values of maximum effort, u_i^{max}. Moreover, the switching time for the optimal isolation strategy can occur after the peak of infection (see the dark gray region in Fig. 3.4(a)). In Fig. 3.4(b), we show that the isolation problem selects for optimal delayed control in a wide range of parameter settings also when the number of infected individuals firstly introduced in the population increases (i.e. $I(0) > 1$). Fig. 3.4(c) displays the optimal starting intervention time (τ^*), the final time for the optimal isolation strategy (T^*, solid curve), and the final time for the constant isolation ($T_{\tau=0}$, dashed curve) as functions of the maximum effort, u_i^{max}. As in the vaccination problem, the optimal starting intervention time for isolation undergoes a "catastrophic" transition from delayed to constant control for increasing values of maximum effort. Fig. 3.4(c) shows that delayed control can be optimal also when $\mathcal{R}_C < 1$, i.e. when an prompt intervention at $t = 0$ could have implied an immediate decline in the number of infected individuals In addition, when delaying the onset of isolation is optimal, the differences in the final time of the epidemic between optimal control and constant control can be significant. Fig. 3.4(d) shows the number of susceptible individuals at the end of the epidemic for the optimal isolation strategy ($S(T^*)$, solid curve) and the constant isolation ($S(T_{\tau=0})$, dashed curve) as functions of the maximum effort, u_i^{max}. Similarly to the switching time, $S(T^*)$ exhibits a discontinuous increase at the boundary between delayed and constant control.

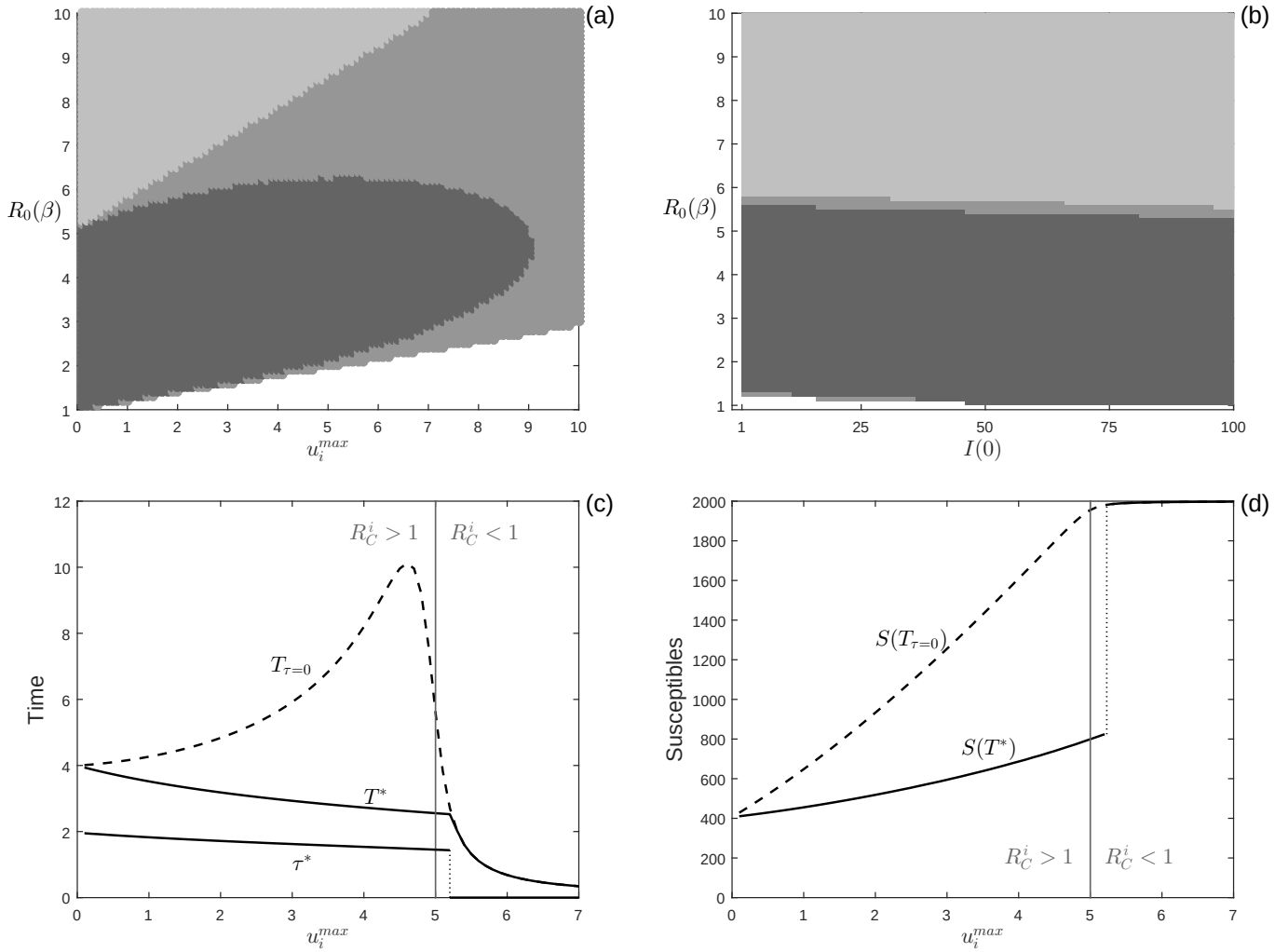

Fig. 3.4. Numerical analysis of the optimal isolation problem. Different colors represent different optimal control types obtained by varying: (a) u_i^{max} and $\mathcal{R}_0(\beta)$; (b) $I(0)$ and $\mathcal{R}_0(\beta)$. Color meanings are specified in Fig. 3.1. (c) Plot of the optimal starting intervention time τ^*, the optimal eradication time T^*, and the eradication time $T_{\tau=0}$ as functions of u_i^{max}, with $\mathbb{R}_0(\beta) = 2$. (d) Number of susceptible individuals at the end of the epidemic obtained using the optimal control, $S(T^*)$, and the constant control $u(t) = u_i^{max}$, $S(T_{\tau=0})$, as functions of u_i^{max}, with $\mathcal{R}_0(\beta) = 2$. In panel (b) $u_i^{max} = 1$. In panels (c)-(d) is also highlighted the value of u_i^{max} for which $\mathcal{R}_C^i = 1$ (in gray). Other parameter values as in Fig. 3.3.

3.5.3 Culling

We consider the culling control, denoted by $u_c(t)$, in the optimal control problem defined in (3.10), with $g_c(\boldsymbol{x})$ as in (3.8). The control reproduction number for culling is defined as $\mathcal{R}_C^c = \beta S(0)/(\mu + u_c^{max})$.

The numerical analyses on the time-optimal culling problem are illustrated in Fig. 3.5. In Fig. 3.5(a), we show the results of the simulations performed in the parameter space $[u_c^{max}, \mathcal{R}_0(\beta)]$. We display that, when $\mathcal{R}_0$ is low, delayed control is selected for small values of culling effort (u_c^{max}), while, when $\mathcal{R}_0$ is high, delayed control is selected for intermediate values of u_c^{max}. In addition, in the aforementioned cases, the starting of the optimal culling generally occurs before the peak of infection (light gray region in Fig. 3.5(a)). However, we can notice that there exists a small region in the parameter space $[u_c^{max}, \mathcal{R}_0(\beta)]$ where the starting of the optimal strategy can occur after the peak of infection (see the dark gray region in the box). Fig. 3.5(b) shows the optimal starting intervention time (τ^*), the final time for the optimal culling strategy (T^*, solid curve), and the final time for the constant culling ($T_{\tau=0}$, dashed curve) as functions of the maximum effort, u_c^{max}. Also in this case the optimal starting intervention time undergoes a "catastrophic" transition from delayed to constant control for increasing values of u_c^{max} and, when delaying the onset of culling is optimal, the differences in the final time between optimal control and constant control is marginal, analogously to the case of vaccination.

3.6 Reduction of transmission policy

We consider SIR model (3.3) with reduction of transmission control, denoted by $u_r(t)$, obtaining an optimal control problem as the one defined in (3.10), with $g_r(\boldsymbol{x})$ as in (3.9) and $0 < u_r^{max} \leq 1$. The control reproduction number for reduction of transmission is defined as $\mathcal{R}_C^r = \beta(1 - u_r^{max})/\mu$. Despite the nonlinearity of this kind of policy, it is possible to find the same type of optimal strategy of the linear term policies.

Theorem 3.6.1. *If u_r^* is the optimal control strategy for the reduction of transmission problem, then u_r^* is a bang-bang control with at most one switching time τ_s^* from no control to maximum control.*

Proof. Let $\boldsymbol{x}(t) = (S(t), I(t))^\mathsf{T}$ denote the optimal solution for the reduction of the transmission control problem, with control term $u_r(t)$, $\boldsymbol{\lambda}(t) = (\lambda_S(t), \lambda_I(t))^\mathsf{T}$ the corresponding adjoint variables and T the optimal eradication time. By the Pontryagin's Minimum Principle, the Hamiltonian function, the switching function and its

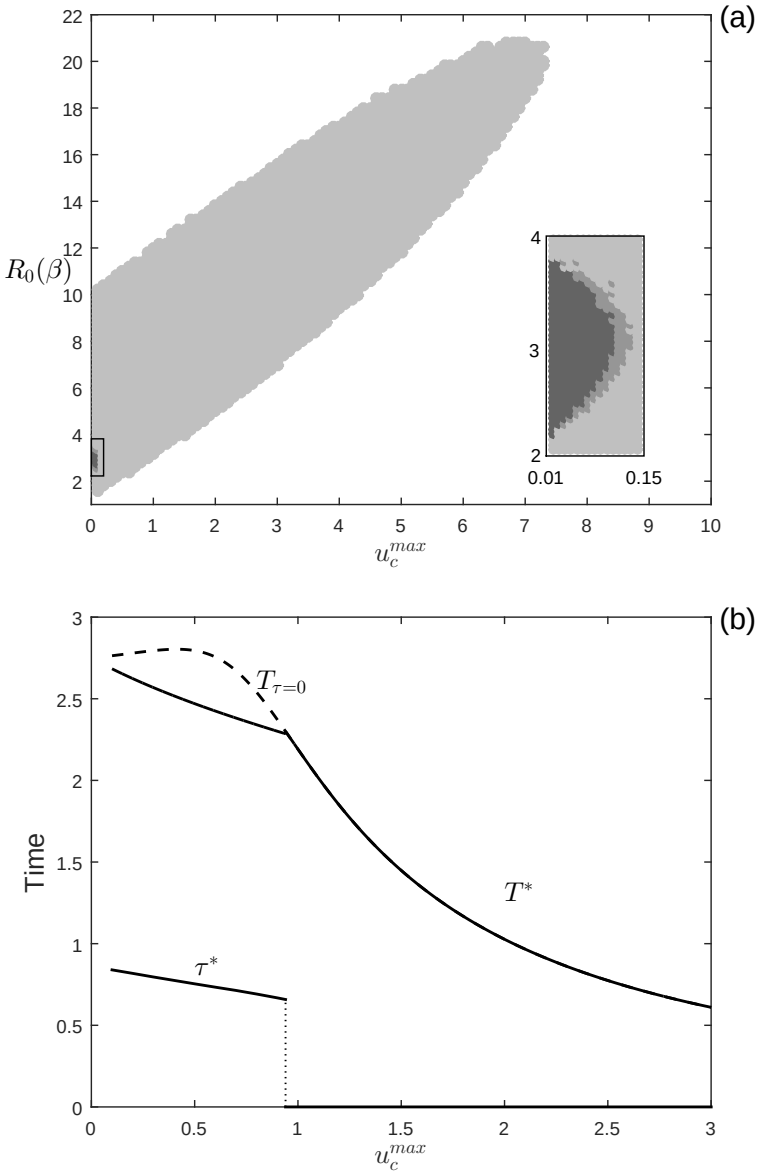

Fig. 3.5. Numerical analysis of the optimal culling problem. (a) Different colors represent different optimal control types obtained by varying u_c^{max} and $\mathcal{R}_0(\beta)$. Color meanings are specified in Fig. 3.1. (b) Plot of the optimal starting intervention time τ^*, the optimal eradication time T^*, and the eradication time $T_{\tau=0}$ as functions of u_c^{max}, with $\mathcal{R}_0(\beta) = 3$. Other Parameter values as in Fig. 3.3.

derivative are respectively:

$$\mathcal{H}(\boldsymbol{x}, \boldsymbol{\lambda}, u_r) = 1 + (\lambda_I - \lambda_S)\beta(1 - u_r)SI - \mu I\lambda_I \tag{3.19}$$

$$\psi(\boldsymbol{x}, \boldsymbol{\lambda}) = (\lambda_S - \lambda_I)\beta SI, \qquad \dot{\psi}(\boldsymbol{x}, \boldsymbol{\lambda}) = -\mu\beta SI\lambda_S, \tag{3.20}$$

and the adjoint variables satisfy the following system of ODEs:

$$\begin{cases} \dot{\lambda_S} &= (\lambda_S - \lambda_I)\beta(1 - u_r)I \\ \dot{\lambda_I} &= (\lambda_S - \lambda_I)\beta(1 - u_r)S + \mu\lambda_I. \end{cases}$$

For the proof of the Theorem, first we show that the control is non-singular, namely that the function ψ vanishes only in isolated points. Suppose that ψ vanishes in an open interval B. Then $\psi = \dot{\psi} = 0$ in B, namely $\lambda_S = \lambda_I = 0$ (see (3.20)), which is in contradiction with the statement of the Theorem 3.3. Therefore, ψ can vanish only in isolated points. Substituting $\lambda_S(T) = 0$ (the transversality condition) in (3.19) and by condition 2 of Theorem 3.3 we get $\lambda_I(T) = -\dot{I}(T)^{-1}$, which is positive, being $\dot{I}(T) < 0$. As a consequence, $\psi(T) < 0$ by (3.20).

Let τ_s be a generic switching time, namely $\psi(\tau_s) = 0$. Then $\lambda_S(\tau_s) = \lambda_I(\tau_s)$ by (3.20) and, by equation (3.19), they are both equal to $(\mu I(\tau_s))^{-1}$. Substituting this value in (3.20) we obtain $\dot{\psi}(\tau_s) = -\beta S(\tau_s)$, which is negative. Therefore, since the sign of the derivative of ψ is constant at every switching time τ_s, there can be at most a unique switch from no control (positive values of ψ) to the maximum rate of control u_r^{max} (negative values of ψ). □

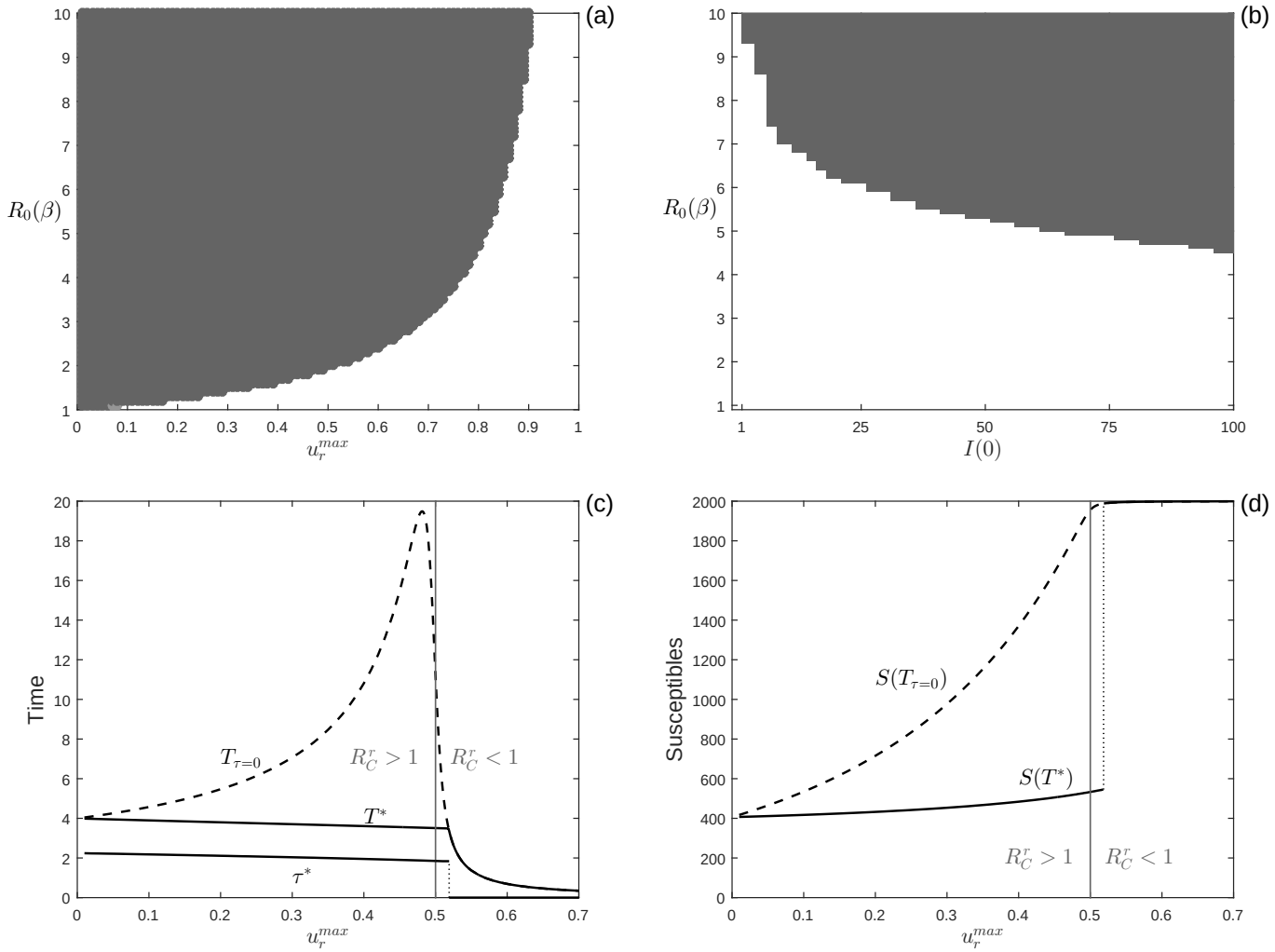

Fig. 3.6. Numerical analysis of the optimal reduction of transmission problem. Different colors represent different optimal control types obtained by varying: (a) u_r^{max} and $\mathcal{R}_0(\beta)$; (b) $I(0)$ and $\mathcal{R}_0(\beta)$. Color meanings are specified in Fig. 3.1. (c) Plot of the optimal starting intervention time τ^*, the optimal eradication time T^*, and the eradication time $T_{\tau=0}$ as functions of u_r^{max}, with $\mathcal{R}_0(\beta) = 2$. (d) Number of susceptible individuals at the end of the epidemic obtained using the optimal control, $S(T^*)$, and the constant control $u(t) = u_r^{max}$, $S(T_{\tau=0})$, as functions of u_i^{max}, with $\mathcal{R}_0(\beta) = 2$. In panel (b) $u_r^{max} = 0.9$. In panels (c)-(d) is also highlighted the value of u_r^{max} for which $\mathcal{R}_C^r$=1 (in gray). Other parameter values as in Fig. 3.3.

The numerical analyses on the time-optimal reduction of transmission problem are illustrated in Fig. 3.6. In Fig. 3.6(a), we show the results of the simulations performed in the parameter space $[u_r^{max}, \mathcal{R}_0(\beta)]$. We display that, when delayed control is selected, the starting of the optimal reduction of transmission generally occurs after the peak of infection (dark gray region in Fig. 3.6(a)). In Fig. 3.6(b), we show that the reduction of transmission problem selects for optimal delayed control in a wide range of parameter settings also when the number of infected individuals firstly introduced in the population increases (i.e. $I(0) > 1$). Fig. 3.6(c) shows the optimal starting intervention time (τ^*), the final time for the optimal reduction of transmission strategy (T^*, solid curve), and the final time for the constant reduction of transmission ($T_{\tau=0}$, dashed curve) as functions of the maximum effort, u_r^{max}. Similarly to the isolation problem, we find that: (i) delayed control for reduction of transmission can be optimal also when $\mathcal{R}_C < 1$; and (ii) when delaying the starting of reduction of transmission is optimal, the differences in the final time of the epidemic between optimal control and constant control can be significant. Fig. 3.6(d) shows the number of susceptible individuals at the end of the epidemic for the optimal reduction of transmission strategy ($S(T^*)$, solid curve) and the constant reduction of transmission ($S(T_{\tau=0})$, dashed curve) as functions of the maximum effort, u_r^{max}. Similarly to the isolation problem, $S(T^*)$ exhibits a discontinuous increase at the boundary between delayed and constant control.

4

Discussion and conclusions

In this Part of the thesis, we investigated the problem of minimizing the epidemic duration by using different control policies. Specifically, we characterized analytically the time-optimal control strategies for prophylactic vaccination, isolation, non-selective culling, and reduction of transmission by using a family of simple SIR models in an optimal control framework [78]. Our analyses led to the non-trivial result that, even in the unconstrained optimal control problem (i.e. without costs of control or resource limitations (*sensu* [44])), using the maximal effort for the entire epidemic period may not be the optimal strategy to minimize the epidemic duration. In addition, we found that, when applying the maximal effort for the entire epidemic is sub-optimal, then a delayed control represents the optimal strategy in all the cases investigated. We even found that the optimal amount of delay applied to the control may be sufficiently large to postpone the beginning of the intervention after the peak of the infection (see Fig. 3.1 and dark gray regions in Figs. 3.4(a), 3.5(a), and 3.6(a)). In addition, we showed that the delayed control may represent the optimal strategy for minimizing the epidemic duration even when a prompt intervention could immediately reduce the number of infected individuals (i.e. reduce $\mathcal{R}_C$ below 1, see Figs. 3.4(c) and 3.6(c)).

The biological explanation for the optimality of delayed controls relies on the remark that, at the beginning of the epidemic, the infection process can be more efficient in depleting the reservoir of susceptibles (which represents the mechanism leading to epidemic extinctions) than the applied control. In other words, reducing via external interventions the number of individuals involved in the infection process at the beginning of the outbreak (especially the infected ones) may lead to slower epidemic dynamics, which implies longer times for the epidemic to go extinct. Two evidences support this explanation: (1) delayed control is generally optimal when the effectiveness of the control is low (i.e. low u^{max}); and (2) isolation and reduction of

transmission policies (which do not reduce directly the number of susceptibles) tend to select for delayed control in wider ranges of parameter settings than vaccination and culling.

Our results differ from those previously obtained for the time-optimal problem in specific epidemic contexts. By analysing a subsystem of an epidemic model describing SARS spread, Jiang [55] proved that, according to Pontryagin's Minimum Principle, maximizing the isolation effort for the entire epidemic period would reduce epidemics in minimum time. Similarly, by numerically testing scenarios in an SIR model where the control always reduces the disease reproduction number below 1, Iacoviello & Liuzzi [53] showed that maximizing the combined vaccination and isolation efforts for the entire epidemic period eradicates epidemics in minimum time.

Our results substantially differ also from those obtained minimizing the total number of infected (or the infectious burden) in SIR epidemic models. By characterizing optimal controls according to Pontryagin's Maximum Principle, different works showed that the unconstrained problems for isolation [44, 88], vaccination [44, 69], and culling [17] only support the trivial solution of applying the maximal effort for the entire epidemic. Then, from our results it follows that the infectious burden may not be minimized while minimizing the epidemic duration in simple SIR models.

Minimizing the infectious burden in the optimal control problem for isolation and reduction of transmission is equivalent to maximize the final number of susceptibles, $S(T)$. Some examples of the tension between minimizing the epidemic duration and the infectious burden can be observed in Figs. 3.4 and 3.6. In particular, Figs. 3.4(c) and 3.6(c) display the eradication time, T, and Figs. 3.4(d) and 3.6(d) display the number of susceptible individuals at the end of the epidemic, $S(T)$, as functions of u^{max} for both the time-optimal control and the constant control (corresponding to the optimal solution for the unconstrained problem of infectious burden minimization). From these figures, we notice that the different objective functions provide similar results when the control efforts are sufficiently large to rapidly lead the epidemic to extinction (high u^{max}), while they provide substantially different results in the case of less efficient strategies (low u^{max}). Specifically, the time-optimal control strategy performs poorly in minimizing the infectious burden at the boundary between delayed and constant control (see Figs. 3.4(d) and 3.6(d)), while the infectious burden minimization strategy performs poorly in minimizing the epidemic duration for slightly higher values of $\mathcal{R}_C$ (see the peak of $T_{\tau=0}$ in Figs. 3.4(c) and 3.6(c)).

Moreover, we find that small changes in the control parameter u^{max} can cause large changes in the shape of the optimal strategies. An analogous result was found by Hansen & Day [44] investigating the problem of minimizing the infectious burden through isolation in a SIR framework with limited resources. Hansen & Day [44] also

found that a "catastrophic" shift in the shape of the isolation strategy corresponds to an abrupt variation in the objective function (i.e. the infectious burden). Conversely, here we find that "catastrophic" shifts in the shape of the control strategies correspond to continuous variations in the objective functions (i.e. the final time of epidemics).

We believe our findings can be useful in throwing light on overlooked results obtained with more complex models developed in specific epidemiological contexts. For instance, Roche et al. [80] investigated the performances of different spatially explicit models for the spread of foot-and-mouth disease in the UK farms, considering different control scenarios. Among other scenarios, they compared the effect of suppressive vaccination strategies started at 7 and 14 days after the outbreak beginning. They found that, in two out of the four models investigated, the medians and/or the 95^{th} percentiles of the epidemic duration decreased when the control is delayed by 7 days [80, see models 'IS+' and 'NL' in table 4 therein]. On the other hand, they found that the number of infected farms always increases when the vaccination is delayed [see table 4 in 80]. In a similar way, by investigating the effectiveness of combined culling and movement restriction to control classical swine fever in Switzerland pig farms, Dürr et al. [33] found that delaying the starting of the control from 6 to 16 days after the outbreak beginning reduced the median outbreak duration in three out of the eight analysed scenarios [see figure 4 in 33].

Previous works have already shown that delayed control might represent an optimal strategy in some epidemiological applications. For instance, Handel et al. [42] and Hansen & Day [43] showed that delaying the controls may be optimal in preventing the re-emergence of the epidemic or the emergence of resistant epidemics. Bolzoni et al. [17] showed that the delayed control may be optimal in wildlife diseases where the host population growth is density-dependent.

The numerical analyses performed here under the assumption of constant control highlighted that increasing the control efforts may lead to a substantial increase of the eradication time. This is especially true in the case of isolation and reduction of transmission, where the eradication time may increase from two- to five-fold with respect to the "do-nothing" alternative (see Figs. 3.4(c) and 3.6(c)). Similar negative effects of constant efforts on disease control have also been highlighted when the target of the intervention was the reduction of the number of infected individuals [15, 16, 23, 79]. All these counter-intuitive findings suggest that the implementation of simple time-dependent strategies may crucially improve the control of infectious diseases.

4.1 Perspectives

Other aspects of diseases control implementation that were not included in the present thesis – such as combined controls [44], the costs of control [9], resources limitation [44], and availability of surveillance information [14] – can play a significant role in shaping the optimal strategy. These aspects are essential in defining optimal protocols of intervention for diseases eradication. However, thanks to the generality of the model formulation, we believe our results can be used as a benchmark for future investigations.

We plan to thoroughly investigate combined controls, namely the application of two or more policies at the same SIR model. We proved that in this case the admissible controls are multidimensional bang-bang controls, for which the existence of an optimal solution can be proved, analogously to what is done inthis thesis for the single policy. However, a numerical scheme that follows the one we used in this thesis is too expensive, and a shooting method (as in [56, 62, 67]) is preferable. This method consists in searching for the zero of a certain shooting function, typically via quasi-Newton methods. The main advantages of this approach lie in the accuracy and low numerical complexity. Also, the dimension of the system of differential ordinary equations that must be solved is $2d$, where d is the state dimension, which is quite low for this kind of problems. Yet, particular care must be taken in using this method: depending on the arbitrary value that initializes the method (which originates the method name "shooting"), the algorithm might not converge at all, or might converge to local minima of the functional, which can assume higher values than the true global minimum.

To overcome this problem, the numerical scheme must provide for a preliminary application of, as an example, a Hamilton-Jacobi-Bellman scheme [25] that allows to select an initializing value for the shooting method that will lead to global minimum. The HJB approach is based on the dynamic programming principle [10]. It consists in considering the functional to be minimized $J(\boldsymbol{u}, \boldsymbol{x}_0)$ as a function of the initial state $\boldsymbol{x}_0$ only ($\mathcal{T}(\boldsymbol{x}) = J(\boldsymbol{x}, \boldsymbol{u}^*)$) and write it as a solution of a first-order non-linear partial differential equation. Once an approximation of the *value function* $\mathcal{T}$ evaluated at the proper $\boldsymbol{x}_0$ is obtained, one can easily obtain both the optimal control $\boldsymbol{u}^*$ in feedback form and, by direct integration, the optimal trajectory $\boldsymbol{x}(t)$ that starts from $\boldsymbol{x}_0$. The method itself is greatly advantageous because it is able to reach the global minimum of the cost functional, even if the problem is not convex. The HJB approach allows also to have a global overview of the reachable sets i.e. the sets of starting points from which it is possible to reach the target. Beside all the advantages listed above, the HJB approach suffers from the well known "curse of dimensionality", so in general

it is restricted to problems in low dimension ($d \leq 3$). Moreover, it is much more expensive than the shooting method. The idea is then to solve the problem via the HJB method on a coarse grid, to have in short time a first approximation of the value function and the structure of the optimal trajectory. Then, we use this information to initialize the PMP shooting method and compute a precise approximation of the global minimum.

We plan also to investigate the case of limited resources (which introduces a further variable for each control used, as in [44]) and the case of linear costs added to the time-optimal request (which modifies the cost functional $J(u) = \int_0^T [1 + Pu(t)]dt$, as in [17]). In both cases we obtain bang-bang controls along with infinite order singular arcs, so the strategy used in this thesis to prove the existence of the optimal control cannot longer be applied and particular care must be used with the numerical solutions that are obtained with a combined method "HJB-shooting".

Part II

Capasso-Serio epidemic model applied to a network

5

Introduction

There is an astonishing number and variety of models and explanations for the spread and cause of epidemic outbreaks [3, 4, 8, 26, 30, 45, 47, 71]. The reason is that epidemiological models and computer simulations are useful experimental tools for building and testing theories, assessing quantitative conjectures, answering specific questions, determining sensitivities to changes in parameter values, and estimating key parameters in a field where data on human-to-human contacts are rare, often incomplete and complicated by many factors not of direct interest. Moreover, they allow to do "experiments" in a field where real experiments are impossible or unethical.

Understanding the transmission characteristics of infectious diseases in communities, regions, and countries can lead to better approaches to decrease their spreading. Mathematical models are used in comparing, planning, evaluating, and optimizing various detection, prevention, therapy, and control programs [46].

Another reason for this huge variety is that different diseases require different models and also, for the same disease, one can construct several models that takes into account different aspects of the underlying mechanisms.

Dependence of modelling conclusions on assumptions made is seldom straightforward. Some conclusions may depend very sensitively on parameter values or, more insidiously, on hypothesis implicit in the type of model chosen, for instance on the way in which it represents units of the population and contacts between them. Clearly good models must be realistic, but this does not mean the inclusion of all possible effects, but rather the incorporation of what appears to be the major components. For this reasons it is important, in the first stage, to keep models clear and simple as far as possible.

One of the simplest deterministic mathematical tool is the SIR model proposed by Kermack and McKendrick in 1927 [58, 59]. As we saw in Section 3.1, it is a three-compartment model that ignores almost every detail of a real epidemic, such as incubation, demographic and social structure of the population and spatial distribution of the individuals. It also neglects birth and natural death phenomena, since the time scale epidemic progress is considered much shorter than lifetime. Despite of these strong simplifications, this model is widely used since it is able to pose important questions with regard to the underlying mechanisms and possible ways of controlling the spread of a disease.

In the SIR model, the interaction term between susceptible and infected individuals is a mass action term proportional to a constant parameter, βSI. Using this type of interaction term we are implicitly assuming that the contact rate β increases linearly with the total population size N [46]. Naively, it might seem plausible that the population density and hence the contact rate would increase with population size, but the daily contact patterns of people are often similar in large and small communities, cities, and regions. Indeed, for human diseases the contact rate seems to be only very weakly dependent on the population size. This strongly suggests that *standard incidence* term, corresponding to an interaction term $\frac{\beta}{N}SI$, is more realistic for human diseases than the simple mass action incidence. This result is consistent with the concept that people are infected through their daily encounters and the patterns of daily encounters are largely independent of community size within a given country.

Even considering an SIR model with standard incidence term, the interaction term is a linearly increasing function of the number of infected individuals. This might be true for a small number of infectives, but appears quite unrealistic if the epidemic has infected a significant part of the population. Indeed, in this case some psychological effects become considerable and cannot be neglected. Capasso and Serio [21] in 1978 proposed a much more realistic model which involves a non-linear bounded interaction term of the form $g(I)S$; here the dependence on the number of infectives occurs via a non-linear bounded map g. This adjustment allows the possibility of introducing such a psychological effects: for I sufficiently high, g can be a decreasing function, since due to the presence of a very large number of infected individuals the population may tend to reduce the number of contacts per unit of time. Mathematically the modified model proposed by Capasso and Serio (hereafter named the CS model), obtained as a modification of the SIR model (3.1), appears as:

$$\begin{cases} \dot{S} = -\dfrac{g(I)S}{N} \\ \dot{I} = \dfrac{g(I)S}{N} - \mu I \\ \dot{R} = \mu I, \end{cases} \tag{5.1}$$

where μ is again the loss rate of infected individuals. We highlight the total population $N = S + I + R$ (that is constant, as in the SIR model) in order to suggest the use of the standard incidence rather than mass action law to model the infection term. Even though the total population is constant in time, and therefore the variable R can be obtained by the dynamics of $S(t)$ and $I(t)$, we do not reduce system (5.1) to a system of two equations, as we did in Section 3.1, because we want to use these epidemic models to create a network of dynamical systems that takes into account the three compartments.

In order to assure positivity, global existence and uniqueness of the solution of system (5.1), supplemented by a set of initial conditions as in (3.2), we will assume that the function $g : \mathbb{R}_+ \to \mathbb{R}$ satisfies the following conditions:

i) $\forall x \in \mathbb{R}_+ \ : \ g(x) \geq 0$
ii) $g(0) = 0$
iii) $\exists c \in \mathbb{R}_+ \setminus \{0\}$ s.t. $\forall x \in \mathbb{R}_+ \ : \ g(x) \leq c$
iv) the derivative of g exists and is bounded on any compact interval of $\mathbb{R}_+$, with $g'(0) > 0$
v) $\forall x \in \mathbb{R}_+ \ : \ g(x) \leq g'(0)x$.

It is easy to show that in the CS model, analogously to what happens in the SIR model, there exist an infinite number of equilibria that are located on the S-axis, which are unstable if their value is greater than $\mu/g'(0)$ and stable otherwise. Moreover, in a similar way we can define the basic reproduction number

$$\mathcal{R}_0^{(CS)} = \frac{g'(0)S_0}{N\mu}. \tag{5.2}$$

Also in this case, if its value is greater than 1 then the epidemic will spread among the population, otherwise the number of infectives will tend monotonically to zero.

While the temporal development of diseases and epidemics is widely investigated, the geographic spread of epidemics is less well understood and much less well studied. One of the main issues is how to include and quantify spatial effects. There are mainly two possible approaches: a continuous spatial distribution can be used [7], or

a discrete one that leads to a network of dynamical systems. In the first approach the variables of the system – such as the number of susceptible, infected and removed individuals in case of SIR and CS model – are functions of a space variable x (typically a 2-dimensional vector) as well as time; the spatial dispersal of the population is then modelled adding a diffusion term to each equation [70], converting the problem into a system of partial differential equations. This type of approach may not be always appropriate. Consider as an example a human specific disease that is spread by human-to-human contact in the context of a large country with a small number of potentially large cities, a very sparse or even non-existent rural population and a good transportation system. Then the movements from one city to another are fast, and the (eventual) propagation of an epidemic takes place only at the destination location. In this setting, travel of individuals between discrete geographical regions (cities) must play a relevant role in the spreading of the disease. This is a typical example of the discrete approach where a network structure is added to the system: its nodes determine the geometry of the system, representing the cities, and the disease can spread among the links that mimic the transportation system. The state at time t of each node will be described by its own compartments variables, leading to a number of ordinary differential equations linear in the number of nodes. Therefore the main disadvantage of this approach is the high dimensionality of the resulting model.

This Part of the thesis deals with a network of dynamical systems devised to simulate the spread of an epidemic in highly populated cities. Following the approach used in the paper by Stolerman et al. [85], in Section 6.1 we model the city structure by identifying the nodes of the graph with the neighbourhoods of the city, and using directed weighted edges to represent the fraction of people moving from one neighbourhood to another due to their daily routine activities. While in [85] the SIR model is used to describe the evolution of the disease inside each neighbourhood, we choose the generalized model by Capasso and Serio (5.1) in order to use a more realistic and flexible model that can take into account psychological effects that can arise if a significant part of the district is infected. Therefore, to each node we associate three ordinary differential equations that describe the evolution of the susceptible, infected and removed population that live in the neighbourhood. The equations that describe the dynamics of the compartments are obtained starting from the CS model (5.1) and taking into account the influence of the infected individuals that come from other districts. Then, in Section 6.2 we define the basic reproduction number for our epidemiological network. In Chapter 7 is performed the analytical study of the basic reproduction number for two particular network and parameters configurations, in order to analyse the stability of the disease free equilibrium, focusing on

the dependence upon geometry and heterogeneity of the infection rates of different neighbourhoods. More precisely, we will prove that in a homogeneous (with respect to the epidemiological parameters) network the mobility of people is irrelevant, while in a slightly heterogeneous network it could be an essential ingredient in avoiding an epidemic. Finally, Chapter 8 includes some concluding remarks and comments.

6

The Capasso-Serio epidemic model on a network

In this Chapter we consider a network of dynamical systems that simulates the spread of an epidemic inside a highly populated city. We model the city structure and the human daily routine mobility using a weighted directed network where each node represents a neighbourhood of the city and the weight of a generic directed link $i \to j$ reproduces the fraction of resident population of neighbourhood i that daily moves to node j. The evolution of the disease within each node is described by the Capasso-Serio model [21].

We are interested in determining whether an epidemic outbreak can be expected or not, depending on the parameters of the model. For this purpose, in Section 6.2 we define a proper basic reproduction number for our epidemic network model.

6.1 The model

We assume that the city has $M \geq 2$ neighbourhoods and thus we denote the set of the nodes of the network as $\mathcal{V} = \{1, 2, \dots, M\}$. The vertex i is connected to the vertex j with a directed link if there is a fraction of resident of i that travels to j daily, as an example for work purposes. We observe that the graph is directed, since there may generally be residential districts that are not significant employment centres. We summarize the geometry of the network with the weighted adjacency matrix Φ defined as:

$$\Phi_{M\times M} = \begin{pmatrix} \phi_{11} & \phi_{12} & \cdots & \phi_{1M} \\ \phi_{21} & \phi_{22} & \cdots & \phi_{2M} \\ \vdots & \vdots & \ddots & \vdots \\ \phi_{M1} & \phi_{M2} & \cdots & \phi_{MM} \end{pmatrix},$$

whose entries $\phi_{ij} \in [0, 1]$ are the fraction of resident population daily going from i to j. They can be measured using data from road traffic studies and public transportation companies. We assume that the time scale of the epidemic is sufficiently small such that we can, with a good approximation, consider the population of each district and the fractions of resident moving to others neighbourhoods as constants. Moreover, the out-strength of each node needs to be constant:

$$\sum_{k=1}^{M} \phi_{ik} = 1 \quad \forall i \in \mathcal{V}. \tag{6.1}$$

We assume that the evolution of the epidemic in an isolated district is governed by the differential equations of the Capasso-Serio model (5.1). Therefore, we divide each district population in three compartments: susceptible, infected or removed individuals. Then, the state of every vertex $i \in \mathcal{V}$ at time t is described by the variables $S_i(t)$, $I_i(t)$ and $R_i(t)$. Moreover, we assume that each district $i \in \mathcal{V}$ has its own non-linear incidence function g_i that satisfies conditions i)-v) given in Chapter 5. On the contrary, we suppose that the loss rate of infected individuals $\mu > 0$ is constant in every neighbourhood of the city.

As stated before, the total resident population of the i-th district is constant in time and is given by

$$N_i = S_i(t) + I_i(t) + R_i(t), \quad \forall i \in \mathcal{V}. \tag{6.2}$$

We remark that we are interested in introducing human mobility in this epidemic network model. Therefore, the number of people living in a given district is not the number of people that is present in the district during the day. To obtain this latter quantity, we have to take into account the value $\phi_{ki}N_k$ that represents the population of the vertex k that every day moves to vertex i. So, the present population of the vertex i is given by the individuals that come from all other districts plus $\phi_{ii}N_i$, which represents the population that lives and works in the same district i. So we can define the present population as

$$N_i^p = \sum_{k=1}^{M} \phi_{ki} N_k. \tag{6.3}$$

We use this quantity as normalizing factor for the equations of our modified CS model (5.1).

To define the equations that describe the dynamics of the susceptible individuals of a district we have to recall that they move and spread to all other neighbourhoods.

Therefore, we have to take into account what happens to the fraction of susceptibles of the i-th district that daily move to district j, whose amount is $\phi_{ij}S_i$. In node j they get in contact with the total number of infected individuals that are present during the day, namely

$$I_j^p = \sum_{k=1}^{M} \phi_{kj} I_k.$$

Since in the CS model the interaction term between susceptibles and infected individuals that are present in node j is described by the proper incidence function g_j, we can conclude that the dynamics of infection of the fraction of susceptibles of the i-th district that daily move to district j is given by

$$-g_j(I_j^p)\frac{\phi_{ij}S_i}{N_j^p}.$$

Summing up all the possible destinations of the susceptibles, namely summing over all the neighbourhoods, we obtain the differential equation that describes the evolution of the susceptible population of node i:

$$\dot{S}_i(t) = -\sum_{j=1}^{M} g_j \left(\sum_{k=1}^{M} \phi_{kj} I_k \right) \frac{\phi_{ij} S_i}{N_j^p}$$

The dynamics of the infected of node i will contain an analogous gain term from the susceptible population of that district and a loss term due to the mortality, recovery or isolation that is given by $-\mu I_i$. This term is much simpler than the previous one, since the loss rate μ is constant over the network. Clearly, this loss term becomes a gain term in the removed equations. Therefore the dynamics of the i-th node can be written as:

$$\begin{cases} \dot{S}_i = -\displaystyle\sum_{j=1}^{M} g_j \left(\sum_{k=1}^{M} \phi_{kj} I_k \right) \frac{\phi_{ij} S_i}{N_j^p} & \text{(6.4a)} \\ \dot{I}_i = \displaystyle\sum_{j=1}^{M} g_j \left(\sum_{k=1}^{M} \phi_{kj} I_k \right) \frac{\phi_{ij} S_i}{N_j^p} - \mu I_i & \text{(6.4b)} \\ \dot{R}_i = \mu I_i & \text{(6.4c)} \end{cases}$$

We observe that, since the resident population (6.2) is constant, the number of removed individuals can be obtained by

$$R_i(t) = N_i - S_i(t) - I_i(t),$$

and therefore we can focus on the dynamics of the susceptible and infected population only.

6.2 The basic reproduction number

In this Section we define the basic reproduction number $\mathcal{R}_0$ of this particular epidemic network model. We recall that, by definition, $\mathcal{R}_0$ is the number of secondary infections produced by a single infected individual who is introduced in a wholly susceptible population. If, as a mean value, more than one secondary infection is produced, obviously an epidemic occurs and this clarifies the importance of this parameter of the model.

To define the basic reproduction number typically one uses the definition and consider an infected unit inside a wholly susceptible population. In our case care must be taken. In fact, to insert an infected individual inside the population, we have to select a neighbourhood to whom he belongs, fixing as an example $I_i(0) = 1$ and $I_j(0) = 0$ in the other districts. Starting from that configuration, the number of secondary infections will strongly depend on the selected neighbourhood i, so this is not a good definition.

In order to establish $\mathcal{R}_0$ for our epidemic network model, we begin by introducing vector notation that takes into account the state of each vertex at time t. Thus we define

$$\boldsymbol{S}(t) = (S_1(t), S_2(t), \dots, S_M(t))^{\mathsf{T}}, \qquad \boldsymbol{I}(t) = (I_1(t), I_2(t), \dots, I_M(t))^{\mathsf{T}}.$$

For the purpose of defining the basic reproduction number we consider the disease free status of the system given by $\boldsymbol{S}^* = (N_1, N_2, \dots, N_M)^{\mathsf{T}}$ and $\boldsymbol{I}^* = (0, 0, \dots, 0)^{\mathsf{T}}$, which turns out to be an equilibrium for the system. We are interested in determining if a little perturbation in the number of infected individuals will cause the spread of the disease or won't affect the situation.

In this context, we say that the *disease spreads* if there exist at least one node i where $I_i(t) > I_i(0)$ for some $t > 0$.

First we define the perturbation vectors $\Delta\boldsymbol{S}(t) = \boldsymbol{S}(t) - \boldsymbol{S}^*$ and $\Delta\boldsymbol{I}(t) = \boldsymbol{I}(t) - \boldsymbol{I}^*$. Their dynamics come from the differential equation (6.4b) and in particular they are given by:

$$\begin{cases} \dfrac{d\Delta S_i}{dt} = -\displaystyle\sum_{j=1}^{m} g_j \left(\sum_{k=1}^{M} \phi_{kj} \Delta I_k \right) \frac{\phi_{ij}(\Delta S_i + N_i)}{N_j^p} \\ \dfrac{d\Delta I_i}{dt} = \displaystyle\sum_{j=1}^{N} g_j \left(\sum_{k=1}^{M} \phi_{kj} \Delta I_k \right) \frac{\phi_{ij}(\Delta S_i + N_i)}{N_j^p} - \mu \Delta I_i \\ i = 1, \dots, M \end{cases} \tag{6.5}$$

We consider the complete system of $2M$ equations (6.5) and we linearise it around the origin (that corresponds to the disease free equilibrium). Some simple calculations lead to the Jacobian matrix of the system evaluated at $\Delta \boldsymbol{S} = 0$, $\Delta \boldsymbol{I} = 0$ that can be written as a block matrix

$$J(0,0) = \begin{pmatrix} 0_{M\times M} & -\mu\mathcal{K} \\ 0_{M\times M} & \mu(\mathcal{K} - \mathbb{I}_{M\times M}) \end{pmatrix},$$

where

$$\mathcal{K} = \frac{1}{\mu}\begin{pmatrix} \sum_{j=1}^{M} \phi_{1j}^2 \frac{N_1}{N_j^p} g_j'(0) & \sum_{j=1}^{M} \phi_{1j}\phi_{2j} \frac{N_1}{N_j^p} g_j'(0) & \cdots & \sum_{j=1}^{M} \phi_{1j}\phi_{Mj} \frac{N_1}{N_j^p} g_j'(0) \\ \sum_{j=1}^{M} \phi_{2j}\phi_{1j} \frac{N_2}{N_j^p} g_j'(0) & \sum_{j=1}^{M} \phi_{2j}^2 \frac{N_2}{N_j^p} g_j'(0) & \cdots & \sum_{j=1}^{M} \phi_{2j}\phi_{Mj} \frac{N_2}{N_j^p} g_j'(0) \\ \vdots & \vdots & \ddots & \vdots \\ \sum_{j=1}^{M} \phi_{Mj}\phi_{1j} \frac{N_M}{N_j^p} g_j'(0) & \sum_{j=1}^{M} \phi_{Mj}\phi_{2j} \frac{N_M}{N_j^p} g_j'(0) & \cdots & \sum_{j=1}^{M} \phi_{Mj}^2 \frac{N_M}{N_j^p} g_j'(0) \end{pmatrix} \tag{6.6}$$

Therefore the linearised system is given by

$$\begin{cases} \dfrac{d\Delta \boldsymbol{S}}{dt} = -\mu\mathcal{K}\Delta \boldsymbol{I} \\ \dfrac{d\Delta \boldsymbol{I}}{dt} = \mu(\mathcal{K} - \mathbb{I})\Delta \boldsymbol{I}. \end{cases} \tag{6.7}$$

Let us focus on the infective equations. Using a uniform time mesh with time-step Δt we obtain the discrete equations:

$$\Delta \boldsymbol{I}(t_{n+1}) = [\mathbb{I} + \mu(\mathcal{K} - \mathbb{I})\Delta t]\Delta \boldsymbol{I}(t_n). \tag{6.8}$$

Now if we fix the time-step $\Delta t = 1/\mu$ in (6.8) we obtain $\Delta \boldsymbol{I}(t_{n+1}) = \mathcal{K}\Delta \boldsymbol{I}(t_n)$ and remembering that $\boldsymbol{I}^* = 0$ we end up with

$$\boldsymbol{I}(t_{n+1}) = \mathcal{K}\boldsymbol{I}(t_n).$$

Therefore, using some simple iterative arguments, we obtain the following result.

Proposition 6.1. *Let* $(\mathcal{V}, \Phi_{M\times M}; \{g_j\}_{j\in\mathcal{V}}, \mu)$ *be the Capasso-Serio epidemic network model defined by the set of nodes* $\mathcal{V}$*, the weighted adjacency matrix* Φ *and the set of non-linear incidence functions* $\{g_j\}_{j\in\mathcal{V}}$*, one for each node. Then, by considering a uniform time mesh with time step* $\Delta t = \mu$ *and* $\mathcal{K}$ *as in* (6.6)*, we have that*

$$\boldsymbol{I}(t_n) = \mathcal{K}^n \boldsymbol{I}(0) \tag{6.9}$$

describes the discrete dynamics of the infected individuals of the system linearised around the disease free equilibrium $(S_i^*, I_i^*) = (N_i, 0)$*,* $i \in \mathcal{V}$*.*

We can than observe that if the norm of the matrix $\mathcal{K}$ is greater than one then the norm of $\boldsymbol{I}$ will tend to infinity, and consequently the infection will spread among the population. On the contrary, if $||\mathcal{K}|| < 1$ the number of infected individuals will tend monotonically to 0. Therefore the matrix $\mathcal{K}$, or a function of that matrix, is a suitable candidate for the role of $\mathcal{R}_0$.

We follow the work by Diekmann et al. [31] and define the basic reproduction number using the norm of the matrix $\mathcal{K}$.

Definition 6.2. *The basic reproduction number* $\mathcal{R}_0$ *for the Capasso-Serio epidemic network model* $(\mathcal{V}, \Phi_{M\times M}; \{g_j\}_{j\in\mathcal{V}}, \mu)$ *is defined to be*

$$\mathcal{R}_0 = \lim_{n\to\infty} ||\mathcal{K}^n||^{\frac{1}{n}}, \tag{6.10}$$

namely the spectral radius $\rho(\mathcal{K})$*, where* $\mathcal{K}$ *is the matrix given in* (6.6) *and* $||\cdot||$ *is the matrix norm induced by the vector norm* $||\cdot||_1$*.*

Remark 1. The construction of $\mathcal{R}_0$ that is performed in this Section seems to depend on the chosen value of the time-step Δt: indeed, different values of Δt lead to different matrices in the discrete dynamics (6.9), whose spectral radius is used to define the basic reproduction number. However, we prove that $\mathcal{R}_0 = \rho(\mathcal{K})$ is a suitable choice for the basic reproduction number of the Capasso-Serio epidemic network model, regardless the chosen value of the time-step used to obtain the discrete dynamics. More precisely, we investigate the stability of the disease free equilibrium using the first Lyapunov criterion and prove that it is asymptotically stable if and only if $\rho(\mathcal{K}) < 1$.

Let us consider the second equation of the linearised system (6.7). It is a linear autonomous system, so it is well known that its solution $\Delta\boldsymbol{I}(t)$ tends asymptotically to zero if and only if for all eigenvalues $\lambda_{\mathcal{A}}$ of the matrix $\mathcal{A} = \mu(\mathcal{K} - \mathbb{I})$, $\mathrm{Re}(\lambda_{\mathcal{A}}) < 0$. There is a one-to-one correspondence between the eigenvalues of $\mathcal{A}$ and those of $\mathcal{K}$; more precisely if $\lambda_{\mathcal{A}}$ is an eigenvalue of $\mathcal{A}$, then $\lambda_{\mathcal{K}} = 1 + \lambda_{\mathcal{A}}/\mu$ is the corresponding

eigenvalue of $\mathcal{K}$. Therefore, the condition $\mathrm{Re}(\lambda_{\mathcal{A}}) < 0$ can be read as $\mathrm{Re}(\lambda_{\mathcal{K}}) < 1$ in terms of $\mathcal{K}$-eigenvalues.
Now we prove that the asymptotic stability of the disease free equilibrium, namely $\mathrm{Re}(\lambda_{\mathcal{K}}) < 1$, is equivalent to $\rho(\mathcal{K}) < 1$. Thanks to the Perron-Frobenius Theorem [49] we know that the spectral radius $\rho(\mathcal{K})$ is one of the (real) eigenvalues of $\mathcal{K}$, being $\mathcal{K}$ a non-negative matrix. So, if $\mathrm{Re}(\lambda_{\mathcal{K}}) < 1$ by hypothesis, then it is straightforward that $\rho(\mathcal{K}) < 1$. On the contrary, if $\rho(\mathcal{K}) < 1$, then for each eigenvalue $\lambda_{\mathcal{K}}$:

$$\mathrm{Re}(\lambda_{\mathcal{K}}) \leq |\lambda_{\mathcal{K}}| \leq \rho(\mathcal{K}) < 1.$$

7

The analytical study

Let us consider a Capasso-Serio epidemic network model $(\mathcal{V}, \Phi_{M\times M}; \{g_j\}_{j\in\mathcal{V}}, \mu)$, where the functions $\{g_j\}$ and μ define the epidemiological parameters of the model, while $\mathcal{V}$ and Φ define the underlying network. We model the epidemic dynamics by using the set of equations (6.4). Our purpose is to find some conditions under which the epidemic occurs. In the previous Chapter we proved that the epidemic occurs if and only if $\mathcal{R}_0 > 1$, where $\mathcal{R}_0$ is the basic reproduction number defined for this specific model in Definition 6.2.

Unfortunately, since it implies the calculation of the maximum eigenvalue of a $M \times M$ matrix which contains a large number of parameters (precisely M^2+2M+1 that take into account the elements of the weighted adjacency matrix, the present population numbers N_j^p for all $j \in \mathcal{V}$, the derivatives at the origin of g_j for all $j \in \mathcal{V}$, and finally the parameter μ), this is not a simple task. In particular, a general theory encompassing all possible network models will be difficult to develop. Therefore, as in paper [85], we will present results for a small but significant class of network models.

Definition 7.1. *We define a strictly homogeneous epidemic network model as the Capasso-Serio epidemic network model where all the nodes have the same incidence function $g_j(I) = g(I)$ for all $j \in \mathcal{V}$.*

Definition 7.2. *We define a homogeneous epidemic network model as the Capasso-Serio epidemic network model where the incidence function of each node has the same derivative at the origin, namely $g_j'(0) = g_0'$ for all $j \in \mathcal{V}$. We define as heterogeneous epidemic network models the Capasso-Serio epidemic network model that do not satisfy that condition.*

Instinctively, if we want to model a city where all the neighbourhoods have the same "epidemiological properties", it is natural to think about a strictly homogeneous epidemic network. This is the case of epidemics driven by human-to-human contact,

where local variation in human behaviours might be neglected, leading to a strictly homogeneous epidemic network model with respect to the rates of infection. However, we will see that the same basic reproduction number and the same stability results holds for a wider class of models, that is what we call homogeneous epidemic network models class. On the contrary, heterogeneous epidemic network models can be used to model vector-driven epidemics; as an example, in dengue fever different rates of infections are related to variations in mosquito densities among the city neighbourhoods.

Making this distinction between homogeneous and heterogeneous epidemic network allows us to distinguish the roles played by epidemic and movement parameters.

7.1 Homogeneous epidemic network models

The following theorem shows that when the Capasso-Serio epidemic network model is homogeneous, namely all the vertices have incidence functions g_j, $j \in \mathcal{V}$ such that their derivatives at the origin coincide, then the basic reproduction number is simply $\mathcal{R}_0^{hom} = g_0'/\mu$. This implies that the infection will spread if $g_0' > \mu$, independently of the geometry of the network, the human fluxes between different districts, the type of non-linearity of the incidence function, nor the number of susceptible individuals.

We observe that this result does not even need the network to be connected. This is a further proof of the fact that the value of the basic reproduction number can tell *if* the disease will spread through the city, but not *where*.

Theorem 7.3. *Let $(\mathcal{V}, \Phi_{M\times M}; \{g_j\}_{j\in\mathcal{V}}, \mu)$ be a Capasso-Serio epidemic network model whose dynamics are described by the differential system (6.4). Suppose that the epidemic network is homogeneous, namely that $g_j'(0) = g_0'$ for all $j \in \mathcal{V}$. Then the basic reproduction number is $\mathcal{R}_0^{hom} = g_0'/\mu$, therefore the epidemic will spread if and only if $g_0' > \mu$.*

Proof. It is easy to see that in this case the matrix $\mathcal{K}$ is given by

$$\mathcal{K} = \frac{g_0'}{\mu}\mathcal{C},$$

where

$$\mathcal{C} = \begin{pmatrix} \sum_{j=1}^{M} \phi_{1j}^2 \frac{N_1}{N_j^p} & \sum_{j=1}^{M} \phi_{1j}\phi_{2j} \frac{N_1}{N_j^p} & \cdots & \sum_{j=1}^{M} \phi_{1j}\phi_{Mj} \frac{N_1}{N_j^p} \\ \sum_{j=1}^{M} \phi_{2j}\phi_{1j} \frac{N_2}{N_j^p} & \sum_{j=1}^{M} \phi_{2j}^2 \frac{N_2}{N_j^p} & \cdots & \sum_{j=1}^{M} \phi_{2j}\phi_{Mj} \frac{N_2}{N_j^p} \\ \vdots & \vdots & \ddots & \vdots \\ \sum_{j=1}^{M} \phi_{Mj}\phi_{1j} \frac{N_M}{N_j^p} & \sum_{j=1}^{M} \phi_{Mj}\phi_{2j} \frac{N_M}{N_j^p} & \cdots & \sum_{j=1}^{M} \phi_{Mj}^2 \frac{N_M}{N_j^p} \end{pmatrix}. \tag{7.1}$$

We prove that the spectral radius of the matrix $\mathcal{C}$ is $\rho(\mathcal{C}) = 1$. This leads to the thesis, since the spectral radius of $\mathcal{K}$ is $\rho(\mathcal{K}) = \frac{g_0'}{\mu}\rho(\mathcal{C})$ and therefore $\rho(\mathcal{K}) = \frac{g_0'}{\mu}$. To determine the spectral radius of $\mathcal{C}$ we use the following Lemma (see Lemma 8.1.21 in [49]).

Lemma 7.4. *Let $A = (a_{ij})$ be a squared $n \times n$ non-negative matrix. If all the column sums are equal to c, then $\rho(A) = ||A||$, where*

$$||A|| = \max_{r=1,\dots,n} \sum_{s=1}^{n} a_{sr} = \sum_{s=1}^{n} a_{s1} = c$$

is the matrix norm induced by the vector norm $||\cdot||_1$.

Since each element of matrix $\mathcal{C}$ is given by the sum of non-negative quantities, the matrix itself is non-negative. Moreover, the sum of the elements of the generic column r is:

$$\begin{aligned} \sum_{s=1}^{n} \mathcal{C}_{sr} &= \sum_{s=1}^{n} \sum_{j=1}^{M} \phi_{sj}\phi_{rj} \frac{N_s}{N_j^p} \\ &= \sum_{j=1}^{M} \frac{\phi_{rj}}{N_j^p} \underbrace{\sum_{s=1}^{n} \phi_{sj} N_s}_{N_j^p} = \underbrace{\sum_{j=1}^{M} \phi_{rj}}_{\text{out-strength}} = 1, \end{aligned}$$

where we have used definition (6.3) and property (6.1).

□

7.2 Heterogeneous fully connected epidemic network models with constant fluxes

Starting from an homogeneous epidemic network, we want to introduce an inhomogeneity in the rates of infection by modifying the incidence function of one of the nodes. The crucial question is whether this perturbation can qualitatively change the stability of the disease free equilibrium; in other words, we want to test the robustness of an homogeneous network. We focus on the simplest network structure: a fully connected network where the resident population and the fluxes between the nodes are constant. We do this choice in order to simplify the study and, more important, to focus on the modification of the incidence terms.

Let us consider a Capasso-Serio epidemic network model $(\mathcal{V}, \Phi_{M\times M}; \{g_j\}_{j\in\mathcal{V}}, \mu)$ where the resident population of each node is constant: $N_i = N_{\text{res}} > 0$ for all $i \in \mathcal{V}$. We assume that the network is fully connected and that the fractions of movements between any two nodes is a positive constant ϕ_0. Then the components of the weighted adjacency matrix Φ are defined by

$$\phi_{ij} = \begin{cases} \phi_0 & \text{if } i \neq j \\ 1-(M-1)\phi_0 & \text{if } i = j, \end{cases} \tag{7.2}$$

where $0 < \phi_0 \leq \frac{1}{M-1}$, so the weighted adjacency matrix has nonnegative entries, and the value of ϕ_{ii} is chosen to satisfy the conservation of the out-strength of each node (6.1).

We arbitrarily choose a node that will have a different non-linear incidence function. Without loss of generality, suppose that

$$g_j(I) = g(I), \quad j = 1, 3, 4, \ldots, M, \qquad g_2(I) = h(I), \tag{7.3}$$

where both g and h are incidence functions that satisfy conditions i)-v) of Chapter 5. We will prove that the spreading results will depend on the derivative only, as in the homogeneous case. More specifically, we will be interested only in the values $g'(0)$ and $h'(0)$. Let us define the ratio between the two as

$$\zeta = \frac{h'(0)}{g'(0)}. \tag{7.4}$$

Theorem 7.5. *Let $(\mathcal{V}, \Phi_{M\times M}; \{g_j\}_{j\in\mathcal{V}}, \mu)$ be a Capasso-Serio epidemic network model whose dynamics are described by the differential system (6.4). Suppose that the resident population at the nodes are equal, $N_i = N_{res} > 0$ for all $i \in \mathcal{V}$, and that*

the weighted adjacency matrix Φ is defined as in (7.2). Moreover, suppose that each node has the same incidence function g, except the second one, as stated in (7.3). Under these conditions we can obtain conditions guaranteeing the stability of the disease free equilibrium. More precisely, suppose that g and μ are given such that the disease in the homogeneous case does not spread, namely $\mathcal{R}_0^{hom} = g_0'/\mu < 1$. Then, considering the ratio ζ defined in (7.4) we can state that:

- *the disease free equilibrium is stable if*

$$\zeta < \frac{1}{\mathcal{R}_0^{hom}};$$

- *the disease free equilibrium is unstable if*

$$\zeta > \zeta^{crit} = 1 + \frac{1 - \mathcal{R}_0^{hom}}{\mathcal{R}_0^{hom}} M;$$

- *if $\dfrac{1}{\mathcal{R}_0^{hom}} < \zeta < \zeta^{crit}$ the stability depends upon the value ϕ_0; more specifically, the disease free equilibrium is stable if $\phi_0 \in \mathcal{I}$, where*

$$\mathcal{I} = \left(\frac{1}{M} - \tilde{\phi_0},\ \min\left\{ \frac{1}{M} + \tilde{\phi_0},\ \frac{1}{M-1} \right\} \right)$$

and

$$\tilde{\phi_0} = \frac{1}{M} \sqrt{\frac{\mathcal{R}_0^{hom}\zeta + \mathcal{R}_0^{hom}(M-1) - M}{\mathcal{R}_0^{hom}(\mathcal{R}_0^{hom} M\zeta - M\zeta + \zeta - 1)}},$$

otherwise it is unstable.

Proof.

7.2.1 Conditions for stability

We want to find conditions on the parameters of the model such that all the eigenvalues of the matrix $\mathcal{K}$ relevant to our system are within the unit circle, so that $\rho(\mathcal{K}) = \mathcal{R}_0 < 1$.

We recall that the components of matrix $\mathcal{K}$ are given by:

$$\mathcal{K}_{rs} = \frac{1}{\mu} \sum_{j=1}^{M} \phi_{rj}\phi_{sj} \frac{N_r}{N_j^p} g_j'(0). \tag{7.5}$$

Moreover, we observe that under our hypothesis:

$$N_j^p = \sum_{k=1}^{M} \phi_{kj} N_k = N_{\text{res}} \sum_{k=1}^{M} \phi_{kj} = N_{\text{res}},$$

since the weighted adjacency matrix in this case is symmetric and holds (6.1). Substituting this value in (7.5) and recalling that $N_r = N_{\text{res}}$ for all $r \in \mathcal{V}$ we obtain

$$\mathcal{K}_{rs} = \frac{1}{\mu} \sum_{j=1}^{M} \phi_{rj} \phi_{sj} g_j'(0).$$

Using proper values of the weights ϕ_{ij} given in (7.2) and the hypothesis on the incidence functions (7.3) we obtain, after some simple but lengthy calculations, that the matrix $\mathcal{K}$ for our heterogeneous fully connected epidemic network models with constant fluxesis given by

$$\mathcal{K}^{het} = \mathcal{P} + \mathcal{D},$$

where

$$\mathcal{P} = \frac{g_0'}{\mu} \begin{pmatrix} p & q & p & \cdots & \cdots & p \\ q & p & q & \cdots & \cdots & q \\ p & q & p & \cdots & \cdots & p \\ \vdots & \vdots & \vdots & \ddots & \vdots & \vdots \\ \vdots & \vdots & \vdots & \vdots & p & p \\ p & q & p & \cdots & p & p \end{pmatrix}, \qquad \mathcal{D} = \frac{g_0'}{\mu} \begin{pmatrix} d_1 & 0 & 0 & \cdots & \cdots & 0 \\ 0 & d_2 & 0 & \cdots & \cdots & 0 \\ 0 & 0 & d_1 & 0 & \cdots & 0 \\ \vdots & \vdots & 0 & \ddots & \ddots & \vdots \\ \vdots & \vdots & \vdots & \ddots & \ddots & 0 \\ 0 & 0 & 0 & \cdots & 0 & d_1 \end{pmatrix},$$

given the constant values

$$\begin{aligned} p &= \phi_0 \big[2 - (M+1)\phi_0 + \phi_0 \zeta\big] \\ q &= \phi_0 \big[1 - \phi_0 + \big(1 - (M-1)\phi_0\big)\zeta\big] \\ d_1 &= (M\phi_0 - 1)^2 \\ d_2 &= (M\phi_0 - 1)\big[2\phi_0 + \big(M\phi_0 - 2\phi_0 - 1\big)\zeta\big]. \end{aligned} \tag{7.6}$$

Using the diagonal expansion method [24] we can write the characteristic polynomial that gives the eigenvalues λ of $\mathcal{K}$. More specifically, we have to calculate the determinant $|\mathcal{P} + \mathcal{D}'|$, where $\mathcal{D}' = \mathcal{D} - \lambda \mathbb{I}$. Let us consider a generic subset $\theta \subset \mathcal{V}$ of the vertex set and denote by $\bar{\theta}$ the complement of θ in $\mathcal{V}$. Given an $M \times M$ matrix A we denote by $A(\theta)$ the submatrix obtained by deleting all rows and columns not

indexed by θ. Using the diagonale expansion method, the characteristic polynomial can be expanded as a summation over all possible submatrices:

$$|\mathcal{P}+\mathcal{D}'| = \sum_{\theta\subset\mathcal{V}} |\mathcal{P}(\theta)||\mathcal{D}'(\bar{\theta})|.$$

It is easy to see that $\mathcal{P}$ has rank two, therefore all its submatrices bigger than 2×2 have determinant zero. The only subsets θ such that $|\mathcal{P}(\theta)| \neq 0$ are the empty set $\emptyset$, the singleton sets $\{k\}$ for each $k \in \mathcal{V}$, the two-elements sets $\{2,k\}$ for $k = 1,3,4,\ldots,M$. Therefore we can simplify

$$|\mathcal{P}+\mathcal{D}'| = |\mathcal{P}(\emptyset)||\mathcal{D}'(\mathcal{V})| + \sum_{k\in\mathcal{V}} |\mathcal{P}(\{k\})||\mathcal{D}'(\overline{\{k\}})| + \sum_{k\in\mathcal{V}} |\mathcal{P}(\{2,k\})||\mathcal{D}'(\overline{\{2,k\}})|.$$

Again, some simple and lengthy calculations bring to

$$\begin{aligned}|\mathcal{P}+\mathcal{D}'| = (\mathcal{R}_0^{hom}d_1-\lambda)^{M-2}\Big(&\lambda^2 - \mathcal{R}_0^{hom}(d_1+d_2+pM)\lambda \\ &+ (\mathcal{R}_0^{hom})^2\big(d_1d_2 + p(M-1)d_2 + pd_1 + (M-1)(p^2-q^2)\big)\Big).\end{aligned} \tag{7.7}$$

Clearly, $\mathcal{R}_0^{hom}d_1 = \mathcal{R}_0^{hom}(M\phi_0-1)^2$ is an eigenvalue of the matrix $\mathcal{K}$, with molteplicity $M-2$ and therefore the first condition in order to have stability is

$$\mathcal{R}_0^{hom}(M\phi_0-1)^2 < 1. \tag{7.8}$$

Indeed, since $0 < \phi_0 \leq \frac{1}{M-1}$ and $\mathcal{R}_0^{hom} < 1$ by hypothesis, (7.8) turns out to be a trivial condition that is always satisfied.

In order to study the remaining eigenvalues we use Jury conditions [71], which allow us to force the eigenvalues module inside the unit circle without explicitly calculating them.

The Jury conditions that assure that the roots of a second order polynomial $P(\lambda) = \lambda^2 + a_1\lambda + a_0$ lay inside the unit circle are the following:

$$P(1) = 1 + a_1 + a_0 > 0, \quad P(-1) = 1 - a_1 + a_0 > 0, \quad P(0) = a_0 < 1. \tag{7.9}$$

In our case, substituting proper value of the constants given in (7.6), the coefficient of the polynomial given in (7.7) become

$$\begin{aligned}a_0 &= (\mathcal{R}_0^{hom})^2\zeta(M\phi_0-1)^2 \\ a_1 &= -\mathcal{R}_0^{hom}(1 + M\phi_0^2 + \zeta M^2\phi_0^2 - \zeta M\phi_0^2 - 2\zeta M\phi_0 - 2\phi_0 + 2\zeta\phi_0 + \zeta).\end{aligned}$$

If we use this constants to evaluate the Jury conditions given in (7.9) we obtain

$$P(1) = 1 + \mathcal{R}_0^{hom}\left[\zeta(\mathcal{R}_0^{hom}(M\phi_0 - 1)^2 - (M-1)\phi_0(M\phi_0 - 2) - 1) + \phi_0(2 - M\phi_0) - 1\right]$$
$$P(-1) = 1 + \mathcal{R}_0^{hom}\left[\zeta(\mathcal{R}_0^{hom}(M\phi_0 - 1)^2 - (M-1)\phi_0(M\phi_0 - 2) + 1) - \phi_0(2 - M\phi_0) + 1\right]$$

And therefore the three conditions that we want to hold are:

$$1 + \mathcal{R}_0^{hom}[\zeta(\mathcal{R}_0^{hom}(M\phi_0 - 1)^2 - (M-1)\phi_0(M\phi_0 - 2) - 1) + \phi_0(2 - M\phi_0) - 1] > 0 \tag{7.10}$$
$$1 + \mathcal{R}_0^{hom}[\zeta(\mathcal{R}_0^{hom}(M\phi_0 - 1)^2 - (M-1)\phi_0(M\phi_0 - 2) + 1) - \phi_0(2 - M\phi_0) + 1] > 0 \tag{7.11}$$
$$(\mathcal{R}_0^{hom})^2\zeta(M\phi_0 - 1)^2 < 1. \tag{7.12}$$

We prove that condition (7.11) is always satisfied, thanks to our hypothesis. We prove that the term contained in square brackets is positive. Clearly $\mathcal{R}_0^{hom}(M\phi_0 - 1)^2 > 0$. The remaining of the coefficient of ζ is a second order polynomial in the variable ϕ_0 with negative discriminant, therefore always positive. Let us focus on the remaining of the sum, supposing $M \geq 3$:

$$1 - 2\phi_0 + M(\phi_0)^2 \geq 1 - \frac{2}{M-1} + M(\phi_0)^2 > 0,$$

thanks to the range of acceptable values of ϕ_0. Whereas, if $M = 2$, then $1 - 2\phi_0 + M(\phi_0)^2$ is again a second order polynomial with negative discriminant, thus always positive.

Therefore, in order to assure stability of the disease free equilibrium, we have to verify conditions (7.10) and (7.12).

7.2.2 The case $\zeta < 1/\mathcal{R}_0^{hom}$

We prove that conditions (7.10) and (7.12) are true if $\zeta < 1/\mathcal{R}_0^{hom}$. This threshold comes from the study of the weakly connected network where ϕ_0 is very small. Indeed, in this case we can neglect second order terms ϕ_0^2 and the conditions for stability, rephrased to highlight the variable ζ, become

$$\zeta < \frac{1}{(\mathcal{R}_0^{hom})^2 - 2M(\mathcal{R}_0^{hom})^2\phi_0}$$
$$\zeta < \frac{(1 - \mathcal{R}_0^{hom}) + 2\phi_0\mathcal{R}_0^{hom}}{\mathcal{R}_0^{hom}((1 - \mathcal{R}_0^{hom})(1 - 2M\phi_0) + 2\phi_0)}.$$

In the limit $\phi_0 \to 0$, these conditions become $\zeta < 1/(\mathcal{R}_0^{hom})^2$ and $\zeta < 1/\mathcal{R}_0^{hom}$, respectively. Since $\mathcal{R}_0^{hom} < 1$, the latter condition is more restrictive, so we can conclude that $\zeta = \dfrac{1}{\mathcal{R}_0^{hom}}$ is a threshold for the stability of a weakly connected network.

Now we prove that under this threshold the disease free equilibrium is always stable, no matter the value of $\phi_0 \in (0, (M-1)^{-1}]$. If $\zeta < 1/\mathcal{R}_0^{hom}$, then condition (7.12) is always verified since

$$\mathcal{R}_0^{hom}\zeta(M\phi_0 - 1)^2 < \mathcal{R}_0^{hom}(M\phi_0 - 1)^2 < 1.$$

Let us consider condition (7.10). Since we want to use the hypothesis $\zeta < 1/\mathcal{R}_0^{hom}$, we evaluate the sign of the coefficient of parameter ζ. It can be seen as a second order polynomial in the variable ϕ_0:

$$\alpha(\phi_0) = M(\mathcal{R}_0^{hom}M - M + 1)\phi_0^2 - 2(\mathcal{R}_0^{hom}M - M + 1)\phi_0 + \mathcal{R}_0^{hom} - 1.$$

Its reduced discriminant is given by $\mathcal{R}_0^{hom}M - M + 1$, which is also the coefficient of the second order term. If it is negative, then $\alpha(\phi_0) < 0$ for every admissible value of ϕ_0. If it is equal to zero, then the polynomial reduces to $\alpha(\phi_0) = \mathcal{R}_0^{hom} - 1 < 0$. On the contrary, if it is positive, it is easy to see that the polynomial is negative between its two roots $\phi_0^{(-)}$ and $\phi_0^{(+)}$ that contains the admissibility range of ϕ_0: $(0, (M-1)^{-1}] \subset (\phi_0^{(-)}, \phi_0^{(+)})$. As a consequence, the coefficient $\alpha(\phi_0)$ is negative for each value of $\mathcal{R}_0^{hom} < 1$, $M \geq 2$ and $0 < \phi_0 \leq (M-1)^{-1}$.

Therefore, for condition (7.10) holds:

$$\begin{aligned} &1 + \mathcal{R}_0^{hom}\alpha(\phi_0)\zeta + \mathcal{R}_0^{hom}\phi_0(2 - M\phi_0) - \mathcal{R}_0^{hom} \\ &> 1 + \alpha(\phi_0) + \mathcal{R}_0^{hom}\phi_0(2 - M\phi_0) - \mathcal{R}_0^{hom} \\ &= (\mathcal{R}_0^{hom}M - M + 1 - \mathcal{R}_0^{hom})(M\phi_0^2 - 2\phi_0). \end{aligned}$$

The first factor is always negative, since it can be decomposed in $(M-1)(\mathcal{R}_0^{hom} - 1)$, and also the latter factor is negative, since for $M \geq 2$ it holds $1/(M-1) \leq 2/M$.

As a result, all Jury conditions are satisfied and therefore the disease free equilibrium is stable, whenever $\zeta < 1/\mathcal{R}_0^{hom}$.

7.2.3 The case $\zeta > 1/\mathcal{R}_0^{hom}$

Suppose now that $\zeta > 1/\mathcal{R}_0^{hom}$. We want to determine values of the parameters for which conditions (7.10) and (7.12) hold. Rephrasing condition (7.10) we obtain as usual a second order polynomial in the variable ϕ_0:

$$p(\phi_0) = M\mathcal{R}_0^{hom}(\mathcal{R}_0^{hom}M\zeta - M\zeta + \zeta - 1)\phi_0^2 - 2\mathcal{R}_0^{hom}(\mathcal{R}_0^{hom}M\zeta - M\zeta + \zeta - 1)\phi_0 + (\mathcal{R}_0^{hom}\zeta - 1)(\mathcal{R}_0^{hom} - 1) > 0.$$

Since the constant term $(\mathcal{R}_0^{hom}\zeta - 1)(\mathcal{R}_0^{hom} - 1)$ is negative, if the discriminant of the polynomial is also negative, then condition (7.10) can't be satisfied. So we look for conditions on the parameters for which the discriminant has positive value, which turn out to be $1/\mathcal{R}_0^{hom} < \zeta < \zeta^{crit}$ and, if $(M-1)/M < \mathcal{R}_0^{hom} < 1$, also $\zeta > \bar{\zeta}$, where

$$\zeta^{crit} = 1 + M\frac{1 - \mathcal{R}_0^{hom}}{\mathcal{R}_0^{hom}}, \qquad \bar{\zeta} = \frac{1}{\mathcal{R}_0^{hom}M - M + 1}. \tag{7.13}$$

In the latter case, the polynomial $p(\phi_0)$ is a parabola opening to the top; some simple calculations prove that the interval $(0, (M-1)^{-1}]$ is contained within the zeroes of the parabola, therefore $p(\phi_0)$ is negative for each admissible value of ϕ_0. So the only possible range of stability for the disease free equilibrium is $1/\mathcal{R}_0^{hom} < \zeta < \zeta^{crit}$, where $p(\phi_0)$ is a parabola opening on the bottom. Its zeroes are

$$\phi^{\pm} = \frac{1}{M} \pm \frac{1}{M}\sqrt{\frac{\mathcal{R}_0^{hom}\zeta + \mathcal{R}_0^{hom}(M-1) - M}{\mathcal{R}_0^{hom}(\mathcal{R}_0^{hom}M\zeta - M\zeta + \zeta - 1)}}. \tag{7.14}$$

By Descartes' rule of sign, we easily prove that both zeroes of the polynomial are positive. Depending on the values of the parameters, ϕ^+ can be greater or less than $(M-1)^{-1}$, so the values of ϕ_0 for which condition (7.10) is satisfied are those belonging to

$$\mathcal{I} = \left(\phi_0^-, \min\left\{\phi_0^+, \frac{1}{M-1}\right\}\right). \tag{7.15}$$

Summing up these results, condition (7.10) is satisfied if

$$\zeta \in \left(\frac{1}{\mathcal{R}_0^{hom}}, \zeta^{crit}\right), \qquad \phi_0 \in \mathcal{I},$$

where ζ^{crit} and $\mathcal{I}$ are defined in (7.13) and (7.15). For these values of the parameters we verify condition (7.12), by proving that

$$\sup_{\zeta \in \left(1/\mathcal{R}_0^{hom}, \zeta^{crit}\right)} \sup_{\phi_0 \in \mathcal{I}} \zeta(M\phi_0 - 1)^2 < \frac{1}{(\mathcal{R}_0^{hom})^2}.$$

It is easy to prove that $(M\phi_0 - 1)^2$ attains its maximum value in ϕ_0^-, which is the radicand of (7.14). Then we have to prove that

$$\sup_{\zeta\in\left(1/\mathcal{R}_0^{hom},\,\zeta^{crit}\right)} \underbrace{\zeta\frac{\mathcal{R}_0^{hom}\zeta+\mathcal{R}_0^{hom}(M-1)-M}{(\mathcal{R}_0^{hom}M-M+1)\zeta-1}}_{f(\zeta)} < \frac{1}{\mathcal{R}_0^{hom}}.$$

By a simple analysis of the rational function $f(\zeta)$ we find that it is defined and monotonically decreasing in the whole domain $\left(1/\mathcal{R}_0^{hom},\,\zeta^{crit}\right)$. At its border the value of the function is

$$f\left(\frac{1}{\mathcal{R}_0^{hom}}\right)=1, \qquad f(\zeta^{crit})=0$$

And therefore the supremum of $f(\zeta)$, which is also a maximum, is the constant value 1. From our hypothesis, the resulting condition $1<\mathcal{R}_0^{hom}$ is straightforward. Therefore, whenever condition (7.10) is satisfied, then also condition (7.12) holds, and with that stability of the disease free equilibrium is achieved.

□

8

Discussion and conclusions

In this Part of the thesis we have proposed a network of dynamical systems that simulates the spread of a human-to-human disease in a highly populated city. The population of the city has been divided in three compartments: susceptibles, infected and removed individuals. Their dynamics are described by a Capasso-Serio model, with non-linear incidence function, which is a model that is able to take into account psychological effects that derives from the spread of an epidemic. We have supposed that the city is divided in several neighbourhoods and we have allowed each of them to have different incidence function, namely different epidemiological parameters. We have described the topology of the city using a weighted directed graph where each node represents a neighbourhood and the intensity of the directed links represents the fraction of people moving from one neighbourhood to another due to their daily routine activities. Therefore, in describing the dynamics of the resident population of district i, we took into account that: (i) there is a fraction of susceptibles of node i that spends most of its time in the other districts; (ii) the fraction of susceptibles of node i that during the day stays in node j might be infected by an infective individual that is present in district j, which can come from another district k. Therefore, the dynamics of the susceptibles of node i is influenced by infected individuals of all other nodes.

We have looked for a suitable definition of the basic reproduction number for our epidemiological network model; such a definition had to respect the classical threshold role: if the value of the basic reproduction number is greater than one, then the infection will spread among the population, otherwise it will die out monotonically.

Then we have considered two particular epidemiological network model, focusing on epidemiological parameters. First we have considered an homogeneous epidemic network, where each neighbourhood had the same derivative calculated at the origin of the non-linear incidence term $g'_j(0) = g'_0$, for all $j \in \mathcal{V}$. We have proved that the

conditions that determine the spread of the disease only concern the epidemiological parameters of the model, while are independent of the geometry of the system. Then, in order to test the robustness of the homogeneous epidemic network, we have considered a slightly heterogeneous epidemic network by modifying the derivative of the non-linear incidence function of a single district: $g_j'(0) = g_0'$, for all $j \neq 2$, $g_2'(0) = \zeta g_0'$. We have taken as geometry of the system the simple as possible: we have considered that the flux of individuals between two different nodes is constant. We have proved that, if the factor ζ is sufficiently high, then the epidemic can spread for some values of the other epidemiological and geometrical parameters. Moreover, if ζ overcomes a critical value, then the epidemic will always spread, independently of the other parameters of the model.

Therefore, we proved that if the epidemiological parameters are heterogeneous, the geometry of the system (intended as the movement rates set-up) becomes crucial in determining if the epidemic will spread: indeed, even in a simple fully connected network with identical weights, the value of the constant movement rate may condition the evolution of the disease. Moreover, we remark that we found same condition for the spread of the epidemic in slightly heterogeneous systems as the one found in [85], even if the SIR model is not a particular case of the Capasso-Serio model, since it does not satisfy condition iii) on the non-linear incidence function (see Chapter 5). The main reason is that the study is performed linearising the dynamics of the complex network around the origin. The linearised models obtained both starting from SIR epidemic model and from CS epidemic model coincide, provided the identification of β_j and $g_j'(0)$.

In our opinion, future perspectives and developments may involve the modification of the underlying epidemiological model that describes the evolution of the disease within the single node, as an example SEIR or SIRS models [46]. Furthermore, in order to make the introduction of the psychological effects more realistic, we can introduce the dependence on the number of infected individuals of district i and j in the movement coefficients relevant to those districts: if the epidemic overwhelm one of the two nodes, we expect a change in the behaviour of both resident populations. A peculiarity of this model is that the movement rates of susceptible and infected individuals coincide. This can be the case of diseases that induce mild symptoms such as cold, whereas, if the disease is more limiting, different movement rates for susceptible and infected individuals are more accurate. Therefore, a possible improvement of the model is the introduction of an additional parameter $c \leq 1$: if ϕ_{ij} is the movement rate of susceptible individuals from node i to node j, then $c\phi_{ij}$ will represent the movement rate of the corresponding infected individuals. We observe

that in the limit case $c = 1$ we recover the model that is here presented, while if its value tends toward zero we are describing a disease that induces severe symptoms.

As further development of the model, we can add a control (such as vaccination or isolation) that can be applied at different rates in each neighbourhood and look for the optimal solution that eradicates the disease in minimum time, possibly with resources or cost constraints.

We expect that these improvements of the model lead to a more detailed and realistic description of the diffusion of the epidemic through the districts. Although the used model is quite simple, we found a rich behaviour in the epidemic spread. We hope that the introduction of psychological effects and the study of an optimal control might help in planning efficient control strategies.

Part III

A network landscape model: stability analysis and numerical tests

9

Introduction

The problem of understanding the governing principles of ecosystems can be even found in a paper by Lotka [65] in 1922. But it is at the beginning of this century that the problem of a quantitative evaluation of an environmental system has been posed within the so-called discipline of *Landscape Ecology*. In fact, the European Landscape Convention of 2000 has encouraged all the European countries to define their landscape objectives on the ground of management and planning of territory through government, conservation and protection of landscapes. On this subject it is now possible to find a large bibliography (see amongst others [54, 63, 73] and the bibliography therein).

Landscape Ecology may be considered an interdisciplinary field of research involving at the same time empirical testing and mathematical modelling. In this context an environmental system [37] is considered as a spatially extended heterogeneous system that can be distributed in several Landscape Units (LU), that are sections of the territory whose borders are identified by natural or anthropic barriers (roads, speedways, railways, building, industrial infrastructures, rivers, hill ridges, ...) exchanging flows of materials and bio-energy. Moreover, each LU is formed by different biotopes, each characterized by an uniform land cover of vegetation. From a quantitative point of view each LU, often called *ecological sector*, is characterized by a synthetic index of ecological system functionality, that we will call *bio-energy*, and by its capability of transmitting such an energy to the neighbouring sectors. Such a characterization of an environmental system has been considered in the book [34] where a quantitative evaluation of its ecological state has been proposed by the so-called *ecological graph* which, through the computation of suitable indicators (see [35, 39]) determinable by the *Geographic Information System* (GIS) [72], fixes the values of bio-energy production and flux to the neighbours. On the other hand, the ecological graph may be considered a static picture of the ecological state of the system, whereas natural

ecosystems stand in a meta-stable equilibrium which can be modified later in time in a significant way under strong perturbations due to human land uses impact or to natural events [76, 86]. For this reason, simulation by mathematical models may be an useful and reliable tool for the information about environment trend towards possible future scenarios, presenting even bifurcation phenomena, for some critical values of environmental indicators [77, 87].

A first attempt in this direction has been proposed in papers [38, 39] where a mathematical model represented by a set of ODEs has been derived. In particular, the main idea of these papers, as well as that of the present one, consists in considering that the equilibrium solutions of the equations correspond to possible different scenarios reachable by the environmental system under investigation. Moreover, the stability analysis derived in [38] has pointed out that bifurcations may arise for some critical values of the parameters, as for instance for the *connectivity index* which takes into account the level of bio-energy exchanges between the various LUs present in the territory.

More in details, paper [39] assumes as state variables, for the whole environmental system, a generalized form of bio-energy (indicated with the symbol M) and the total surface of green areas (indicated with V) presenting high ecological quality. In order to obtain a more detailed description of the ecological state of the environment, in the last part of paper [38] another model is proposed where the state variables (the same of paper [39]) are defined at the level of each LU. In these papers the connectivity index (considered as the control parameter of the dynamical system) is included in the model as a coefficient of the equations and the variable M is defined as a product of the so-called Biological Territorial Capacity (BTC) by a parameter accounting for some morphological and physical property of the biotopes belonging to each LU.

In this Part[1] of the thesis we propose a new model called Network Landscape Model (NLM) where the state variables are again defined for each LU. This model differs substantially from that of paper [38]. First of all, while the high ecological quality areas of each LU V is maintained, the state variable M is replaced by the BTC of each LU (indicated with B), that is a synthetic index that assesses the flux of energy that an ecological sector needs to dissipate in order to maintain its meta-stable ecological state. Such a choice, in our opinion, seems to be reasonable since BTC, contrary to M, is a measurable bio-energy. The second difference is that the morphological and physical properties of biotopes are included in the model as coefficients of the equations and not as factors of the state variable M. But the main novelty consists in adding to the model equations a new term accounting for connec-

[1] Most of the contents of this Part appeared on *Communications in Nonlinear Science and Numerical Simulation*, 48 (2017), pp. 569–584[18]

tivity, which represents the coupling between the LUs. Such a term is borrowed from electrical synapses linking neurons, more specifically from the so called electrically coupling networks [12]. These novelties have been introduced with the aim of a better calibration of the model, suggested by the study cases presented in paper [38] and in the master degree thesis [27]. We are interested in finding the equilibria of the NLM, in order to study the long term evolution of the environmental system, and in their asymptotic stability, in order to evaluate its robustness under strong perturbations due to human land uses impact or to natural events.

This Part is organized as follows. In Chapter 10 we present the Network Landscape Model as a network of dynamical systems, each of them having the same qualitative structure, that we call Single LU Model (SLM); the last model represents the case of an environmental system where the LUs are not connected and are completely isolated from each other. In Chapter 11 we perform a theoretical and numerical analysis of the equilibria and of their stability. In particular, in Section 11.1 we perform a stability analysis of the SLM in terms of two bifurcation parameters, detecting general conditions for the number of equilibria, for their existence and stability. In Section 11.2 we consider the network of LUs, composed by n LUs coupled through a diffusive term proportional to the difference between the bio-energies of each LU. We investigate the asymptotic behaviours of the network (in terms of equilibria and their stability) by means of a proper simplified system, whose dynamics is completely determined in terms of two additional bifurcation parameters. Then, in Section 11.3, we show some numerical tests relevant to a network of LUs in an environmental system of the northern side of the Turin Province (Italy), characterized by five LUs where rather compact built-up territorial patches interact with natural reserve areas. The results are compared with those of the simplified system and of the single LU model, in order to underline how the coupling between the LUs may modify the scenarios, thanks to the exchange of bio-energy, and how the simplified system is able to give information about the asymptotic behaviour of the network model, in accordance with the stability analysis performed. Some concluding remarks are reported in Chapter 12.

10

The network landscape model

As discussed in the Introduction of this Part and according to the previous papers [38, 39], the environmental system is described as a landscape of n LUs. Then it is possible to represent it as a network of dynamical systems (see Section 1.2), composed by n nodes, whose *ecological state* at time t is described by vector state variables $\boldsymbol{x}_i(t) \in \mathbb{R}^2$, $i = 1, \ldots, n$, interacting pairwise through a set of links, that encode the network topology. We suppose that each LU, when isolated from the others, has its own dynamics described by a system of two differential equations of type $\dot{\boldsymbol{x}}_i = \boldsymbol{F}_i(\boldsymbol{x}_i)$. Considering the network landscape, the dynamics of each LU is affected by the neighbouring LUs; this can be modelled by adding an interaction term in the single LU model. Then, the evolution of the whole network can be modelled by a system of $2n$ differential equations, given by

$$\begin{cases} \dot{\boldsymbol{x}}_i = \boldsymbol{F}_i(\boldsymbol{x}_i) + \boldsymbol{H}_i(\boldsymbol{x}_1, \ldots, \boldsymbol{x}_n; W) \\ i = 1, \ldots, n, \end{cases} \tag{10.1}$$

where the function $\boldsymbol{F}_i$ describes the dynamics of the i-th LU in the same way as in the single landscape model, whereas the term $\boldsymbol{H}_i$ describes the interaction of the i-th LU with the other LUs, and, thus, $\boldsymbol{H}_i$ depends on all LUs state variables and on the topology of the system depicted by the weight matrix W. In order to complete the network landscape model, we have to specify the variables that describe the ecological state $\boldsymbol{x}_i$, the functions $\boldsymbol{F}_i$ and the interaction terms $\boldsymbol{H}_i$ and W.

Let us start by describing the ecological state variables and the single node dynamics $\boldsymbol{F}_i$. Each LU is formed by m_i biotopes, $i = 1, \ldots n$. Each biotope is characterized by its bio-energy or more precisely by its BTC index [54]. Such an index will be indicated in what follows by B_{ji}, $j = 1, \ldots, m_i$, and assumes values in the range $[0, B_{max}]$, with $B_{max} = 6.5$ Mcal/(m$^2 \cdot$ year). The BTC is a synthetic function which, by taking into account ecosystem metabolism through biomass information, gross primary pro-

duction and respiration, assesses the flux of energy that an ecological system needs to dissipate in order to maintain its meta-stable ecological state. As an example, industrial or mineral extraction sites have BTC index equal to 0 Mcal/(m^2 · year), olive groves BTC index is 1.8 Mcal/(m^2 · year), while the BTC of a coniferous forest is 6.4 Mcal/(m^2 · year) (information about how the BTC index is calculated and values for different types of vegetation can be found in [39, 54]). Moreover, the biotopes having a vegetation with a BTC index greater than 2.5 will be considered hereinafter those of high ecological quality. The total value of BTC of each LU in Mcal/year is given by

$$B_i(t) = \sum_{j=1}^{m_i} B_{ji} s_{ji},$$

where s_{ji} is the area of the j-th biotope belonging to the i-th LU of total area $S_i = \sum_{j=1}^{m_i} s_{ji}$.

Let us assume as state variables the total BTC B_i of each LU and the sum V_i of all the areas of the biotopes of high ecological quality. Then the equations of the SLM for the i-th LU read as

$$\dot{B}_i(t) = a_i B_i(t) \left(1 - \frac{B_i(t)}{B_i^{max}}\right) - \ell_i \left(1 - \frac{V_i(t)}{S_i}\right) B_i(t) \tag{10.2}$$

$$\dot{V}_i(t) = d_i V_i(t) \left(1 - \frac{V_i(t)}{S_i}\right) \frac{B_i(t)}{B_i^{max}} - h_i U_i V_i(t), \tag{10.3}$$

where

$$B_i^{max} = B_{max}\, S_i$$

is the value of the BTC produced by a LU having all the biotopes with a BTC index equal to B_{max}.

Equations (10.2) and (10.3) have the same mathematical structure of those proposed in [38] but with coefficients having a different meaning, as already discussed in Chapter 9. In fact, the parameters $\ell_i \in [0, 1]$ are here defined as the ratio between the areas of the impermeable barriers present in the LUs and S_i, and the parameters a_i take into account the capability of the i-th LU to produce an increment of bio-energy. In particular, the latter are assumed to depend essentially on the solar exposure of the biotopes, and can be computed by the formula proposed in paper [39]:

$$a_i := \frac{w_1 S_i^{SES} + w_2 S_i^{W} + w_3 S_i^{NE}}{S_i} \leq 1,$$

where the ws are suitable weights and S_i^{SES}, S_i^W, S_i^{NE} are the soil surfaces with exposure to south-east-south, west and north-east, respectively.

Another novelty relies on the coefficients d_i of Eqs. (10.3) which are here considered as dependent on solar exposure, relative humidity and ecotonal length (this last quantity is the length of the borders between biotopes). In fact, it is reasonable that the increasing of green areas of high ecological quality depends on the bio-energy produced in the LU, taking into account as well particular features of the biotopes. The coefficients are defined as

$$d_i = \frac{1}{3}(a_i + k_i^{hu} + k_i^{ec}) \leq 1, \qquad k_i^{hu} = \frac{w_4 S_i^h + w_5 S_i^s}{S_i}, \qquad k_i^{ec} = 1 - P_i \Big/ \sum_{j=1}^{m_i} P_{ji},$$

where k_i^{hu} and k_i^{ec} stand for the indices of relative humidity and ecotonal length, S_i^h and S_i^s being, respectively, the areas of soil characterized by humidity and sub-humidity; moreover P_{ji} is the length of the j-th biotope perimeter, and P_i that of the i-th LU.

The last two parameters h_i and U_i, already considered in paper [38] and appearing in Eq. (10.3), take into account the presence of built-up areas inside the LU that causes impact to the flow of bio-energy. The parameter h_i is given by the ratio between the sum of the perimeters of the built-up areas and the total perimeter of the LU, whereas U_i is defined as the ratio between the sum of the built-up areas and the total area S_i of the LU. Therefore, these parameters can be considered as a measure of the dispersion and of the intensity of constructions inside the LU, respectively. According to its definition, the parameter h_i can assume values greater than one (such values mean that construction dispersion in the LU is significantly remarkable); conversely U_i ranges in $[0, 1]$.

It is convenient to normalize Eqs. (10.2)-(10.3) by dividing the former by B_i^{max} and the latter by S_i. By introducing the normalized variables $b_i = B_i/B_i^{max}$ and $v_i = V_i/S_i$, the equations for the i-th LU result in:

$$\begin{cases} \dot{b}_i = F_i^{(1)}(b_i, v_i) = a_i b_i (1 - b_i) - \ell_i (1 - v_i) b_i \\ \dot{v}_i = F_i^{(2)}(b_i, v_i) = d_i v_i (1 - v_i) b_i - h_i U_i v_i. \end{cases} \tag{10.4}$$

Equations (10.4) define the Single Landscape Model (SLM) proposed here. From now on, we will refer to them as SLM equations. They have the form $\dot{\boldsymbol{x}}_i = \boldsymbol{F}_i(\boldsymbol{x}_i)$ with $\boldsymbol{x}_i = (b_i(t), v_i(t))^\mathsf{T}$. Although v_i is strictly related to b_i, their combination is able to characterize more precisely the type of territory and its ecological quality, since the b_i variable is able to represent only a mean value of the total (normalized) bio-energy

allocated inside a single LU. On the other hand, the informations that we extract from v_i help in improving the picture of the landscape unit.

Let us now define the interaction term $\boldsymbol{H}_i$ in (10.1). The coupling between the i-th LU and its k neighbors can be modeled by a linear interaction term proportional to the difference between the bio-energies of the i-th and k-th LU, affecting only the equation for the bio-energies themselves. Therefore

$$\boldsymbol{H}_i(\boldsymbol{x}_1, \boldsymbol{x}_2, \ldots, \boldsymbol{x}_n) = \begin{pmatrix} \displaystyle\sum_{k \in \mathcal{I}_i} c_{ki} \left[b_k(t) - b_i(t) \right] \\ 0 \end{pmatrix}$$

where the set $\mathcal{I}_i$ collects all the indices of the LUs adjacent to the i-th one. The term $\boldsymbol{H}_i$ has the same mathematical structure as the electric coupling in neural networks [12].

Summing up, we can then write the $2n$ equations of the network of LUs as

$$\begin{cases} \dot{b}_i(t) = a_i b_i(t)[1 - b_i(t)] - \ell_i[1 - v_i(t)]b_i(t) + \displaystyle\sum_{k \in \mathcal{I}_i} c_{ki} \left[b_k(t) - b_i(t) \right] \\ \dot{v}_i(t) = d_i v_i(t)[1 - v_i(t)]b_i(t) - h_i U_i v_i(t) \\ i = 1, \ldots n. \end{cases} \tag{10.5}$$

Equations (10.5) define the Network Landscape Model (NLM) proposed in this thesis and we will refer to them as NLM equations.
The coefficients c_{ki} in the expression of $\boldsymbol{H}_i$ are the connectivity indices between the k-th and the i-th LUs and represent the elements of the weight matrix W that defines the topology of the considered networks of dynamical systems. They can be computed (see [38]) by the formula

$$c_{ki} = \frac{H_{ki}}{L_{ki}}, \qquad H_{ki} = \sum_{r=1}^{s} L_{ki}^r p^r, \qquad L_{ki} = \sum_{r=1}^{s} L_{ki}^r,$$

where L_{ki} is the length of the border between the two LUs, which is divided into s parts, each of length L_{ki}^r with a permeability index $p^r \in [0, 1]$, with 0 for impermeable and 1 for completely permeable.

In order to study the dynamics of the NLM, Eqs. (10.5) must be equipped with the initial data

$$b_i(0) = b_{i0}, \qquad v_i(0) = v_{i0}$$

that can be obtained directly from the GIS of the territory under investigation.

11

Theoretical and numerical study

In this Chapter we investigate the dynamics of the isolated landscape unit (SLM) (10.4) by studying in Section 11.1 its equilibria and their stability properties. In Section 11.2 we investigate the dynamics of the network landscape models (NLM) (10.5) by means of a proper simplified system, whose dynamics are completely determined in terms of two additional bifurcation parameters. Lastly, in Section 11.3 we show some numerical tests relevant to a network of LUs in an environmental system of the northern side of Turin Province (Italy).

11.1 Equilibria and stability properties: the case of a single LU

In this Section we investigate the single node dynamics by studying the equilibria of the SLM equations (10.4) and their stability in terms of two bifurcation parameters. In order to simplify the notation, we omit the LU index i.

First of all, we notice that the square $Q = [0,1] \times [0,1]$ in the (b, v) plane is an invariant region for the SLM equations (10.4) and this guarantees the consistency of the model with the assumption that the normalized variables b, v are meaningful only if they range between 0 and 1. An important property of the SLM (10.4) is its cooperative structure [84], namely it can be put in the form $\dot{\boldsymbol{x}} = \boldsymbol{F}(\boldsymbol{x})$, where $\boldsymbol{x} = (b, v)$ and $\boldsymbol{F}$ is a cooperative vector field, meaning that $\partial F^{(k)}/\partial x_j \geq 0$ for $k = 1, 2$ and $j \neq k$. As a consequence, since the dynamics is confined in the compact set Q, the long time behavior is severely limited: there will be at least one stable equilibrium, there are no periodic orbits and trajectories will always converge (eventually monotonically) to a stable equilibrium [48, 84].

By setting the right hand sides of the SLM equations (10.4) equal to zero, we compute the equilibrium solutions of the model. Simple calculations lead to four equilibria given by

$$E_0 = (0,0), \quad E_1 = (b_1, 0) = (1-\alpha, 0),$$
$$E_*^{\pm} = (b_*^{\pm}, v_*^{\pm}) = \left(b_*^{\pm}, 1 - \frac{r}{b_*^{\pm}}\right) = \left(\frac{1 \pm \sqrt{1-4\alpha r}}{2}, 1 - \frac{1 \mp \sqrt{1-4\alpha r}}{2\alpha}\right), \quad (11.1)$$

where

$$\alpha = \ell/a, \qquad r = hU/d.$$

Let us comment that the equilibrium E_0 corresponds to a scenario where the system tends to gradually loose its ecological quality and presents a strong landscape fragmentation. The second equilibrium E_1 represents a scenario with no high quality vegetation, but with some production of bio-energy: such scenarios are typical of territories where agricultural production is predominant. Finally, the coexistence equilibria $E_*^{\pm}$ show a good level of bio-energy production in presence of a certain amount of high ecological quality (green) areas.

Since b and v are normalized variables, these equilibria are significant only if their components are between 0 and 1. In particular, it is easy to see that the first equilibrium E_0 is admissible for every choice of the parameters, while E_1 lies in Q if and only if $\alpha < 1$, namely low presence of impermeable barriers (small values of ℓ), together with a good solar exposure (large values of a). The admissibility of the coexistence equilibria $E_*^{\pm}$ depends on both r and α (see Fig. 11.1); standard calculations allow us to prove that

$$E_*^+ \in Q \ \text{ iff } \ r \le \begin{cases} 1-\alpha & \text{when } \alpha < 1/2 \\ 1/(4\alpha) & \text{when } \alpha \ge 1/2 \end{cases}; \quad E_*^- \in Q \ \text{ iff } \ \begin{cases} \alpha \ge 1/2 \\ 1-\alpha \le r \le 1/(4\alpha) \end{cases}. \quad (11.2)$$

Remark 2. The ecological meaning of the parameters allows us to characterize the quality of a territory in terms of α and r. More precisely, low presence of constructions (small values of h and U) together with good environmental parameters (large values of d) yield small value of the parameter r; low presence of impermeable barriers (low values of ℓ) and high capability to increment the bio-energy (high values of a) lead to small values of parameter α. Therefore, we expect small values of α and r to be related to fertile areas, while high values of both parameters represent highly built-up areas or desert zones. Indeed, for high values of α and r the only feasible equilibrium is E_0 that will be globally attractive, owing to the cooperative structure of the SLM (10.4).

The coexistence equilibria $E_*^{\pm} = (b_*^{\pm}, v_*^{\pm})$ are related to territories with a certain amount of high ecological quality areas and a good production of bio-energy, while $E_1 = (b_1, 0)$ represents lower quality territories with predominance of agricultural production. By simple calculations, it is possible to show that the corresponding equilibrium values $b_*^{\pm}$ of the bio-energy are always greater than the equilibrium value b_1, in accordance with the ecological meaning of the equilibria.
The coexistence equilibria $E_*^{\pm}$ are admissible when r is sufficiently small, with threshold decreasing with α; in other words, unfavorable parameters ℓ and a must be balanced by proper favorable values of h, U and d to get the coexistence of the high ecological quality areas and a good production of bio-energy. In addition, when α and r are both small enough (highest quality territory) the equilibrium state E_*^-, less valuable than E_*^+, is not present.

Proposition 1.

(i) E_0 *is locally asymptotically stable if and only if* $\alpha > 1$*;*
(ii) E_1 *is locally asymptotically stable if and only if* $r > 1 - \alpha$*;*
(iii) E_*^+ *is locally asymptotically stable, while* E_*^- *is a saddle (when they are admissible).*

Proof. In order to study the local stability of the equilibria we evaluate the Jacobian matrix of SLM equations (10.4)

$$J = \begin{pmatrix} a[(1-2b) - \alpha(1-v)] & a\alpha b \\ dv(1-v) & d[b(1-2v) - r] \end{pmatrix}$$

at each equilibrium.
(i) It is easy to see that $J(E_0)$ is a diagonal matrix, whose eigenvalues are $\lambda_1 = a(1-\alpha)$ and $\lambda_2 = -rd$, and then both are negative iff $\alpha > 1$.
(ii) The Jacobian matrix evaluated at E_1 is an upper triangular matrix, whose eigenvalues are $\lambda_1 = a(\alpha - 1)$ and $\lambda_2 = d(1 - \alpha - r)$. The first eigenvalue is always negative when E_1 is admissible (i.e. $\alpha < 1$), while the second one is negative if and only if $r > 1 - \alpha$.
(iii) The Jacobian matrix evaluated at the coexistence equilibria can be written in the compact form

$$J(E_*^{\pm}) = \begin{pmatrix} -ab_*^{\pm} & a\alpha b_*^{\pm} \\ dv_*^{\pm}(1 - v_*^{\pm}) & -db_*^{\pm} v_*^{\pm} \end{pmatrix}. \tag{11.3}$$

The determinant of $J(E_*^{\pm})$, by simple calculations, results:

$$\det(J(E_*^{\pm})) = adv_*^{\pm} b_*^{\pm}(b_*^{\pm} - \alpha(1 - v_*^{\pm})) = \pm adv_*^{\pm} b_*^{\pm} \sqrt{1 - 4\alpha r}.$$

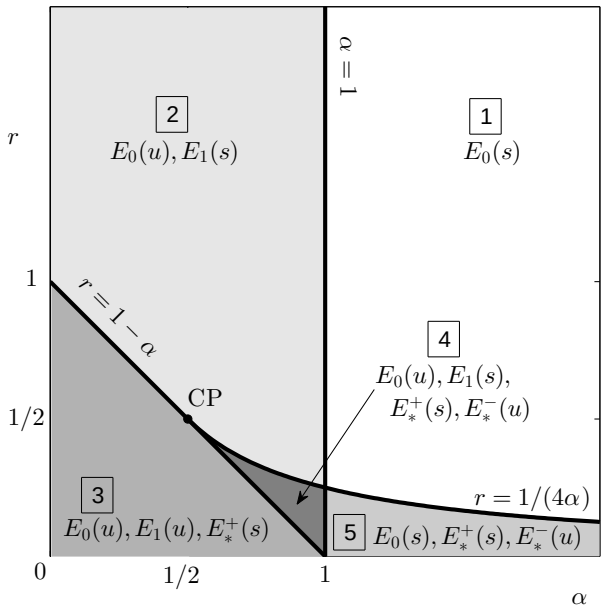

Fig. 11.1. Existence and stability regions of the equilibria given in (11.1) of the SLM (10.4) in the parameter plane (α, r). Stable (resp. unstable) equilibria are denoted by "s" (resp. "u"); CP denotes the cusp point.

We notice that the square root is well defined, thanks to the admissibility conditions (11.2) for the coexistence equilibria since $1-\alpha < 1/(4\alpha)$ for $\alpha < 1/2$. The determinant of $J(E_*^-)$ turns out to be always negative and therefore E_*^- is a saddle point, whenever it is admissible. The determinant of $J(E_*^+)$ is instead always positive. As regards the sign of the trace of $J(E_*^\pm)$, the diagonal elements of the matrix (11.3) are both negative, therefore $\mathrm{tr}J(E_*^+) < 0$.

□

The results about existence and stability of equilibrium states are summarized in Fig. 11.1. In the parameter space (α, r) the lines $r = 1-\alpha$, $\alpha = 1$ and the hyperbola $r = 1/(4\alpha)$ divide the first quadrant in five regions, which are qualitatively different either for the number of equilibria or for their stability. In three of these regions, labeled by 1, 2 and 3, there exists a single locally stable equilibrium that will be always globally asymptotically stable, in accordance with the theory of cooperative systems [84]. In the two remaining regions 4 and 5, the bistability occurs. In both regions, the stable manifold of the saddle E_*^- plays the role of separatrix between the basins of attraction of the stable equilibria, while the unstable manifolds provide

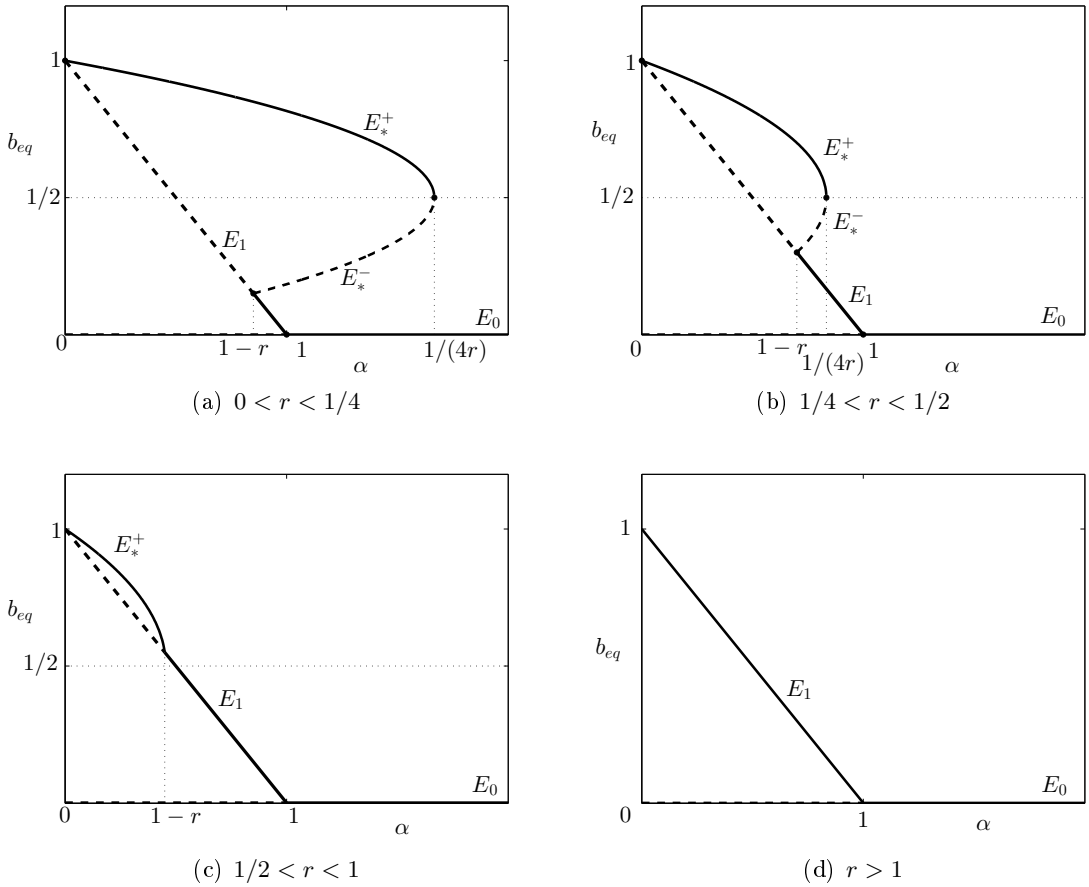

Fig. 11.2. Bifurcation diagrams: equilibrium values of bio-energy b_{eq} versus α for different values of r. Solid curves represent stable equilibria, dashed curves represent unstable equilibria.

heteroclinic orbits connecting E_*^- with them. As a consequence, the system can evolve towards a "good" equilibrium (E_*^+) or a "poor" equilibrium (E_0 or E_1) equilibrium depending on the initial state. Moreover, when considering interventions in these regions, a parameter change can drive an initial situation either to extinction, or to the absence of high quality green areas only, or to the best coexistence of bio-energy and high quality green areas, depending on the parameter values.

All the boundary curves between these five regions are stationary bifurcation curves. In particular, on the vertical line $\alpha = 1$ the system shows transcritical bifurcation points involving the equilibria E_1 and E_0. This is also the case of the line $r = 1 - \alpha$, which involves transcritical bifurcations between the equilibrium E_1 and

a coexistence one (E_*^+ or E_*^-, depending on the parameter values), while the curve $r = 1/(4\alpha)$ is a saddle-node bifurcation curve involving the equilibria E_*^+, E_*^-. In addition, these last two bifurcation curves intersect at the critical point $CP = (1/2, 1/2)$ in the parameter space, where the three equilibrium states E_1, E_*^+, E_*^- coincide. At this point, the two bifurcation curves share a common tangent; then CP is a mathematical cusp in the (α, r) plane. All these results indicate the presence of a cusp singularity, according to Whitney's theory [6], for the equilibrium surface in the space (α, r, b).

The bifurcation process is described also in Fig. 11.2, where the values of b at equilibria are reported versus α for different values of r. With reference also to Fig. 11.1, we can see in detail in Fig. 11.2 how the equilibrium states collide and disappear. The four panels can be obtained by slicing the diagram in Fig. 11.1 with lines $r = const$.

When r is sufficiently small (Fig. 11.2(a)), by varying α we can pass from region $\boxed{3}$, characterized by the best ecological parameters and where E_*^+ is the only attractor, to the region $\boxed{4}$, where the system is bistable with both E_*^+ and E_1 being attractors, then to the region $\boxed{5}$, where bistability is between E_*^+ and E_0, and finally to the region $\boxed{1}$, where E_0 is the only attractor. By increasing r (Fig. 11.2(b)) towards $1/2$, varying α we pass from regions $\boxed{3}$ to $\boxed{4}$ by a transcritical bifurcation between E_1 and E_*^-, then from $\boxed{4}$ to $\boxed{2}$ by the saddle-node bifurcation involving $E_*^\pm$, and finally from regions $\boxed{2}$ to $\boxed{1}$ by transcritical bifurcation between E_1 and E_0. When $r = 1/2$, the vertex of the parabola, representing the saddle-node bifurcation point, lies on the line $r = 1 - \alpha$ and we have coincidence of $E_*^\pm$ and E_1 (cusp point). For r above $1/2$, bistability is no more feasible and the equilibrium E_*^+ interacts with E_1 by transcritical bifurcation as long as $r < 1$ (Fig. 11.2(c)) and by increasing α we cross regions $\boxed{3}$, $\boxed{2}$ and $\boxed{1}$. Finally for $r > 1$, there is only a transcritical bifurcation between E_1 and E_0 when we pass from region $\boxed{2}$ to region $\boxed{1}$.

11.2 A preliminary analysis of network dynamics

In this Section we consider the NLM (10.5) and investigate the effect of the coupling between the LUs. Typically, networks of dynamical systems may present rich behaviors, such as synchronization, periodic solutions, chaos [12]. The NLM (10.5) is however a system of $2n$ differential equations of cooperative type [84], since it can be easily proved that its Jacobian matrix has nonnegative off-diagonal entries in the compact invariant hypercube $[0, 1]^{2n}$. Therefore, under mild restrictions [48], it is possible to show that the trajectory of almost every initial state converges to

an equilibrium in the compact hypercube and that there are no attracting periodic orbits other than equilibria, because every attractor contains a stable equilibrium.

The analytical study of equilibria for the NLM equations (10.5) is substantially impracticable; we can only easily verify that the null state is an equilibrium point and using the first Lyapunov criterion, we can investigate its stability. The Jacobian of NLM (10.5), when evaluated at the null state, is a block diagonal matrix of order $2n$, with two blocks of order n. One block is a diagonal matrix with negative entries $-h_i U_i$, corresponding to the partial derivatives of the terms on the r.h.s of the equations for the high quality green areas v_i with respect to v_i. The other block is symmetric with the off-diagonal entries equal to c_{ji} and diagonal elements $a_i - c_i - \ell_i$. Thanks to the localization Gershgorin theorem [89], the eigenvalues relevant to this block are bounded from below by $a_i - 2c_i - \ell_i$ and from above by $a_i - \ell_i = a_i(1-\alpha_i)$. Then, if $a_i - \ell_i < 0 \ \forall \ i$, namely if the parameter α in each LU is greater than 1, the null equilibrium state is locally asymptotically stable. This scenario refers to the case in which all LUs belong to regions $\boxed{1}$ or $\boxed{5}$ (Fig. 11.1), the only ones where E_0 is stable for the SLM. Moreover, if there exists an index i such that $c_i < (a_i - \ell_i)/2$, then the null equilibrium state is unstable.

To proceed further and get indications about the network asymptotic behavior, we follow a simplified strategy which involves a planar system of ODEs, with the aim of understanding how the connectivity among LUs quantitatively modifies equilibrium states with respect to those of the single LUs.

In Subsection 11.2.1 we detail the construction of this simplified model, then in Subsection 11.2.2 we study its equilibria and their asymptotic stability in terms of two bifurcation parameters, and finally we complete the analysis by characterizing in Subsection 11.2.3 the stability regions in different parameter planes.

11.2.1 The simplified system

Let $(\bar{b}_i, \bar{v}_i), i = 1, \ldots, n$ be an equilibrium point for the NLM (10.5); then, the r.h.s. of NLM equations (10.5) evaluated at this point is zero, namely

$$\begin{cases} a_i \bar{b}_i[1 - \bar{b}_i] - \ell_i[1 - \bar{v}_i]\bar{b}_i - c_i \bar{b}_i + \bar{I}_i = 0 \\ d_i \bar{v}_i[1 - \bar{v}_i]\bar{b}_i - h_i U_i \bar{v}_i = 0 \\ i = 1, \ldots n, \end{cases}$$

where the coupling terms have been rewritten in terms of the in-strength of each node and a set of constants that depends both on the topology of the network and on the bio-energy equilibrium values:

$$c_i = \sum_{k \in \mathcal{I}_i} c_{ki}, \qquad \bar{I}_i = \sum_{k \in \mathcal{I}_i} c_{ki} \bar{b}_k. \tag{11.4}$$

We remark that the dependence of the i-th LU on the neighboring LUs is incorporated in the term $\bar{I}_i$, ranging from 0 to c_i, which is a proper unknown constant at equilibrium for each subsystem relevant to the single LU. In order to get information about the equilibria $(\bar{b}_i, \bar{v}_i), i = 1, \ldots, n$, and their stability, we consider the simplified assumption that the landscape network is composed by $n-1$ LUs at equilibrium, playing the role of a background, and we connect an additional LU to it (labeled by i). For a landscape network, it is reasonable to expect that the $n-1$ LUs of the background will not be affected by this insertion. This intuitive assumption deserves however further investigation, that will be matter of future work. Then, the i-th LU will relax to equilibrium according to the dynamics given by the system

$$\begin{cases} \dot{b}_i(t) = a_i b_i(t)[1 - b_i(t)] - \ell_i[1 - v_i(t)]b_i(t) - c_i b_i(t) + I_i \\ \dot{v}_i(t) = d_i v_i(t)[1 - v_i(t)]b_i(t) - h_i U_i v_i(t) \end{cases}$$

where we have replaced $\bar{I}_i$ with an additional generic parameter, let's say I_i, constant but a priori unknown, dependent on the (unknown) equilibrium values of the bioenergies of the other LUs of the background.

We omit the LU index i in order to simplify the notation, and then consider the simplified system

$$\begin{cases} \dot{b}(t) = ab(t)[1 - b(t)] - \ell[1 - v(t)]b(t) - cb(t) + I \\ \dot{v}(t) = dv(t)[1 - v(t)]b(t) - hUv(t) \end{cases} \tag{11.5}$$

for a generic value of the parameter I, with $0 \leq I \leq c$. First we observe that, as for the SLM (10.4), $Q = [0, 1]^2$ is an invariant set for the simplified model and that system (11.5) has a cooperative structure too, therefore there are no periodic orbits, and the trajectories will converge, eventually monotonically, to an equilibrium.

11.2.2 Equilibria and their asymptotic stability

Simple calculations lead to equilibrium (the subscript N stands for "network")

$$E_{1_N} = (b_{1_N}, 0) = \left(\frac{a - c - \ell + \sqrt{(a - c - \ell)^2 + 4aI}}{2a}, 0 \right) \tag{11.6}$$

which characterizes agricultural areas, and to two coexistence equilibria

$$E^{\pm}_{*_N} = \left(b^{\pm}_{*_N}, v^{\pm}_{*_N}\right) = \left(\frac{a - c \pm \sqrt{(a-c)^2 + 4a(I - a\alpha r)}}{2a}, 1 - \frac{r}{b^{\pm}_{*_N}}\right). \tag{11.7}$$

We notice that the expression of the first component of E_{1_N} is found as the positive root of a second order polynomial. The other root is negative for $0 < I \leq c$; when $I = 0$ the positive root reduces to 0 if $a - c - \ell < 0$, otherwise the negative root does it. It follows that, only when $I = 0$, the simplified system (11.5) admits also the null equilibrium state $E_{0N} = (0, 0)$.

As for the single LU model, since b and v are normalized variables, these equilibria are significant only if their components are between 0 and 1. As regards the equilibrium E_{1_N}, it is easy to see that it is well defined since the radicand is always positive and also that its first component is positive. In fact, the condition $b_{1_N} \leq 1$ is equivalent to $I \leq c + \ell$, which is true by the hypothesis on the parameter I ($I \leq c$). Therefore, the equilibrium E_{1_N} always belongs to $Q = [0, 1] \times [0, 1]$.

To determine the parameter values for which $E^{-}_{*_N}$ is admissible we have to impose five conditions: the radicand must be nonnegative and the equilibrium components $b^{-}_{*_N}$, $v^{-}_{*_N}$ must range from 0 to 1. By some calculations, we obtain

$$E^{-}_{*_N} \in Q \iff \begin{cases} (a-c)^2 + 4a(I - a\alpha r) \geq 0 \\ r \leq b^{-}_{*_N} \leq 1 \end{cases} \iff \begin{cases} a(1 - r - \alpha) < c \leq a(1 - 2r) \\ f(c) \leq I \leq g(c) \\ r < 1/2 \end{cases} \tag{11.8}$$

where

$$f(c) = a\left(\alpha r - \frac{(a-c)^2}{4a^2}\right), \qquad g(c) = r[a(r + \alpha - 1) + c]. \tag{11.9}$$

The last condition in (11.8) is due to the fact that c must be a positive parameter. Moreover, we can find a suitable c only if $a(1 - r - \alpha) < a(1 - 2r)$, namely $r < \alpha$.

Similarly, the admissibility conditions of the equilibrium $E^{+}_{*_N}$ are given by

$$\begin{cases} (a-c)^2 + 4a(I - a\alpha r) \geq 0 \\ r \leq b^{+}_{*_N} \leq 1 \end{cases} \tag{11.10}$$

which admits solutions only if $r < 1$. After some calculation we obtain

$$E^{+}_{*_N} \in Q \iff \begin{cases} c \geq a(1 - 2r) \\ I \geq g(c) \\ r < 1 \end{cases} \quad \vee \quad \begin{cases} c < a(1 - 2r) \\ I \geq f(c) \\ r < 1/2. \end{cases}$$

Remark 3. It can be noticed that a necessary condition for the admissibility of both $E^+_{*_N}$ and $E^-_{*_N}$ is $r < 1$, namely $hU < d$, which means that both intensity and dispersion of built-up areas must be sufficiently low. This fact is in accordance with the comments in Remark 2 for the single LU model. As in the single case, standard calculations show that the bio-energy value of the coexistence equilibrium $E^+_{*_N}$ is always greater than the bio-energy value of E_{1_N}, namely $b^+_{*_N} > b_{1_N}$.

Proposition 2.

(i) E_{0N}, *admissible for* $I = 0$, *is locally asymptotically stable if and only if* $a - c - \ell < 0$.

(ii) E_{1_N} *is locally asymptotically stable if and only if* $\begin{cases} c > a(1 - r - \alpha) \\ 0 < I < g(c). \end{cases}$

(ii) $E^+_{*_N}$ *is locally asymptotically stable, while* $E^-_{*_N}$ *is a saddle (when they are admissible).*

Proof. In order to study the local stability we evaluate the Jacobian matrix of the simplified system (11.5)

$$J = \begin{pmatrix} a[(1-2b) - \alpha(1-v)] - c & \ell b \\ dv(1-v) & d[b(1-2v) - r] \end{pmatrix}$$

at each equilibrium and determine the sign of its eigenvalues.
(i) The Jacobian matrix evaluated at E_{0N} is a diagonal matrix with eigenvalues $\lambda_1 = a - c - \ell$ and $\lambda_2 = -dr$.
(ii) The Jacobian matrix evaluated at E_{1_N} is an upper triangular matrix, whose eigenvalues are $\lambda_1 = a(1 - \alpha - 2b_{1_N}) - c$ and $\lambda_2 = d(b_{1_N} - r)$. By simple calculations we find that the first eigenvalue is always negative, while the second one is negative if and only if $b_{1_N} < r$. Such condition, by some algebra, expresses the thesis.
(iii) The Jacobian matrix evaluated at the coexistence equilibria can be written in the compact form

$$J(E^\pm_{*_N}) = \begin{pmatrix} a(1 - \alpha r/b^\pm_{*_N} - 2b^\pm_{*_N}) - c & \ell b^\pm_{*_N} \\ dv^\pm_{*_N}(1 - v^\pm_{*_N}) & d(r - b^\pm_{*_N}) \end{pmatrix}.$$

The determinant, by simple calculations, results to be:

$$\det(J(E^\pm_{*_N})) = d(a - c - 2ab^\pm_{*_N})(r - b^\pm_{*_N}).$$

The last term of this product is always negative, due to the admissibility conditions (11.8) and (11.10). Moreover, after some calculations, the second term of the product,

$(a-c-2ab^{\pm}_{*_N})$, can be reduced to $\mp\sqrt{(a-c)^2+4a(I-a\alpha r)}$. Therefore the sign of the determinant is constant, in particular $J(E^{-}_{*_N})$ is negative (and therefore $E^{-}_{*_N}$ is a saddle), while $J(E^{+}_{*_N})$ is positive. To determine the stability of $E^{+}_{*_N}$ we have to study the sign of the trace of $J(E^{+}_{*_N})$, which can be written as:

$$\begin{aligned}\mathrm{tr}(J(E^{+}_{*_N})) &= a(1-\alpha r/b^{\pm}_{*_N}-2b^{\pm}_{*_N})-c+d(r-b^{\pm}_{*_N})\\ &= -a\alpha r/b^{\pm}_{*_N}+d(r-b^{\pm}_{*_N})-\sqrt{(a-c)^2+4a(I-a\alpha r)}\end{aligned}$$

which is negative, since all its addends are negative, and then the thesis holds. □

Remark 4. The case $I=0$ for the simplified system (11.5) is strictly related to the null equilibrium of the whole network, discussed at the beginning of this Section. In fact, $I=0$ can be obtained only if the background is at the null state and it is remarkable that the stability condition for E_{0N} is analogous to the ones found for the stability of the null equilibrium state for the network.

11.2.3 Stability regions

The stability analysis of the system (11.5) turns out to depend also on the additional parameters c and I, besides r and α. The representation of the behaviors of the system in terms of equilibria and their stability is then much more complicated and it is schematized in Fig. 11.3. In the parameters plane (α, r) (panel (a)) we identify six different regions, which present different scenarios. Regions $\boxed{A}$ - $\boxed{E}$ are represented in panels (b)-(f) in the parameters plane (c, I), respectively, while region $\boxed{F}$ is not further detailed since only the equilibrium E_{1_N} is admissible and it is locally asymptotically stable (and also globally stable, according to the theory of cooperative systems which holds for system (11.5)). In each panel (b)-(f) different tonalities represent different number of admissible equilibria or different stability properties. In particular, white regions denote sets of non admissible parameter values, since admissibility requires $I \le c$; in the light gray regions there exists only the equilibrium E_{1_N} and it is locally (and globally) asymptotically stable; in the gray regions there exist the equilibria E_{1_N} (unstable) and $E^{+}_{*_N}$ (asymptotically stable); in the dark gray regions there exist the equilibrium E_{1_N} (locally asymptotically stable) and both coexistence equilibria $E^{+}_{*_N}$ (locally asymptotically stable) and $E^{-}_{*_N}$ (unstable).

Remark 5. If we analyze the effect of the coupling on the position of the equilibria, we find that if the constant input I is sufficiently high, then the bio-energy at equilibrium of the simplified model (11.5) is greater than the corresponding value of the single LU, in fact

$$b_{1_N} > b_1 \quad \Longleftrightarrow \quad I > c(1-\alpha) = cb_1. \tag{11.11}$$

This is also the case of the equilibrium $E^+_{*_N}$, whenever it is admissible, in fact by some algebra we get

$$b^+_{*_N} > b^+_*, \quad v^+_{*_N} > v^+_* \quad \Longleftrightarrow \quad I > cb^+_*. \tag{11.12}$$

On the contrary, the bio-energy and the fraction of high quality areas of the equilibrium $E^-_{*_N}$, whenever it is admissible, are greater than their respective values of the isolated LU if I is sufficiently small, namely

$$b^-_{*_N} > b^-_*, \quad v^-_{*_N} > v^-_* \quad \Longleftrightarrow \quad I < \min\left\{cb^-_{*_N}, \frac{ac-c^2}{2a}\right\}.$$

The coupling can also force the system to tend to a different equilibrium type. It can be seen that

$$b_{1_N} > b^+_* \quad \Longleftrightarrow \quad I > b^+_*(c+\ell) - \ell r, \tag{11.13}$$

namely that the bio-energy b_{1_N} of the simplified model is greater than the bio-energy b^+_* of the single LU if I is sufficiently high.

A first consequence of this analysis is that the sectors that belong to region $\boxed{F}$ in the (α, r) plane (see Fig. 11.3(a)) can evolve only towards the equilibrium E_{1_N} regardless of the values of c and I, while in the single LU model they can reach either the equilibrium E_0 or the equilibrium E_1 (see Fig. 11.1), depending on the initial data.

As it can be seen in Figs. 11.3(b)-11.3(f), in all the other regions $\boxed{A}$ - $\boxed{E}$ the number and the stability of equilibria do not depend only on α and r. Nevertheless, for regions $\boxed{A}$, $\boxed{B}$, $\boxed{D}$ and $\boxed{E}$ we can still find conditions on the parameter c for which the system admits only one stable equilibrium, regardless of I. More specifically, it is possible to find a threshold $\tilde{c}$, that depends on the region, below which either E_{1_N} or $E^+_{*_N}$ are locally asymptotically stable. Therefore in this case, given the set of parameters and since c is a geometric parameter that can be calculated from the connectivity indices with formula (11.4), we can a priori determine to which equilibrium the system will tend, without knowing I. As an example, let us consider region $\boxed{A}$ of Fig. 11.3(a). For these values of α and r the isolated system only admits a stable equilibrium, namely E^+_* (see Fig. 11.1). For the simplified model (11.5), as it can be seen by Fig. 11.3(b) and due to the previous considerations, if $c < \tilde{c} = a(1-r-\alpha)$ then the trajectory tends to the coexistence equilibrium $E^+_{*_N}$, of the same type of the isolated case. On the contrary, if $c > \tilde{c}$, either the equilibrium E_{1_N} or $E^+_{*_N}$ could be locally asymptotically stable, depending on the value of I. Similar comments hold for the other regions, except for region $\boxed{C}$, where for each

c both equilibria E_{1_N} and $E^+_{*_N}$ can be stable, depending on I. Moreover, as can be seen in Figs. 11.3(c), 11.3(d), 11.3(e), there are bistability regions (dark gray color) in which the estimated I does not determine univocally the attractor of the system.

11.3 Application to a case study in Northern Italy

We consider an environmental system located in the northern side of the Turin Province (Italy). We focus in particular on five LUs of this region where rather compact built-up territorial patches interact with natural reserve areas. Table 11.1 provides the initial data and the values of the parameters (indicators) that identify the different ecological sectors of the territory under investigation; Table 11.2 contains the geometric parameters that characterize the borders of the LUs. The data have been obtained from the GIS measurements in the master degree thesis [27], where a territory of 24 LUs centered around the municipality of Cirié (Turin) has been taken into account. For the purposes of the present paper, which is mainly devoted to show the effects of connectivity between different patches of a territory, we have selected only 5 sectors which better fit our aims since the remaining other 19 sectors, not here examined, are generally not well connected to the five LUs we have chosen. The data of Table 11.1 can be commented in order to better characterize each LU, in the sense that the numerical values of the indicators highlight immediately some peculiarities of each LU. In fact, LU18 and LU20 present a good production of BTC (b_0) together with a rather high value of solar exposure (a). Conversely, LU19 has a low value of high ecological quality green area (v_0) and a strong intensity of construction (U) which of course implies high presence of barriers (high value of ℓ). A peculiarity characterizing LU20 is a low value of construction which conversely is strongly dispersed ($h = 2.2$). By examining also Table 11.2 it comes out the peculiarity of the connection between LU17 and LU19 which present a connectivity index equal to zero: this is not surprising, since these two sectors are completely divided by two contiguous cities.

On the basis of these data we can know a "priori" how many stable equilibria are present in each (isolated) LU, as represented in Fig. 11.4(a) by the points which locate the sectors in the proper region of the (α, r) plane. The positions of sectors LU18 and LU1 in the (α, r) plane are quite close to each other, and their dynamical behaviors are expected to be very similar.

The network composed by the five LUs, modeled by the NLM equations (10.5), is characterized by the weight matrix

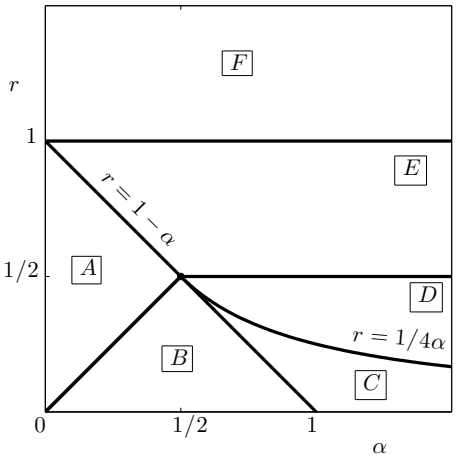

(a) (α, r) plane

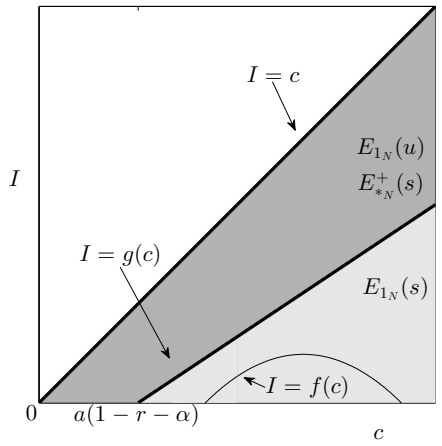

(b) Region $\boxed{A}$ - (c, I) plane

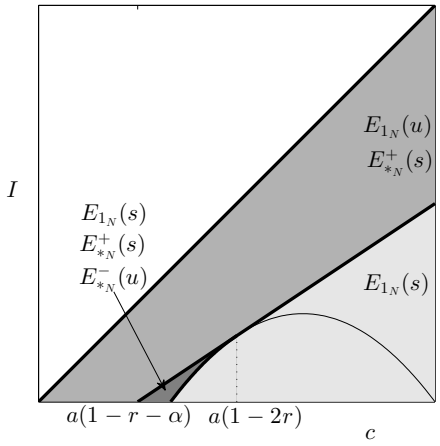

(c) Region $\boxed{B}$ - (c, I) plane

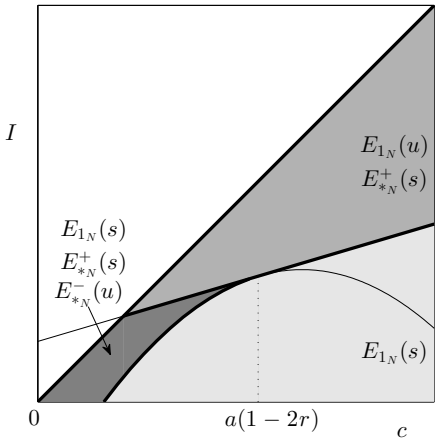

(d) Region $\boxed{C}$ - (c, I) plane

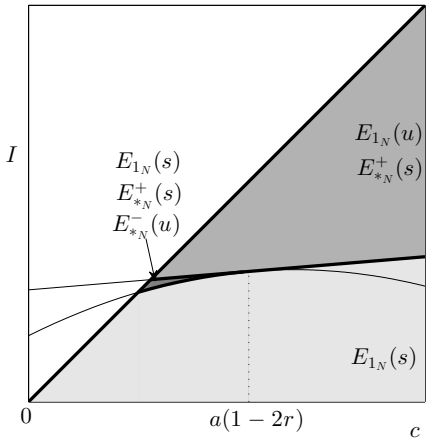

(e) Region $\boxed{D}$ - (c, I) plane

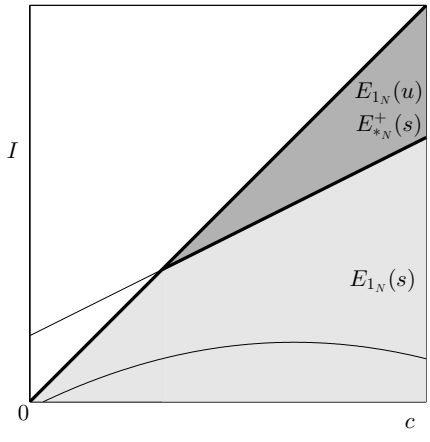

(f) Region $\boxed{E}$ - (c, I) plane

Fig. 11.3. Existence and stability regions of the equilibria given in (11.6)-(11.7) for the simplified model (11.5). Curves $I = f(c)$ and $I = g(c)$ are defined in (11.9). Light gray regions: E_{1_N} locally asymptotically stable. Gray regions: E_{1_N} (unstable) and $E^+_{*_N}$ (locally asymptotically stable). Dark gray regions: E_{1_N} (locally asymptotically stable), $E^+_{*_N}$ (locally asymptotically stable) and $E^-_{*_N}$ (unstable).

LU	S_i	P_i	b_{i0}	v_{i0}	a_i	ℓ_i	d_i	h_i	U_i	$\alpha_i = \ell_i/a_i$	$r_i = h_i U_i/d_i$
1	19156648	25248	0.19	0.30	0.39	0.05	0.35	1.83	0.09	0.128	0.471
17	6369795	12599	0.13	0.26	0.32	0.11	0.26	1.58	0.21	0.344	1.276
18	69754645	60482	0.34	0.31	0.44	0.04	0.40	1.97	0.07	0.091	0.345
19	4589299	18604	0.17	0.13	0.31	0.32	0.28	1.88	0.61	1.032	4.096
20	42953048	38826	0.45	0.30	0.51	0.05	0.26	2.20	0.09	0.098	0.761

Table 11.1. Data of the landscapes in the considered environmental system.

Interacting LUs	H_{ki}	L_{ki}	$c_{ki} = H_{ki}/L_{ki}$
1 – 17	3017	7543	0.4
1 – 18	3664	9543	0.38
17 – 18	5429	8671	0.63
17 – 19	0	5421	0
18 – 19	3352	8953	0.37
18 – 20	5390	10780	0.5
19 – 20	1553	3106	0.5

Table 11.2. Geometric parameters and connectivity indices that describe the interaction between the LUs.

$$C = \begin{bmatrix} 0 & c_{17,1} & c_{18,1} & 0 & 0 \\ c_{1,17} & 0 & c_{18,17} & c_{19,17} & 0 \\ c_{1,18} & c_{17,18} & 0 & c_{19,18} & c_{20,18} \\ 0 & c_{17,19} & c_{18,19} & 0 & c_{20,19} \\ 0 & 0 & c_{18,20} & c_{19,20} & 0 \end{bmatrix}$$

where $c_{ki} = c_{ik}$ are the connectivity indices that describe how the LUs interact to each other; their numerical values, for the network under consideration, follow from the geometric parameters reported in Table 11.2.

In Figs. 11.4 we present the trend to equilibrium of each LU when the initial data are the ones reported in Table 11.1. More precisely, we compare the time evolution of the state variables (b, v) of each LU under investigation when it is connected (black solid lines, solutions to the NLM equations (10.5)) or isolated (gray dashed lines, solutions to SLM equations (10.4)), with parameters and initial conditions given in Tables 11.1 and 11.2. These figures show the effect of the coupling in the network model and its ability to modify or not the asymptotic behaviours of the single LU. As we can see, there are situations in which the network drives a sector towards a better scenario, characterized by higher level of green areas and bio-energy, but this is not the rule. More precisely, LU17, when connected to the others, evolves towards the same qualitative (single) scenario of predominant agricultural production, with however a slight improvement in the level of bio-energy; both LU1 and LU18 as a part of the network evolves towards the same kind of scenario, that is good quality

of bio-energy in presence of a certain amount of high quality areas, but the values of the components of the network equilibrium point relevant to LU1 and LU18 are both worse than the corresponding values in the single LU model. In sectors LU19 and LU20 there is a more evident difference in the asymptotic behaviours, since the network causes a change of the attractor: in the single model, LU19 tends to gradually loose its ecological quality in presence of a strong landscape fragmentation, while it evolves towards the agricultural scenario when connected to the other sectors, improving its quality; on the contrary, LU20 gets worse in the network, in terms of bio-energy and percentage of high quality areas, evolving towards the agricultural scenario when instead would reach the high quality equilibrium in absence of the network. We point out that in this case study the null state is not reached by the network, even if it could be locally stable; in other words, such environmental system takes advantage of the coupling. As a further remark, we can see in Fig. 11.4(e) for LU19 that the time evolution of the state variable v in the single LU model is almost indistinguishable from that in the network model. A possible explanation is that since r_{19} is rather large (see Table 11.1), the differential equation for the variable v_{19} in both SLM (10.4) and NLM (10.5) has a dominant term that does not contain the variable b_{19} (that is the variable influenced by the connected LUs):

$$v'_{19}(t) = d_{19}[v_{19}(t)(1 - v_{19}(t))b_{19}(t) - r_{19}v_{19}(t)] \approx -d_{19}r_{19}v_{19}(t),$$

and then the same exponential decrease can be expected for the single LU model and for the network system. This comment also applies to the v variable relevant to LU17 (see Fig. 11.4(c)). Summing up, the interactions within the network improve the dynamics of LUs 17 and 19 and, at the same time, deteriorate the dynamics of LUs 1, 18 and 20.

In Fig. 11.5 we compare the trajectories in the phase subspace (b, v) obtained by integrating the SLM equations (10.4) (dashed gray lines), the NLM equations (10.5) (black solid lines) and also that of the simplified model (11.5) (gray solid lines). The value of I (one for each LU) used in the simplified model has been numerically evaluated a posteriori, according to (11.4), from the NLM simulation when the network has reached its equilibrium (with parameters and initial data given in Tables 11.1 and 11.2). It is remarkable that the simplified and the network models evolve towards the same equilibrium states in each LU, as expected; relaxation to equilibrium for the simplified model is instead different with respect to the one prescribed by the NML equations, since the simplified model describes essentially the dynamics of each LU when inserted in a network at equilibrium (background), thus under particular assumptions on the relaxation times. The relation between the

trend-to-equilibrium dynamics of the simplified and NLM systems deserves however further investigation, that will be matter of future work.

As an additional test of validity of our simplification, we have numerically checked the expression (11.6) and (11.7) of the equilibrium states for the parameter values of Tables 11.1 and 11.2. To do this we have integrated the NLM equations (10.5) and, as already discussed, each LU reaches a steady state (Fig. 11.5). Then we have computed the value of I in system (11.5) of the simplified model at the network equilibrium, and we have obtained a value for the equilibria (11.6) and (11.7) for each LU. The obtained values turn out to be in agreement with the equilibrium values obtained integrating the NLM equations (10.5), with an error of order 10^{-8} due to numerical approximations.

The behavior of the NLM can be explained on the basis of the analysis performed in Section 11.2 for the simplified system (11.5). In Figure 11.6(a) the position of each LU in the (α, r) plane for our case study is shown. In particular, sectors LU17 and LU19 belong to region $\boxed{F}$ in the (α, r) plane. This fact explains a priori the change of equilibrium type to which LU19 converges: the trajectory tends to E_0 in the single LU model and to E_{1_N} in the coupled system, as can be seen in Fig. 11.5(d). Also sector LU17 belongs to region $\boxed{F}$ and it tends to the equilibrium denoting an agricultural scenario both in the single LU model and in the network case. Moreover, from the simulations we observe that the value b_{1_N} of the bio-energy at the equilibrium for LU17 in the coupled case is greater than b_1 of the isolated one. This is in agreement with the condition (11.11) where $I = I_{17}$ is estimated a posteriori using the simulation outcomes and formula (11.4), and turns out to be greater than cb_1.

The other sectors, instead, belong to region $\boxed{A}$ and, as it can be seen in Fig. 11.6(b), the connectivity values c_1, c_{18} and c_{20} (dashed lines) are greater than the respective thresholds $\tilde{c}$, so we have to compute I_1, I_{18} and I_{20} using the simulation outcomes and formula (11.4) to determine the stable equilibrium. We find that parameters of sectors LU1 and LU18 lie in the gray region, so they evolve to the coexistence equilibrium $E^+_{*_N}$, while the parameters of LU20 are in the light gray region, therefore the trajectories tend to E_{1_N}. This is in agreement with the network simulations reported in Fig. 11.5 and more specifically it explains the change of equilibrium type of LU20.

Thanks to the theoretical study of the simplified model (11.5) and in particular to the Remark 5, we can justify the decrease in the bio-energy at the equilibrium from the single LU model to the network one, observed for sectors LU1, LU18 and LU20. In fact, the computed values of I in such cases are smaller than the respective thresholds in conditions (11.12) and (11.13).

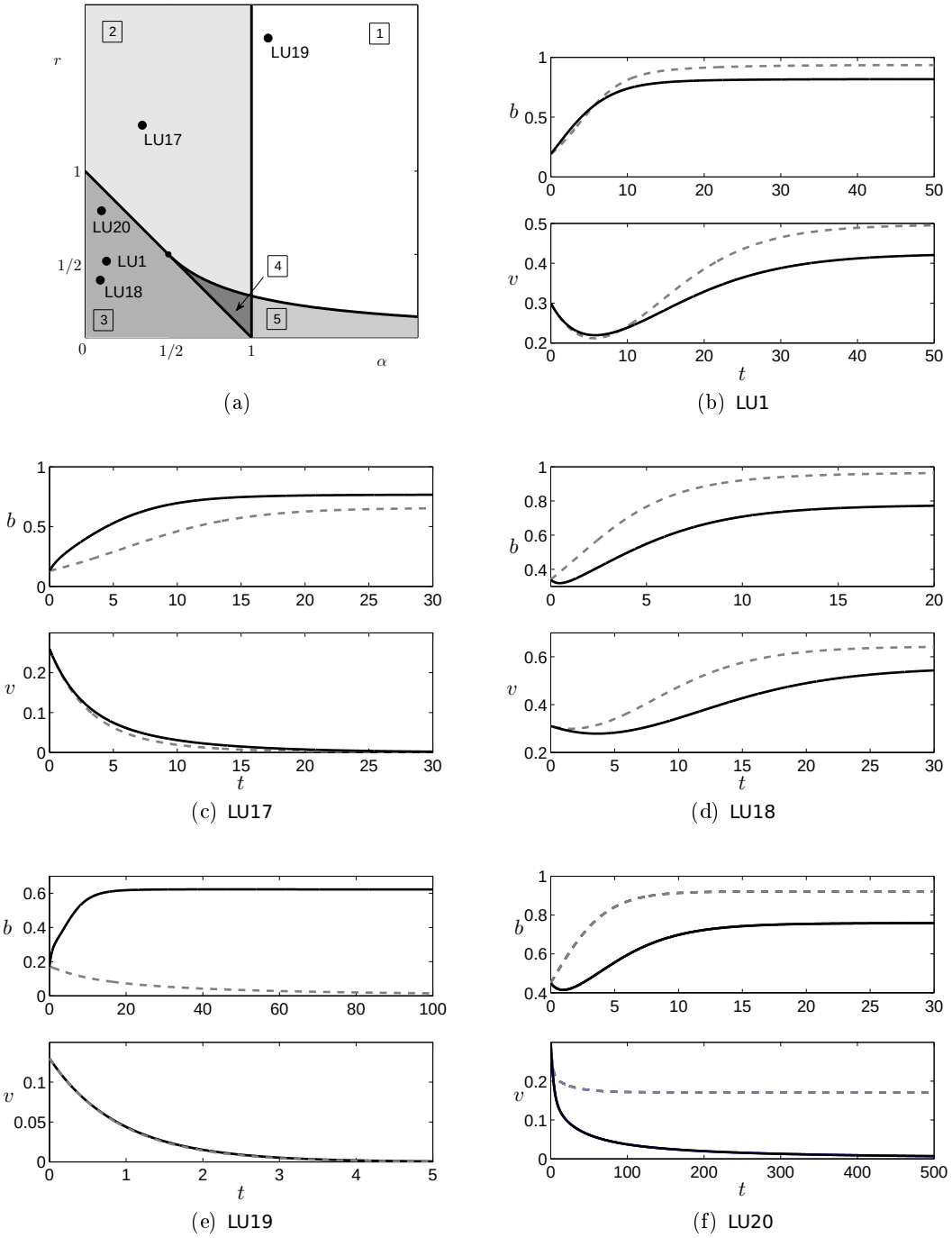

Fig. 11.4. Panel (a): Black points indicate the position in the (α, r) plane of the five considered LUs belonging to the northern Turin Province, whose parameters are reported in Table 11.1. The LUs belong to regions $\boxed{1}$, $\boxed{2}$, $\boxed{3}$ in which there is only one stable equilibrium of the single LU model, namely E_0, E_1, E_*^+ respectively. Panels (b)-(f): time evolution of the solutions $b(t)$ and $v(t)$ of the SLM equations (10.4) (dashed lines) and for the NLM equations (10.5) (solid lines) for the LUs 1, 17, 18, 19 and 20. LU1, LU17, LU18 evolve towards the same kind of scenario in the two cases; LU19, LU20 reach different scenarios when connected in the network.

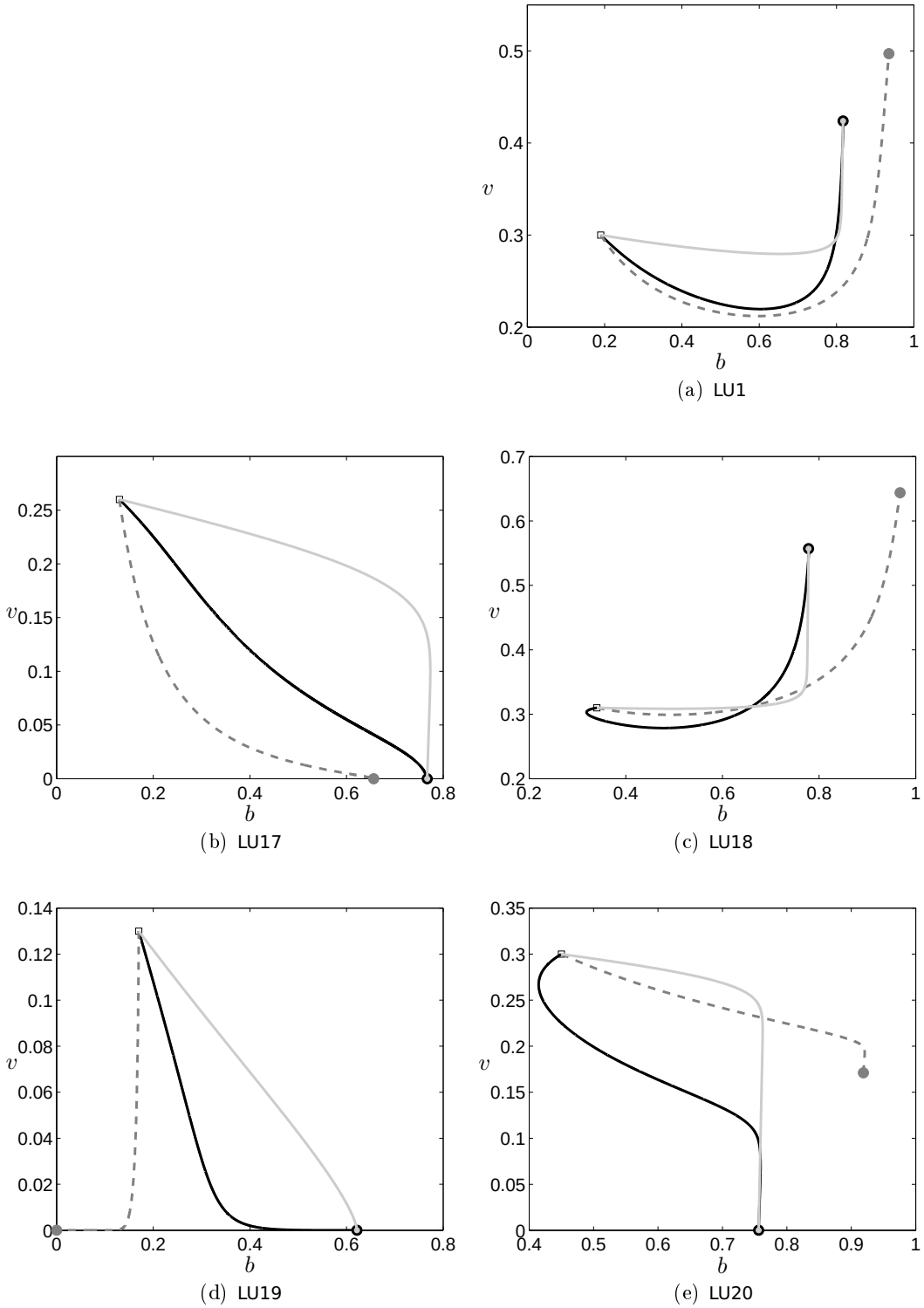

(a) LU1

(b) LU17

(c) LU18

(d) LU19

(e) LU20

Fig. 11.5. Trajectories in the phase subspace of each LU for the SLM (10.4) (dashed gray lines), for the NLM (10.5) (solid black lines) and for the simplified model (11.5) (solid gray lines); squares indicate initial conditions; points denote the steady states.

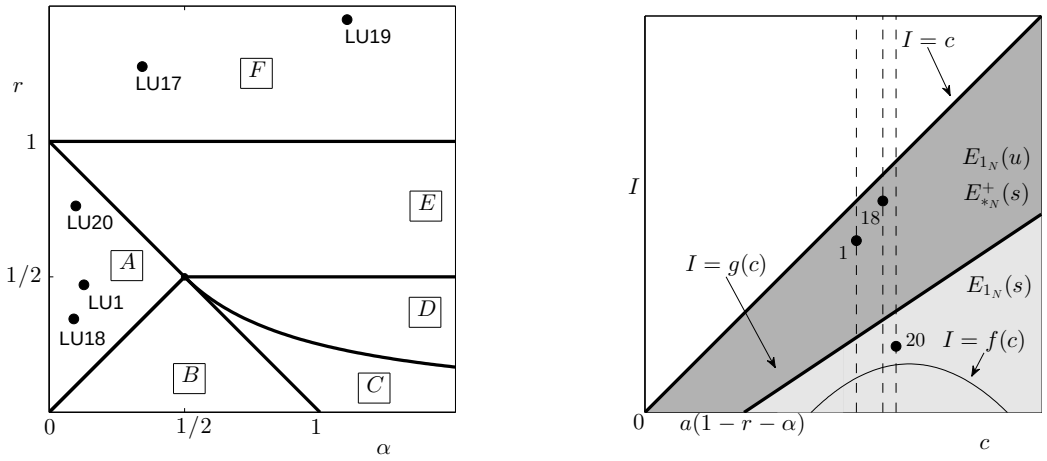

(a) (α, r) plane

(b) (c, I) plane

Fig. 11.6. Panel (a): Black points indicate the position in the (α, r) plane of the five considered LUs belonging to the northern Turin Province, whose parameters are reported in Table 11.1. Panel (b): Position in the (c, I) plane of the three LUs belonging to region $\boxed{A}$ of the (α, r) plane. This is a qualitative figure, since the position of the curves $I = f(c)$ and $I = g(c)$ depends on the chosen LU.

12

Discussion and Conclusions

We have proposed a model for an environmental system, distributed in several sectors (LUs) as an ecological network, using as state variables the production of bio-energy and the percentage of high ecological quality areas in each sector. The LUs are coupled to each other by a linear interaction term proportional to the difference between the bio-energies and constitute a network of dynamical systems. First we have considered the single LU model and analyzed its evolution towards a stable equilibrium state. Then we have focused our attention on the network model. Our analysis has shown that the interaction between the LUs can lead each ecological sector both to a better or to a worse ecological scenario, with respect to the single LU model, depending on the values of the state variables of the nearest LUs. In fact, the case study has shown clearly that LU1 and LU18 commute to a worse situation when they are connected in the network. On the contrary, LU17 improves its bio-energy value. In addition, LU19 and LU20 present even a change of equilibrium state passing from an attractor to another one: these behaviors can be interpreted as examples of different kinds of resilience of landscape systems under the effect of environmental stress.

The simplified system, representing the situation of a single LU added to a network at the equilibrium (background), has proved to be an useful tool of investigation of the network. For instance, the simplified model univocally determines the asymptotic behavior of sectors LU17 and LU19, regardless of the initial conditions.

In our opinion future perspectives and developments may involve the modification of the connectivity term in order to better detail the interaction. In particular, we plan to consider time-dependent connectivity parameters $c_{ij}(t)$ that depend on the bio-energy flux through the boundaries, similarly to what has been proposed in paper [38] where the connectivity index is defined in a different way.

Furthermore, another modification to the model could take into account a coupling term also in the differential equations relevant to the v_i variables. More specifically, a loss term on the i-th LU depending on the extension of the low ecological quality areas of its neighbors (namely proportional to $1 - v_k(t)$, for $k \in \mathcal{I}_i$) could be considered. This term should describe the negative impact of the low quality areas of the LUs surrounding the i-th itself. Conversely, also a gain term, accounting for an increase in the quality of the ecological sector, can be introduced, in order to take into account the pollination phenomena that eventually may arise thanks to the presence of high quality areas in the nearby LUs.

We expect that these improvements of the model lead to a more detailed and realistic description of the phenomena characterizing an environmental system, even if the analysis developed in this paper shows that a simple linear coupling term is able to reproduce some relevant aspects of such an interaction. Therefore, these new models can be employed to aid the management and the decision process in defining planning strategies by the prediction of possible future scenarios of the environment and to help in preventing incidental risks of the territory.

References

[1] A. Abakuks, *An optimal isolation policy for an epidemic*, Journal of Applied Probability, 10 (1973), pp. 247–262.

[2] ——, *Optimal immunization policies for epidemics*, Advances in Applied Probability, 6 (1974), pp. 494–511.

[3] R. Anderson and R. May, *Population biology of infectious diseases: Part I*, Nature, 280 (1979), pp. 361–367.

[4] R. M. Anderson, R. M. May, and B. Anderson, *Infectious diseases of humans: dynamics and control*, vol. 28, Wiley Online Library, 1992.

[5] J. Arino and P. Van den Driessche, *A multi-city epidemic model*, Mathematical Population Studies, 10 (2003), pp. 175–193.

[6] V. I. Arnol'd, *Catastrophe Theory*, Springer Science & Business Media, 2003.

[7] N. T. Bailey, *Spatial models in the epidemiology of infectious diseases*, in Biological Growth and Spread, Springer, 1980, pp. 233–261.

[8] N. T. Bailey et al., *The mathematical theory of infectious diseases and its applications*, Charles Griffin & Company Ltd, 5a Crendon Street, High Wycombe, Bucks HP13 6LE., 1975.

[9] H. Behncke, *Optimal control of deterministic epidemics*, Optimal Control Applications and Methods, 21 (2000), pp. 269–285.

[10] R. Bellman, *Dynamic Programming*, Courier Corporation, 2013.

[11] L. D. Berkovitz, *Optimal Control Theory*, vol. 12, Springer Science & Business Media, 1974.

[12] S. Boccaletti, V. Latora, Y. Moreno, M. Chavez, and D.-U. Hwang, *Complex networks: Structure and dynamics*, Physics reports, 424 (2006), pp. 175–308.

[13] L. Bolzoni, E. Bonacini, M. Groppi, and C. Soresina, *Time-optimal control strategies in SIR epidemic models*, Mathematical Biosciences, (2017). In press, minor revision requested.

[14] L. Bolzoni and G. A. De Leo, *A cost analysis of alternative culling strategies for the eradication of classical swine fever in wildlife*, Environment and Development Economics, 12 (2007), pp. 653–671.

[15] ——, *Unexpected consequences of culling on the eradication of wildlife diseases: the role of virulence evolution*, American Naturalist, 181 (2013), pp. 301–313.

[16] L. Bolzoni, L. Real, and G. De Leo, *Transmission heterogeneity and control strategies for infectious disease emergence*, Plos ONE, 2 (2007), p. e747.

[17] L. Bolzoni, V. Tessoni, M. Groppi, and G. A. De Leo, *React or wait: which optimal culling strategy to control infectious diseases in wildlife*, Journal of Mathematical Biology, 69 (2014), pp. 1001–1025.

[18] E. Bonacini, M. Groppi, R. Monaco, A. Soares, and C. Soresina, *A network landscape model: stability analysis and numerical tests*, Communications in Nonlinear Science and Numerical Simulation, 48 (2017), pp. 569 – 584.

[19] F. Brauer, P. Van den Driessche, and J. Wu, *Mathematical Epidemiology*, Springer, Berlin-Heidelberg, 2008.

[20] C. Büskens, *NUDOCCCS, user's manual*, Universität Münster, (1996).

[21] V. Capasso and G. Serio, *A generalization of the Kermack-McKendrick deterministic epidemic model*, Mathematical Biosciences, 42 (1978), pp. 43–61.

[22] B. Chachuat, *Nonlinear and dynamic optimization: from theory to practice*, tech. report, Automatic Control Laboratory, EPFL, Switzerland, 2007.

[23] M. Choisy and P. Rohani, *Harvesting can increase severity of wildlife disease epidemics*, Proceedings of the Royal Society B, 273 (2006), pp. 2025–2034.

[24] B. J. Collings, *Characteristic polynomials by diagonal expansion*, The American Statistician, 37 (1983), pp. 233–235.

[25] E. Cristiani and P. Martinon, *Initialization of the shooting method via the Hamilton-Jacobi-Bellman approach*, Journal of Optimization Theory and Applications, 146 (2010), pp. 321–346.

[26] D. J. Daley and J. Gani, *Epidemic Modelling: an Introduction*, vol. 15, Cambridge University Press, 2001.

[27] I. De Palma, *Methodologies of landscape ecology and mathematical models for environments evaluation and ecoservice systems estimate*, master degree thesis, Politecnico di Torino, 2014.

[28] DEFRA/DCMS, *Economic cost of foot and mouth disease in the UK*, tech. report, Joint Working Paper of the Department for the Environment, Food and Rural Affairs and the Department of Culture, Media and Sport, UK, 2002.

[29] M. Diehl, D. B. Leineweber, and A. A. Schäfer, *MUSCOD-II users' manual*, Universität Heidelberg. Interdisziplinäres Zentrum für Wissenschaftliches Rechnen [IWR], 2001.

[30] O. Diekmann and J. A. P. Heesterbeek, *Mathematical epidemiology of infectious diseases: model building, analysis and interpretation*, vol. 5, John Wiley & Sons, 2000.

[31] O. Diekmann, J. A. P. Heesterbeek, and J. A. Metz, *On the definition and the computation of the basic reproduction ratio R_0 in models for infectious diseases in heterogeneous populations*, Journal of mathematical biology, 28 (1990), pp. 365–382.

[32] K. Dong-Hyun, *Structural factors of the middle east respiratory syndrome coronavirus outbreak as a public health crisis in Korea and future response strategies*, Journal of Preventive Medicine and Public Health, 48 (2015), pp. 265–270.

[33] S. Dürr, H. zu Dohna, E. Di Labio, T. E. Carpenter, and M. G. Doherr, *Evaluation of control and surveillance strategies for classical swine fever using a simulation model*, Preventive Veterinary Medicine, 108 (2013), pp. 73–84.

[34] P. Fabbri, *Paesaggio, pianificazione, sostenibilità*, vol. 1, Alinea, 2003.

[35] F. Finotto, *Landscape assessment: the ecological profile*, in Landscape Indicators, Springer, 2011, pp. 47–75.

[36] W. H. Fleming and R. W. Rishel, *Deterministic and stochastic optimal control*, vol. 1, Springer Science & Business Media, 1982.

[37] R. T. Forman, *Land Mosaics: The Ecology of Landscapes and Regions (1995)*, Springer, 2014.

[38] F. Gobattoni, G. Lauro, R. Monaco, and R. Pelorosso, *Mathematical models in landscape ecology: stability analysis and numerical tests*, Acta Applicandae Mathematicae, 125 (2013), pp. 173–192.

[39] F. Gobattoni, R. Pelorosso, G. Lauro, A. Leone, and R. Monaco, *A procedure for mathematical analysis of landscape evolution and equilibrium scenarios assessment*, Landscape and Urban Planning, 103 (2011), pp. 289–302.

[40] S. V. Gordon, *Bovine TB: stopping disease control would block all live exports*, Nature, 456 (2008), p. 700.

[41] J. Guckenheimer and P. Holmes, *Nonlinear Oscillations, Dynamical Systems, and Bifurcations of Vector Fields*, vol. 42, Springer Science & Business Media, 2002.

[42] A. Handel, I. Longini, and R. Antia, *What is the best control strategy for multiple infectious disease outbreaks*, Proceedings of the Royal Society B, 274 (2007), pp. 833–837.

[43] E. Hansen and T. Day, *Optimal antiviral treatment strategies and the effects of resistance*, Proceedings of the Royal Society B, 278 (2011), pp. 1082–1089.
[44] ——, *Optimal control of epidemics with limited resources*, Journal of Mathematical Biology, 62 (2011), pp. 423–451.
[45] H. W. Hethcote, *A thousand and one epidemic models*, in Frontiers in mathematical biology, Springer, 1994, pp. 504–515.
[46] ——, *The mathematics of infectious diseases*, SIAM review, 42 (2000), pp. 599–653.
[47] H. W. Hethcote and J. W. Van Ark, *Epidemiological models for heterogeneous populations: proportionate mixing, parameter estimation, and immunization programs*, Mathematical Biosciences, 84 (1987), pp. 85–118.
[48] M. W. Hirsch and H. Smith, *Monotone dynamical systems*, Handbook of differential equations: ordinary differential equations, 2 (2006), pp. 239–357.
[49] R. A. Horn and C. R. Johnson, *Matrix Analysis*, Cambridge university press, 2012.
[50] H. S. Horst, C. J. de Vos, F. H. M. Tomassen, and J. Stelwagen, *The economic evaluation of control and eradication of epidemic livestock diseases*, Revue Scientifique et Technique de l'Office International des Epizoties, 18 (1999), pp. 367–379.
[51] A. M. Hutber, R. P. Kitching, and E. Pilipcinec, *Predictions for the timing and use of culling or vaccination during a foot-and-mouth disease epidemic*, Research in Veterinary Science, 81 (2006), pp. 31–36.
[52] M. Hvistendahl, *Enigmatic bird flu strain races across the U.S. Midwest*, Science, 348 (2015), pp. 741–742.
[53] D. Iacoviello and G. Liuzzi, *Fixed/free final time SIR epidemic models with multiple controls*, International Journal of Simulation Modelling, 7 (2008), pp. 81–92.
[54] V. Ingegnoli, *Landscape ecology: A widening foundation*, 2002.
[55] C. Jiang, *Optimal control of SARS epidemics based on cybernetics*, International Journal of Systems Science, 38 (2007), pp. 451–457.
[56] C. Y. Kaya and J. L. Noakes, *Computational method for time-optimal switching control*, Journal of Optimization Theory and Applications, 117 (2003), pp. 69–92.
[57] M. J. Keeling, L. Danon, M. C. Vernon, and T. A. House, *Individual identity and movement networks for disease metapopulations*, Proceedings of the National Academy of Sciences, 107 (2010), pp. 8866–8870.
[58] W. O. Kermack and A. G. McKendrick, *A contribution to the mathematical theory of epidemics*, in Proceedings of the Royal Society of London A:

mathematical, physical and engineering sciences, vol. 115, The Royal Society, 1927, pp. 700–721.

[59] ——, *Contributions to the mathematical theory of epidemics. ii. the problem of endemicity*, in Proceedings of the Royal Society of London A: Mathematical, Physical and Engineering Sciences, vol. 138, The Royal Society, 1932, pp. 55–83.

[60] M. Koopmans, B. Wilbrink, M. Conyn, G. Natrop, H. van der Nat, H. Vennema, A. Meijer, J. van Steenbergen, R. Fouchier, A. Osterhaus, and A. Bosman, *Transmission of H7N7 avian influenza A virus to human beings during a large outbreak in commercial poultry farms in The Netherlands*, Lancet, 363 (2004), pp. 587–593.

[61] A. J. Kucharski, A. Camacho, S. Flasche, R. E. Glover, W. J. Edmunds, and S. Funk, *Measuring the impact of Ebola control measures in Sierra Leone*, Proceedings of the National Academy of Sciences of the United States of America, 112 (2015), pp. 14366–14371.

[62] S. Lenhart and J. T. Workman, *Optimal Control Applied to Biological Models*, Chapman & Hall /CRC Mathematical and Computational Biology Series, Boca Raton, USA, 2007.

[63] B.-L. Li, *Why is the holistic approach becoming so important in landscape ecology?*, Landscape and Urban Planning, 50 (2000), pp. 27–41.

[64] N. Longworth, M. C. M. Mourits, and H. W. Saatkamp, *Economic analysis of HPAI control in The Netherlands I: Epidemiological modelling to support economic analysis*, Transboundary and Emerging Diseases, 61 (2014), pp. 199–216.

[65] A. J. Lotka, *Contribution to the energetics of evolution*, Proceedings of the National Academy of Sciences, 8 (1922), pp. 147–151.

[66] M.-J. J. Mangen, A. M. Burrell, and M. C. M. Mourits, *Epidemiological and economic modelling of classical swine fever: application to the 1997/1998 Dutch epidemic*, Agricultural Systems, 81 (2004), pp. 37–54.

[67] P. Martinon and J. Gergaud, *Using switching detection and variational equations for the shooting method*, Optimal Control Applications and Methods, 28 (2007), pp. 95–116.

[68] M. P. M. Meuwissen, S. H. Horst, R. B. M. Huirne, and A. A. Dijkhuizen, *A model to estimate the financial consequences of classical swine fever outbreaks: principles and outcomes*, Preventive Veterinary Medicine, 42 (1999), pp. 249–270.

[69] R. Morton and K. Wickwire, *On the optimal control of a deterministic epidemic*, Advances in Applied Probability, 6 (1974), pp. 622–635.

[70] J. D. Murray, *Mathematical Biology. II Spatial Models and Biomedical Applications*, Interdisciplinary Applied Mathematics V. 18, Springer-Verlag New York Incorporated, 2001.

[71] ——, *Mathematical Biology. I An introduction*, Interdisciplinary Applied Mathematics V. 17, Springer-Verlag New York, 2002.

[72] National Geographic website, October 2016. http://education.nationalgeographic.org/encyclopedia/geographic-information-system-gis/.

[73] Z. Naveh, *What is holistic landscape ecology? A conceptual introduction*, Landscape and urban planning, 50 (2000), pp. 7–26.

[74] B. Nerlich and C. Halliday, *Avian flu: the creation of expectations in the interplay between science and the media*, Sociology of Health & Illness, 29 (2007), pp. 46–65.

[75] J. Otte, J. Hinrichs, J. Rushton, D. Roland-Holst, and D. Zilberman, *Impacts of avian influenza virus on animal production in developing countries*, CAB Reviews: Perspectives in Agriculture, Veterinary Science, Nutrition and Natural Resources, 3 (2008).

[76] R. Pelorosso, S. Della Chiesa, U. Tappeiner, A. Leone, and D. Rocchini, *Stability analysis for defining management strategies in abandoned mountain landscapes of the mediterranean basin*, Landscape and Urban Planning, 103 (2011), pp. 335–346.

[77] C. Pettit, W. Cartwright, I. Bishop, K. Lowell, D. Pullar, and D. Duncan, *Landscape Analysis and Visualisation: Spatial Models for Natural Resource Management and Planning*, Springer Science & Business Media, 2008.

[78] L. Pontryagin, V. Boltyanskii, R. Gamkrelidze, and E. Mishchenko, *The Mathematical Theory of Optimal Processes*, International series of monographs in pure and applied mathematics, Interscience Publishers, Los Angeles, USA, 1962.

[79] A. Potapov, E. Merrill, and M. Lewis, *Wildlife disease elimination and density dependence*, Proceedings of the Royal Society B, 279 (2012), pp. 3139–3145.

[80] S. E. Roche, M. G. Garner, R. L. Sanson, C. Cook, C. Birch, J. A. Backer, C. Dubé, K. A. Patyk, M. A. Stevenson, Z. D. Yu, T. G. Rawdon, and F. Gauntlett, *Evaluating vaccination strategies to control foot-and-mouth disease: a model comparison study*, Epidemiology & Infection, 143 (2015), pp. 1256–1275.

[81] G. Rossi, G. A. De Leo, S. Pongolini, S. Natalini, S. Vincenzi, and L. Bolzoni, *Epidemiological modelling for the assessment of bovine tuberculosis*

surveillance in the dairy farm network in Emilia-Romagna (Italy), Epidemics, 11 (2015), pp. 62–70.

[82] M. Shamsi, *A modified pseudospectral scheme for accurate solution of bang-bang optimal control problems*, Optimal Control Applications and Methods, 32 (2011), pp. 668–680.

[83] C. Silva and E. Trélat, *Smooth regularization of bang-bang optimal control problems*, IEEE Transactions on Automatic Control, 55 (2010), pp. 2488–2499.

[84] H. L. Smith, *Monotone Dynamical Systems: an Introduction to the Theory of Competitive and Cooperative Systems*, American Mathematical Soc., 2008.

[85] L. M. Stolerman, D. Coombs, and S. Boatto, *Sir-network model and its application to dengue fever*, SIAM Journal on Applied Mathematics, 75 (2015), pp. 2581–2609.

[86] M. G. Turner, *Landscape ecology: the effect of pattern on process*, Annual review of ecology and systematics, 20 (1989), pp. 171–197.

[87] J. E. Vermaat, F. Eppink, J. C. van den Bergh, A. Barendregt, and J. van Belle, *Aggregation and the matching of scales in spatial economics and landscape ecology: empirical evidence and prospects for integration*, Ecological Economics, 52 (2005), pp. 229–237.

[88] K. Wickwire, *Optimal isolation policies for deterministic and stochastic epidemics*, Mathematical Biosciences, 26 (1975), pp. 325–246.

[89] J. H. Wilkinson, *The Algebraic Eigenvalue Problem*, vol. 87, Clarendon Press Oxford, 1965.

[90] J. Zhang, J. Lou, Z. Ma, and J. Wu, *A compartmental model for the analysis of SARS transmission patterns and outbreak control measures in China*, Applied Mathematics and Computation, 162 (2005), pp. 909–924.

Journal publications

Papers relevant to thesis's subject

- E. Bonacini, M. Groppi, R. Monaco, A.J. Soares, C. Soresina, *A network model for landscape evolution: stability analysis and numerical tests*, Communications in Nonlinear Science and Numerical Simulation, 48 (2017) 569?584.

- E. Bonacini, L. Bolzoni, M. Groppi and C. Soresina, *Time-optimal control strategies in SIR epidemic models*, requested minor revisions Mathematical Biosciences.

Other papers

- E. Bonacini, R. Burioni, M. di Volo, M. Groppi, C. Soresina, A. Vezzani, *How single node dynamics enhances synchronization in neural networks with electrical coupling*, Chaos, Solitons & Fractals, 85 (2016) 32-43.

Communications

- "Time-optimal control strategies in SIR epidemic models", XLI Summer School on Mathematical Physics, 17 September 2015, Ravello (Italy).
- "Synchronization in neural networks: the Connection Graph Stability approach", XXXIX Summer School on Mathematical Physics, 18 September 2014, Ravello (Italy).
- "Mathematical modeling of neural networks and methods for the study of synchronization", Computational and Theoretical Neuroscience Reading Group Seminar, 12 May 2014, University of Milano.

Posters

- "Time-optimal control strategies in SIR epidemic models" during the poster session of the School *Methods and Models of Kinetic Theory*, June 2016, Porto Ercole (Grosseto) Italy.

- "Time-optimal control strategies in SIR epidemics models" during the poster session of the workshop *Mathematical and Computational Epidemiology*, August 2015, Erice (Trapani) Italy.

- "How single node dynamics enhance synchronization in neural networks with electrical coupling" during the poster session of the School *Methods and Models of Kinetic Theory*, June 2014, Porto Ercole (Grosseto) Italy.

Parma, 23/09/2017